Secondary Control in Inverter-Based Microgrids

vorgelegt von

Ajay Krishna

an der Fakultät IV - Elektrotechnik und Informatik
der Technischen Universität Berlin
zur Erlangung des Akademischen Grades

Doktor der Ingenieurwissenschaften
- Dr.-Ing. -
genehmigte Dissertation

Promotionsausschuss:

Vorsitzender: Prof. Dr.-Ing. Sergio Lucia
Gutachter : Prof. Dr.-Ing. Jörg Raisch
Gutachter : Prof. Dr.-Ing. Johannes Schiffer
Gutachter : Dr. Frank Hellmann

Tag der wissenschaftlichen Aussprache: 17. Juni 2020

Berlin 2020

Abstract

The concept of microgrids is foreseen as a promising solution to tackle challenges arising due to the increasing integration of renewable energy sources (RESs) into electric power systems. Due to the high share of RESs, various challenging problems arise in controlling a microgrid. In the present work, some vital control problems such as network frequency regulation, power sharing, load voltage restoration and, voltage stability in an islanded microgrid are investigated. The contributions of this thesis are twofold, i.e., (a) *distributed secondary frequency control* and (b) *distributed voltage control*.

In the former case, the main contributions are as follows: (i) Steady-state performance of various distributed secondary frequency controllers are compared in the presence of clock drifts, which is a non-negligible parameter uncertainty observed in microgrids. (ii) Necessary and sufficient conditions for accurate active power sharing and network frequency regulation are derived. (iii) A novel secondary frequency controller, termed as generalized distributed averaging integral (GDAI) control, is proposed to address the aforementioned control objectives in the presence of clock drifts. (iv) A tuning criterion is derived, which guarantees asymptotic convergence of the closed-loop system trajectories with the GDAI control to a desired synchronized motion.

The section on *distributed voltage control* considers microgrids with parallel-connected inverters connected to a joint load at the point of common coupling (PCC). This is a commonly encountered microgrid application. In such a network, achieving steady-state proportional reactive power sharing and PCC/load voltage regulation are two important control objectives, especially in the case with highly inductive power lines. The contributions falling under this section are as follows: (i) The existence and uniqueness properties of a positive voltage solution to the algebraic equations corresponding to the aforementioned control objectives are established. (ii) A distributed voltage control law that yields the desired unique voltage solution is proposed. (iii) A stability criterion which renders local asymptotic stability of the closed-loop equilibrium point is derived. Finally, via simulation, the performance of the control approaches presented in this thesis are validated for modeling errors and disturbances.

Zusammenfassung

Das Konzept von Microgrids könnte entscheidend zur Bewältigung von Herausforderungen durch die zunehmende Integration erneuerbarer Energiequellen in elektrische Energiesysteme beitragen. Die fluktuierende und dezentrale Einspeisung erneuerbarer Energien führt zu vielen anspruchsvollen und neuen Aufgaben für die Regelung von Microgrids. In der vorliegenden Arbeit werden daher einige wichtige Regelungsprobleme wie Netzfrequenzregelung, Leistungsaufteilung, Lastspannungswiederherstellung und Spannungsstabilität in einem Inselnetz untersucht. Die wissenschaftlichen Beiträge dieser Arbeit sind (a) verteilte Sekundärregelung der Frequenz und (b) verteilte Spannungsregelung.

Im ersten Fall sind die Hauptbeiträge: (i) Die stationäre Performance verschiedener Sekundärregler wird unter Einfluss von Taktversatz (clock drifts) verglichen, welche eine nicht vernachlässigbare Parameterunsicherheit in Microgrids darstellen. (ii) Es werden notwendige und hinreichende Bedingungen für eine genaue Aufteilung der Wirkleistung und für die Netzfrequenzwiederherstellung hergeleitet. (iii) Ein neuartiger Frequenzsekundärregler mit der Bezeichnung GDAI-Regelung (Generalized Distributed Averaging Integral) wird vorgeschlagen, welcher oben genannte Regelziele bei Vorhandensein von Taktversatz (clock drifts) einhält. (iv) Es wird ein Auslegungskriterium hergeleitet, das asymptotische Konvergenz der geschlossenen Regelkreistrajektorien mit dem GDAI-Regler zu einer gewünschten synchronisierten Bewegung garantiert.

Der Abschnitt verteilte Spannungsregelung betrachtet Microgrids mit parallel angeschlossenen Wechselrichtern, die am Point of Common Coupling (PCC) mit einer gemeinsamen Last verbunden sind. Dies stellt eine typische Microgrid-Anwendung dar. In einem solchen Netzwerk stellen stationäre proportionale Blindleistungsaufteilung und PCC-/Lastspannungsregulierung zwei wichtige Regelziele dar, insbesondere bei hochinduktiven Stromleitungen. Hier sind die wissenschaftlichen Beiträge wie folgt gegliedert: (i) Es werden Existenz- und Eindeutigkeitseigenschaften einer positiven Spannungslösung für die algebraischen Gleichungen gemäß der oben genannten Regelziele aufgestellt. (ii) Es wird ein verteiltes Spannungsregelgesetz, das die gewünschte eindeutige Spannungslösung erzielt, vorgeschlagen. (iii) Es wird ein Stabilitätskriterium, welches lokale asymptotische Stabilität des Gleichgewichtspunkts im geschlossenen Regelkreis betrachtet, hergeleitet. Schließlich wird durch Simulation die Performance der in dieser Arbeit vorgestellten Regelansätze hinsichtlich Modellierungsfehlern und Störungen validiert.

എന്റെ അമ്മയ്ക്ക്
To my mother

Acknowledgements

First of all, I would like to express my sincere gratitude to Jörg Raisch for allowing me to pursue my Ph.D. I highly appreciate your relaxed style of offering lots of freedom to explore one's research interests. In addition to academic matters, there are many other things I have learned from you, thanks Jörg.

Secondly, I thank you, Johannes Schiffer, for being an excellent supervisor and friend. Starting with my master's thesis in 2013, to this date, you were an inspiration to me. You know that, without your support, probably, I would not have started research on the topic *control of microgrids*. Your patience and willingness while listening to my ideas–which often were quite stupid–have always amazed me. This quality is something that I will try to follow for the rest of my career.

A big thanks to Christian A. Hans, providing everything needed to start a Ph.D. at the Microgrids Group, TU Berlin. You were always there as an experienced researcher and as a friend who encourages early-stage researchers like me. I cherish our after-work beer sessions at Cafe-A. Almost all the pictures presented in this thesis use your base code. Thanks a lot, Christian.

Likewise, I would like to thank all my colleagues at the Control Systems Group, TU Berlin. Especially a big thanks to my wonderful office mate, Lia Strenge. I was always so comfortable in our office, mainly because I never had to be conscious of anything. I was happy to keep the office as messy as I wanted to, thanks to you, Lia. Similarly, the last three years would not have been so enjoyable without you, Philipp Zitzlaff, Josep Theune, Ajay K. Sampathirao, and Steffen Hoffmann.

I am thankful to DAAD (German Academic Exchange Service) for financing my studies at TU Berlin and many thanks to Frank Hellmann and Sergio Lucia for joining my Ph.D. committee. I want to thank my collaborators, Christian A. Hans, Nima Monshizadeh, and Thomas Kral, for their guidance, contributions, and comments at various stages of my research. Furthermore, I am very much grateful to the proofreaders of this thesis, Shyam K.C. Neelakandhan (Sakha), Hisham Jamal, Lia Strenge, and Ajay K. Sampathirao.

I thank my family in India, especially my mother, Usha, for supporting me throughout my life. You are the strongest woman I have ever seen, and without your support, I probably wouldn't have even made to the school, thank you Amme. A big thanks to my little family in Berlin, Aparna, Nabeel, Nilufar, and our cute

little Noah. With the positive vibes you fellows create, my time at home has always been so chilled and relaxed. Aparna, you know how our journey has been, thanks a lot for your phenomenal support. I thank all my friends for their love.

Finally, I am very much thankful to the *society* for providing necessary socio-economic-geographic privileges so that I got the opportunity to *learn*.

Contents

List of Figures

Abbreviations

AC	alternating current
DAE	differential algebraic equation
DAI	distributed averaging integral
DC	direct current
DG	distributed generator
DoS	denial of service
ESS	energy storage system
GDAI	generalized distributed averaging integral
GFI	grid-forming inverter
LHS	left hand side
LMI	linear matrix inequality
LV	low voltage
MV	medium voltage
ODE	ordinary differential equation
PCC	point of common coupling

PI	proportional integral
PV	photovoltaic
RES	renewable energy source
RHS	right hand side
SRF-PLL	synchronous reference frame phase locked loop
UPS	uninterruptible power supply
ZIP	constant power/current/impedance

Symbols

$\mathbb{R}$	set of real numbers
$\mathbb{R}_{\geq 0}$	set of non-negative real numbers
$\mathbb{R}_{>0}$	set of positive real numbers
$\mathbb{R}_{<0}$	set of negative real numbers
$\mathbb{T}$	set of real points on the unit circle (mod 2π)
∇g	gradient of a function $g : \mathbb{R}^n \to \mathbb{R}$
$\|\cdot\|_2$	Euclidean norm
$A^\top$	transpose of a square matrix A
$\|\mathcal{W}\|$	cardinality of a set $\mathcal{W}$
$\mathcal{N}$	set of network nodes
$\mathcal{N}_i$	set of neighboring nodes connected to node i
δ_i	voltage phase angle at node i
V_i	voltage amplitude at node i
V_i^d	desired voltage amplitude at node i
B_{ij}	susceptance of the power line connecting node i and j
B_{ii}	shunt susceptance at node i
G_{ii}	shunt conductance at node i
a_i	weighting coefficient for reactive power sharing at node i
$\mathcal{X}_i$	weighting coefficient for active power sharing at node i
ω_i	electrical frequency at node i
$\bar{\omega}_i$	internal frequency at node i
ω^d	desired nominal network frequency
μ_i	clock drift value at inverter i
P_i	active power injection at node i
P_i^m	measured active power injection at node i
P_i^d	desired active power set point at node i
Q_i	reactive power injection at node i
Q_i^m	measured reactive power injection at node i
Q_i^d	desired reactive power set point at node i

τ_i	time constant of the power measurement filter at node i
S_i^N	nominal power rating of an inverter connected at node i
$\mathscr{L}$	Laplacian matrix of a communication network
$\mathscr{B}$	Incidence matrix of a communication network
$\mathbf{W}$	Edge weight matrix of a communication network

Chapter 1

Introduction

1.1 Motivation

The electric power systems are considered as the backbone of any modern industrialized society [1–3]. A power system can be broadly classified into power generators, transmission system, distribution system, and load centres [1, 4]. In conventional power networks, a significant share of power generated is through synchronous generators, which often use fossil-fuel-based energy sources [4, 5], substantially contributing to greenhouse gas emissions. Motivated by this, to reduce greenhouse gas emissions and fossil fuel consumption in the area of power systems, the worldwide usage of renewable energies has increased remarkably in the recent years [6,7]. Nonetheless, the increasing integration of renewable energy sources (RESs) results in various technological as well as structural changes in the existing power grid [8–11].

In comparison to conventional generators, RESs are small-sized, i.e., the power generated is relatively lower. Hence, most RESs are interfaced to MV (medium voltage) or LV (low voltage) levels [8, 10, 11]. Also, while replacing a conventional generator that typically delivers a high amount of power [12], a large number of RESs need to be installed for balancing power demand and supply. Thus, power generation is moving from a relatively small number of large scale power stations to a huge number of small-scale distributed generators (DGs). This is a major structural change in the existing power grid structure [6, 9].

An immediate consequence of this structural change is that power generation and consumption have become geographically closer to each other, with RESs as the primary source of power generation. Alternatively stated, such a set up can be understood as a distribution system which–in contrast to conventional

power systems– has localized power generation and consumption involved in it. Besides, the presence of a large number of DGs poses some crucial control challenges. For instance, in conventional power systems, the number of power generators is relatively small, and hence a centralized control solution would work satisfactorily [1]. However, in a power grid with a large number of DGs, a centralized control solution turns out to be inefficient [13], mainly because that a central unit has to communicate to all the numerous DGs connected in the network. Such a one-to-all communication system would increase the overall communication burden, and at the same time, would pose the risk of single-point-failures [13].

On top of the above-mentioned structural changes, a crucial technological challenge is as follows. RESs connected in the grid mostly produce DC (direct current) or variable frequency AC (alternating current) power output. Hence, they are interfaced to the grid using power electronic inverters. The physical characteristics of inverters largely differ from that to synchronous generators, see, e.g. [3, 14–16]. As a consequence, control strategies used in conventional power systems need to be redesigned and/or readjusted for power networks having a large number of inverter-interfaced RESs [14, 15, 17].

One promising solution to address these issues is by using the concept of *microgrids* [8, 10, 17–19]. A microgrid is a locally controllable electrical network with generators, storage units, and loads. The concept of microgrids is foreseen as a critical element in future electric power systems [10, 20]. In a general setting, microgrids may interact with each other [21], but - by matching generation and consumption within the microgrid as far as possible - transmitted power is reduced, and transmission losses are decreased. Microgrids can usually be operated in two modes, namely *grid-connected mode* where it is connected to the utility grid and *islanded* or *stand-alone* mode where it works as an isolated power network [10, 18, 19]. In comparison to grid-connected mode, in islanded mode, control actions have to be undertaken by the units connected within the network, making it challenging [22–27]. Thus, this thesis focusses on the topic of *control of islanded microgrids*.

1.2 Contributions

The present work is dedicated to addressing the following control problems in an islanded microgrid:

1. Accurate network frequency restoration,

2. Active power sharing,
3. Load voltage regulation,
4. Reactive power sharing and
5. Voltage stability.

A brief overview of the relevance of the considered control objectives is given in the sequel.

Similar to any isolated power network, maintaining a stable operating point is of tremendous importance in an islanded microgrid [22–24,28–31]. At the same time, restoring the network frequency to the nominal value and maintaining voltage amplitudes at all the buses within a specific limit is also very important [27,32,33]. In some microgrid applications, like a battery energy storage system (ESS) or a distributed uninterruptible power supply (UPS) system, it is often the case that the DGs are connected in parallel and are feeding a common load connected at the PCC [34,35]. In such applications, restoring the voltage amplitude at the PCC/load bus is of great relevance [34,35]. Finally, in any microgrid network, sharing the total system loads among the generation units in a fair manner is a crucial control objective [22,23,26,27,35].

The aforementioned contributions of this work can be divided into two main sections. At first, the problem of distributed frequency control [13,25,32,36,37] in a microgrid with arbitrary topology (also termed as a *meshed microgrid*) is investigated. Later, voltage stability and reactive power sharing [24, 27] in a microgrid with parallel-connected DGs connected to a common load [34, 35, 38] are addressed. Unless confusion arises, such a network is called a *parallel microgrid* in the rest of this thesis.

Next, the main contributions falling under these two sections are briefly described.

1.2.1 Distributed secondary frequency control

Inspired by conventional power systems, a hierarchical control architecture is advocated for microgrids, which has primary, secondary, and tertiary control layers [39,40]. The chapter entitled *distributed secondary frequency control* in this thesis focusses on exploring the robustness and performance of distributed secondary frequency controllers in the presence of a non-negligible parameter

uncertainty, known as *clock drifts*, commonly observed in inverter-based microgrids.

Microgrids are distributed systems where distributed computing is involved. It is a well-known fact that distributed computing applications suffer from clock drifts [41, 42]. In the presence of clock drifts, the steady-state performance of primary [16,43] and secondary frequency control [44–48] employed in a microgrid are adversely affected. The contributions of this thesis regarding these issues can be summarized as follows.

1. A general distributed integral frequency control structure is proposed to compare the steady-state performance of various distributed secondary frequency controllers in the presence of clock drifts. This approach assumes that in the primary control layer, the standard frequency droop control [38] is implemented.

2. Based on the proposed general controller structure, necessary and sufficient conditions for steady-state accurate frequency restoration and active power sharing in the presence of clock drifts are derived. Later, a novel secondary frequency controller, termed as generalized distributed averaging integral (GDAI) controller is presented to achieve the above-mentioned control objectives in the presence of clock drifts.

3. A tuning criterion in the form of a set of linear matrix inequalities (LMIs) is derived that, if feasible, guarantees asymptotic stability [49, 50] of the closed-loop equilibrium point. The tuning criterion is derived using the standard decoupling assumption utilized in power networks with inductive lines[1], see e.g., [1, 22, 24, 27, 32].

4. The results are validated extensively, via simulation, and are compared with other distributed secondary frequency controllers proposed in the literature, e.g. [13, 32, 51, 52].

1.2.2 Distributed voltage control

This section outlines the contributions of this thesis to the topic of *voltage control in parallel microgrids*. Two important control objectives in a parallel microgrid with dominantly inductive power lines are (i) reactive power sharing and (ii) load/PCC voltage restoration, see, e.g. [34, 35, 38]. In this regard, the following results are summarized in this thesis.

[1] Also referred to as *lossless* lines [1].

1. At first, the existence and uniqueness properties of a stationary solution to the set of algebraic equations corresponding to steady-state proportional reactive power sharing and PCC voltage restoration are established.

2. A distributed voltage controller which drives the closed-loop system trajectories asymptotically [49, 50] to the desired unique stationary solution is proposed.

3. Via a numerical case study, the performance of the proposed distributed voltage controller towards further modeling errors and load disturbances is evaluated. Operational compatibility of the proposed control approach with the standard frequency droop control [38] is also investigated.

1.2.3 Structure of the thesis

The present thesis is arranged as six chapters with a common conclusion. The main contents of each chapter are described concisely in the following.

Chapter 2: Preliminaries

In this chapter, some standard results from control theory, algebraic graph theory, and power systems are reviewed. After introducing the mathematical notation used in this thesis, some control theory basics, like Lyapunov stability [49, 50], are recalled. Then, a background on algebraic graph theory [53–55] and consensus protocols [56] are discussed. Finally, some power systems basics [1, 3, 4] required in the present work are presented.

Chapter 3: Problem statement

In this chapter, the microgrid concept and the formal definition of a microgrid [8, 10, 18] are introduced. Furthermore, the main technical challenges in a microgrid are discussed. Later, the hierarchical control structure used in an islanded microgrid [39] is described. Finally, definitions regarding power sharing [26, 27], frequency and voltage restoration [13, 32, 36, 51, 57] are formalized.

Chapter 4: Microgrid model and primary control

The mathematical model of the microgrid studied in this thesis is introduced in this chapter. More precisely, the inverter, the load and the network models required to present the results summarized in this thesis are introduced. Furthermore, the standard droop control [38] used at the primary control layer is described in detail. Later, the model of a droop-controlled inverter in the presence of clock drifts is derived [43, 58] Finally, the steady-state performance of

frequency droop control in the presence of clock drifts and voltage droop control in lossless microgrids are discussed in detail.

Chapter 5: Distributed secondary frequency control

This chapter focusses on the performance of secondary frequency control in microgrids with explicit consideration of clock drifts. More precisely, achieving control objectives of steady-state

1. accurate network frequency restoration and
2. active power sharing,

with various distributed secondary frequency controllers in the presence of clock drifts are studied.

A general distributed control representation is proposed, which can be parameterized into the control approaches presented in [13, 32, 37, 51]. Based on this general controller representation, necessary and sufficient conditions for achieving secondary frequency control objectives in the presence of clock drifts are derived. The control approaches advocated in [13, 32, 37, 51] were found to be not satisfying the derived necessary and sufficient conditions. Yet in this section, a novel secondary frequency controller, termed as GDAI control is proposed, which fulfils the above-mentioned control objectives in the presence of clock drifts.

In the second part of this chapter, a tuning criterion that guarantees asymptotic stability of the closed-loop (with the GDAI control) equilibrium point is presented. For deriving this result, concepts from the classical Lyapunov function-based stability analysis employed in power networks were used, see, e.g. [25, 59].

Chapter 6: Distributed voltage control

In this chapter, the problem of voltage control in a parallel microgrid is investigated. More precisely, three important control objectives of

1. reactive power sharing,
2. PCC voltage restoration and
3. voltage stability,

in a parallel microgrid with inductive lines are addressed.

In the first part of this chapter, the existence and uniqueness properties of a stationary voltage solution to the steady-state algebraic equations of reactive power sharing and PCC voltage restoration are established. Then, inspired by [27, 30], a distributed voltage controller is proposed, which at equilibrium yields the desired stationary solution mentioned above. A stability criterion that guarantees local asymptotic stability of the closed-loop equilibrium point is also derived in this chapter.

Chapter 7: Case study

In the first section of this chapter, the performance of the GDAI controller is validated and is compared with other distributed control approaches [13, 32, 51] in the presence of clock drifts. To evaluate the robustness of the GDAI control towards typical modeling uncertainties, a small line resistance is considered in the simulated microgrid.

In the second part of this chapter, the performance of the distributed voltage controller designed for a parallel microgrid is validated. Furthermore, the operational compatibility of the same with the frequency droop control [38] is tested.

1.3 Related works

1.3.1 Introduction

In conventional power systems, synchronous generators that operate as grid forming units are responsible for maintaining a desired stable operating point [3]. However, in inverter-based microgrids, inverter-interfaced sources or, more precisely, *grid-forming inverters* replace synchronous generators [14, 15]. A grid forming inverter is a voltage source inverter controlled using voltage and frequency references provided by the designer [14–16].

Motivated by the control strategies used in conventional power systems, a hierarchical control approach has been advocated for microgrids [13, 39, 60]. One typically distinguishes primary and secondary control layers (as in conventional power systems), while the top control level, which is mostly referred to as operational management or tertiary control, is mainly concerned with generation scheduling, see, e.g. [21, 61]. Primary control layer consists of a *decentralized* proportional control, called *droop control*. The decentralized aspect of droop control

facilitates that each inverter[2] requires *only local* information for its operation, and does not need any communication with other inverters. In microgrids with inductive power lines, droop control can be divided into two, *frequency droop control* and *voltage droop control*. In frequency droop control, the frequency of an inverter depends linearly on the active power injection. Frequency droop control achieves frequency stability and active power sharing [22, 62]. In the case of voltage droop control, voltage amplitude at each inverter is in proportion to its reactive power injection [38].

In the rest of this section, some relevant works on the topics focussed on in this thesis are reviewed.

1.3.2 Distributed secondary control

In islanded microgrids, frequency stability and proportional active power sharing are typically provided by the primary frequency droop control [22, 26, 38, 62, 63]. Despite many advantages, a major drawback of the frequency droop control is that the steady-state frequency usually deviates from the nominal value (50 or 60 Hz). The first part of this thesis is devoted to secondary frequency control, which is responsible for correcting the steady-state frequency error caused by the primary control layer [39]. In this regard, some related works on secondary frequency control are outlined in the sequel.

As most of the electrical devices are designed to operate at the nominal frequency of 50 or 60 Hz, restoring the network frequency to the desired nominal value is very important [1]. Conventionally, a central integral control [63] is advocated for this task, where a central unit communicates with all the generation units. Yet, considering the complexity and the number of generation units connected in a microgrid, centralized approaches significantly increase the communication burden and are also vulnerable to single-point-failures [13]. As a consequence, distributed secondary control architectures are being increasingly proposed for this task [13, 25, 32, 36, 37, 51, 64]. Most distributed controllers only need a sparsely connected communication network for their operation. The sparsity of the communication network stems from the fact that each unit in the network has to communicate only with its neighbors [56], thus avoiding undesired all-to-all and one-to-all communication requirements. Typically, a distributed secondary frequency controller is implemented by means of *consensus-based* algorithms, see e.g., [13, 25, 32, 36, 37, 51, 64].

[2] Unless confusion arises, a *grid-forming inverter* is denoted simply as an *inverter* in the rest of this work.

There are various important aspects to be considered while designing a distributed control law for a networked system like a microgrid, e.g. communication delay [36, 65, 66] and denial-of-service (DoS) [67, 68]. Also, finding an optimal communication topology for the satisfactory operation of a distributed controller is also of great practical relevance [64–66, 69]. Irrespective of such aspects, the main advantage of using a distributed control approach in a microgrid is that it obviates the requirement for a central communication unit, thus improving system reliability and robustness towards single-point-failures [13]. Hence, *secondary frequency control* discussed in this thesis considers *distributed* control solutions and investigates their performance towards a non-negligible parameter uncertainty usually observed in microgrids, that is explained concisely in the following.

1.3.2.1 Performance in the presence of clock drifts

An inverter-based microgrid involves distributed computation, carried out at the digital-controller of each grid-forming inverter. It is a well-known fact that the clocks used to generate time signals of these digital-controllers are not synchronized [41, 42]. This results in *clock drifts* between the inverters. In microgrids, clock drifts create frequency mismatches and disturb steady-state active power sharing [43, 58]. In the context of distributed secondary frequency control, approaches presented in the literature often neglect the effect of clock drifts, see, e.g. [13, 32, 36, 51, 64]. However, recently it has been highlighted that clock drifts have an adverse effect on the performance of secondary frequency control [44–48]. For example, in [70], the detrimental effect of clock drifts on distributed averaging integral (DAI) control presented in [32, 51] has been investigated. It has been shown that the DAI controller is unable to properly achieve usual secondary frequency control objectives in the presence of clock drifts. In [48], a comparative study comprising droop-only, droop-free and various consensus-based distributed control approaches in the presence of clock drifts has been presented. The authors conclude that all the approaches studied in [48] exhibit problems in achieving secondary frequency control objectives in the presence of clock drifts.

In [44], steady-state and transient performance of various decentralized secondary frequency controllers in the presence of clock drifts has been compared. In a similar spirit, in [45], a decentralized secondary control approach has been studied and robustness of this approach towards clock drifts under high load conditions are evaluated experimentally. Although decentralized secondary controllers avoid the requirement of communication, they have the disadvantage that they exhibit inefficient allocation of generation resources and suffer from poor robustness to measurement bias [57]. In contrast to that, a droop-free controller that requires neighboring node communication has been studied in [46]

considering the effect of clock drifts. However, the comparative study presented in [48] shows that the aforementioned droop-free approach under-performs in terms of active power sharing in the presence of clock drifts.

In [47], a consensus-based distributed frequency controller has been studied, where the authors confirm experimentally, that clock drifts induce power sharing errors and frequency deviations. However, the approach investigated in [47] requires that each inverter has to communicate with all other inverters connected in the microgrid. In practice, such an all-to-all communication is undesirable. In a slightly different setting, a consensus-based power control law has been designed in [71] on top of a primary angle droop[3] control layer. The approach presented in [71] is able to achieve frequency consensus and active power sharing at steady-state. Recently, a modified frequency droop control scheme to address power sharing issues in the presence of clock drifts has been presented in [73]. Nonetheless, the approaches proposed in [71, 73] have not yet considered the mandatory secondary frequency control objective of network frequency restoration.

A possible remedy to alleviate the impact of clock drifts is to use a global time synchronization strategy, e.g., [63], where a central unit communicates a global time signal to all the generation units. Again, such a central set up increases communication burden and is prone to single-point-failures. Another interesting option is to use clock synchronization protocols applied in sensor networks, see e.g. [74, 75]. Yet, when it comes to microgrids, for implementing these clock synchronization protocols, an additional clock synchronization control has to be designed and should–probably–be activated before primary and secondary controls are enabled. Adding such an additional control layer would increase the overall complexity of the hierarchical control architecture employed in microgrids [63].

1.3.3 Distributed voltage control

In contrast to primary frequency droop control, the use of primary *voltage droop control* [38] is often not the most preferred solution in microgrids with inductive lines, see e.g. [24, 27, 30, 32]. This can be explained as follows.

In microgrids with inductive lines, voltage droop control [38] yields a proportional relation between the voltage amplitude and the reactive power flow at each inverter. Thereby, even a small mismatch in voltage set points together with the low resistance to inductive reactance (R/X) ratio of the power lines, resulting in

[3] In an angle droop controller, the voltage phase angle of a grid forming inverter is calculated in proportion to the power injected [72].

undesired circulating reactive currents [24]. A detailed investigation regarding poor reactive power sharing in lossless microgrids operated with voltage droop control can be found in [32]. Thus in the sequel, some relevant works from the literature to address accurate proportional reactive power sharing, and additionally, load voltage regulation in a lossless microgrid with parallel-connected inverters is reviewed.

1.3.3.1 Distributed voltage control in parallel microgrids

For improving system redundancy and reliability needed by a critical load, a common practice in some microgrid applications is to connect inverter-interfaced RESs and storage units in parallel to the point of common coupling (PCC) where the load is connected. Such a network is commonly termed as a *parallel microgrid*, see e.g. [34, 35, 38, 76, 77]. Some practical examples of parallel microgrids are battery power plants (also known as energy storage systems (ESSs)) and distributed uninterruptible power supply (UPS) systems [38, 76, 77]. Similar to an islanded microgrid, the issue of power balance and network stability is of tremendous importance in a parallel microgrid.

As mentioned earlier, maintaining all the bus voltage amplitudes within a certain limit is an important control objective in any power network. In a parallel microgrid, the most critical voltage amplitude is at the PCC since there is no generation unit present at that node. Hence, to restore the voltage at the PCC to the nominal value, DGs connected in the microgrid should be controlled accordingly [34, 35, 38]. On the other hand, in a parallel microgrid with inductive power lines, it is also of high relevance to share the reactive power demand of the load proportionally between the DGs [34, 35, 76–81].

The problem of power sharing in parallel microgrids has been investigated in [38, 77–80, 82] using proportional droop control. In [81], a proportional-integral (PI)-based distributed controller has been proposed to address power sharing. In [34, 35], together with power sharing, the objective of PCC voltage regulation also has been addressed using a PI controller. The aforementioned approaches assume that there exists a unique stable operating point. Stability analysis with two droop-controlled inverters connected in parallel has been presented in [83], where the authors linearize the power flow equations at a particular operating point. In contrast to that, a decentralized quadratic voltage droop controller has been proposed in [24] to ensure voltage stability in lossless microgrids. However, accurate proportional reactive power sharing cannot be guaranteed without risking voltage stability [27, 30].

1.4 Publications

A major share of this thesis is based on the following publications, to all of which the author of the present work has made significant contributions.

- A. Krishna, C. A. Hans, J. Schiffer, J. Raisch, and T. Kral. **Steady state evaluation of distributed secondary frequency control strategies for microgrids in the presence of clock drifts.** In *Mediterranean Conference on Control and Automation (MED)*, pages 508-515, Valetta, Malta, 2017.
- A. Krishna, J. Schiffer and J. Raisch. **A Consensus-Based Control Law for Accurate Frequency Restoration and Power Sharing in Microgrids in the Presence of Clock Drifts.** In *European Control Conference*, pages 2575-2580, Limassol, Cyprus, 2018.
- A. Krishna, J. Schiffer and J. Raisch. **Distributed Secondary Frequency Control in Microgrids: Robustness and Steady-State Performance in the Presence of Clock Drifts.** Accepted for publication at *European Journal of Control*.
- A. Krishna, J. Schiffer, N. Monshizadeh, and J. Raisch **A consensus-based voltage control for reactive power sharing and PCC voltage regulation in microgrids with parallel-connected inverters.** In *European Control Conference*, Naples, Italy, 2019.

Chapter 2

Preliminaries

This chapter describes the notations and preliminaries used in this thesis. At first, the employed mathematical terminology is presented. Later, preliminaries about control theory, algebraic graph theory, and power systems needed in this thesis are outlined.

2.1 Notation

Throughout this thesis, the identity matrix of size $n \times n$ is denoted by I_n, the vector of all-ones as $\mathbb{1}_n \in \mathbb{R}^n$ and the vector of all-zeros as $\mathbb{0}_n \in \mathbb{R}^n$. The matrix of all ones (also called the all-ones-matrix [84]) is denoted by $\mathbb{1}_{n\times n} \in \mathbb{R}^{n\times n}$ unless specifically denoted as $\mathbb{1}_n\mathbb{1}_n^\top$. A matrix of all zeros is denoted by $\mathbb{0}_{n\times m} \in \mathbb{R}^{n\times m}$. An $n \times n$ diagonal matrix with entries a_j, $j = 1,\ldots,n$ is denoted by $\mathrm{diag}(a_j)$. The maximum eigenvalue of a square symmetric matrix F is denoted by $\lambda_{\max}(F)$ and the trace of F as $\mathrm{trace}(F)$. The elements below the diagonal of F are denoted by $*$. If F is positive (negative) definite, then it is denoted by $F > 0$ ($F < 0$). Similarly, if F is positive (negative) semidefinite, $F \geq 0$ ($F \leq 0$). Moreover, $A > B$ means that $A - B > 0$.

Let $x = \mathrm{col}(x_i)$ represent a column vector with entries x_i. Then, $[x]$ denotes a diagonal matrix with diagonal entries x_i. Moreover, $X = \mathrm{blockdiag}(X_i)$ denotes a block-diagonal matrix with matrix entries $X_i \in \mathbb{R}^{n_i\times n_i}$. For a function $f(x) : \mathbb{R}^n \to \mathbb{R}$, $\nabla_x f$ denotes the gradient of $f(x)$ with respect to $x \in \mathbb{R}^n$. Finally, $\|\cdot\|_2$ denotes the Euclidean norm and $|\mathscr{U}|$ represents the cardinality of a set $\mathscr{U}$.

2.2 Control theory basics

In this section some standard control theory concepts are surveyed. After recalling the definition of a dynamical system, the notion of stability is introduced. Later, the classical Lyapunov stability results are recalled. These control theory basics are based on [49, 50]. Hence, for the proofs of the theorems presented in this section, the reader is referred to [49, 50].

The class of systems relevant in the context of this thesis are dynamical systems in the form of an ordinary differential equation (ODE) given by [49, 50]

$$\dot{x} = f(x(t)), \tag{2.2.1}$$

where $x(t) : [t_0, \infty) \to \mathbb{R}^n$, $f : \mathbb{R}^n \to \mathbb{R}^n$ is a locally Lipschitz function and $t_0 \in \mathbb{R}$ is the initial time.

2.2.1 Lyapunov stability

Lyapunov stability is a standard tool in control theory to study stability of the equilibrium point of systems of the form (2.2.1). This is formalized in the definition below.

Definition 2.2.1. *[49, Definition 3.1] Consider the system* (2.2.1)*. Let f be a locally Lipschitz continuous function defined over the domain $D \in \mathbb{R}^n$, which contains the origin, and $f(\mathbb{0}_n) = \mathbb{0}_n$. The equilibrium point $x = \mathbb{0}_n$ of the system* (2.2.1) *is*

1. *stable if for each $\epsilon > 0$, there is $\delta = \delta(\epsilon) > 0$ such that*

$$\|x(0)\| < \delta \Rightarrow \|x(t)\| < \epsilon, \forall\, t \geq 0,$$

2. *unstable, if not stable,*

3. *asymptotically stable, if it is stable and δ can be chosen such that*

$$\|x(0)\| < \delta \Rightarrow \lim_{t \to \infty} x(t) = 0.$$

The notion of Lyapunov's stability is formalized in the theorem below.

Theorem 2.2.2. *[49, Theorem 3.3] Consider the system* (2.2.1)*. Let f be a locally Lipschitz continuous function defined over the domain $D \in \mathbb{R}^n$, which contains the*

origin, and $f(\mathbb{0}_n) = \mathbb{0}_n$. *Let* $V(x)$ *be a continuously differentiable function defined over* D *such that*

$$V(\mathbb{0}_n) = 0 \quad \textit{and} \quad V(x) > 0 \quad \forall x \in D \setminus \{\mathbb{0}_n\}, \tag{2.2.2}$$

$$\dot{V}(x) \leq 0 \quad \forall x \in D, \tag{2.2.3}$$

then $x = \mathbb{0}_n$ *is a stable equilibrium point of the system* (2.2.1). *Moreover, if*

$$\dot{V}(x) < 0 \quad \forall x \in D \setminus \{\mathbb{0}_n\}, \tag{2.2.4}$$

then $x = \mathbb{0}_n$ *is asymptotically stable. Furthermore, if* $D = \mathbb{R}^n$, (2.2.2) *and* (2.2.4) *hold for all* $x \neq \mathbb{0}_n$, *and*

$$\|x\| \to \infty \Rightarrow V(x) \to \infty, \tag{2.2.5}$$

then $x = \mathbb{0}_n$ *is globally asymptotically stable.*

2.3 Graph theory and consensus protocols

Graph theory concepts [53–55] are used to describe the communication network required to implement the distributed control strategies presented in this thesis. At first, some preliminary results from algebraic graph theory are recalled in Section 2.3.1. Later in Section 2.3.2, some basic concepts about consensus protocols are introduced.

2.3.1 Algebraic graph theory

A weighted undirected graph of order $n > 1$ is a triple $\mathcal{G} = (\mathcal{N}, \mathcal{E}, \mathcal{W})$ with set of vertices $\mathcal{N} = \{1, \ldots, n\}$. The set of edges is denoted by $\mathcal{E} \subseteq [\mathcal{N}]^2$, $\mathcal{E} = \{e_1, \ldots, e_s\}$ where $s = |\mathcal{E}|$ and $[\mathcal{N}]^2$ represents the set of all two-element subsets of $\mathcal{N}$. Furthermore, $\mathcal{W} : \mathcal{E} \to \mathbb{R}_{>0}$ is a weight function. By assigning a random orientation to the edges, the incidence matrix $\mathcal{B} \in \mathbb{R}^{n \times s}$ can be defined element-wise as $h_{jl} = 1$ if node j is the source of the l-th edge e_l, $h_{jl} = -1$ if node j is the sink of the l-th edge e_l and $h_{jl} = 0$ otherwise. Let $\mathbf{W} = \operatorname{diag}(w_l) \in \mathbb{R}^{s \times s}$ be the edge-weight matrix where $w_l > 0$ is the weight of the l-th edge, $l \in \{1, \ldots, s\}$. The entries of the adjacency matrix $\mathcal{A} \in \mathbb{R}^{n \times n}$ of $\mathcal{G}$ are $a_{ij} = a_{ji} = w_l > 0$ if $\{i, j\} \in \mathcal{E}$ and $a_{ij} = a_{ji} = 0$ otherwise. The set of neighboring nodes of node i is given by $\mathcal{N}_i = \{j \in \mathcal{N} \mid a_{ij} \neq 0\}$. Then, the diagonal degree matrix $\mathcal{D} \in \mathbb{R}^{n \times n}$ is given by $\mathcal{D} = \operatorname{diag}\big(\sum_{j \in \mathcal{N}_i} a_{ij}\big)$. In addition, the Laplacian matrix $\mathcal{L} \in \mathbb{R}^{n \times n}$ of the undirected weighted graph $\mathcal{G}$ is given by $\mathcal{L} = \mathcal{B}\mathbf{W}\mathcal{B}^\top = \mathcal{D} - \mathcal{A}$.

A path is an ordered sequence of nodes such that any pair of consecutive nodes in the sequence is connected by an edge. The graph $\mathcal{G}$ is called connected if there exists a path between every pair of distinct nodes. The matrix $\mathcal{L}$ has a simple zero eigenvalue if and only if $\mathcal{G}$ is connected. A corresponding right eigenvector is $\mathbb{1}_n$, i.e., $\mathcal{L}\mathbb{1}_n = \mathbb{0}_n$, yielding $\mathcal{L} \geq 0$.

2.3.2 Consensus protocols

The use of consensus protocols to address control objectives in multi-agent networked systems have become increasingly popular in the past few decades, see, e.g. [56, 85–88]. The term *consensus* means that a group of agents in a networked system reach an agreement on a common value by negotiating with their neighbors [56]. The interaction rule to achieve this agreement is typically called as *consensus protocol* or *consensus algorithm* [56]. A remarkable advantage of consensus protocols is that, in general, they are distributed in nature. Therefore to reach an agreement among agents, neither an all-to-all communication network nor a central communication setup are required.

Consider an undirected connected weighted graph $\mathcal{G} = (\mathcal{N}, \mathcal{E}, \mathcal{W})$ where $\mathcal{N}, \mathcal{E}$ and $\mathcal{W}$ are defined in Section 2.3.1. A simple consensus protocol which guarantees convergence to a common value can be represented as [56]

$$\dot{x}_i = \sum_{i \in \mathcal{N}_i} a_{ij}(x_j - x_i), i \in \mathcal{N}, j \in \mathcal{N}_i, \tag{2.3.1}$$

where x_i is the information state of the i-th agent, a_{ij} is the (i, j)-th entry of the adjacency matrix $\mathcal{A}$ of graph $\mathcal{G}$ and $\mathcal{N}_i$ is the set of neighboring nodes connected to agent i. The consensus protocol (2.3.1) for the whole network can be written as

$$\dot{x} = -\mathcal{L}x, \tag{2.3.2}$$

where $x = \text{col}(x_i) \in \mathbb{R}^n$ is the information state vector and $\mathcal{L}$ is the Laplacian matrix of the graph $\mathcal{G}$. The dynamics (2.3.2) at steady-state can be expressed as

$$\mathbb{0}_n = \mathcal{L}x^s, \tag{2.3.3}$$

where the super script s denotes the steady-state value. Under the assumption that $\mathcal{G}$ is connected, 0 is a simple eigenvalue of $\mathcal{L}$ with a corresponding right eigenvector $\mathbb{1}_n$. Therefore,

$$\mathcal{L}x^s = \mathbb{0}_n \Leftrightarrow x^s = \alpha\mathbb{1}_n, \quad \alpha \in \mathbb{R}. \tag{2.3.4}$$

Let $x(0) \in \mathbb{R}^n$ be the initial condition of of $x(t)$. Then [56]

$$\alpha = \frac{1}{|\mathcal{N}|} \sum_{i \in \mathcal{N}} x_i(0).$$

Hence, the systems of the form (2.3.2) are also known as *continuous time distributed averaging* systems [56, 87].

2.4 Power system basics

Following the standard practice in AC power systems, power is typically generated, transmitted, and distributed in the form of three-phase signals [4, 12, 89]. Therefore, the present work focuses on three-phase AC power networks. It is assumed that the three-phase signals considered in this thesis are symmetric [4, 89, 90], see also [23, Section 2.4].

In light of these assumptions, the following sections summarize some power systems preliminaries required throughout the present work. At first, the network model is introduced, and expressions for active and reactive power flows are presented later. Finally, a commonly used network reduction technique used in power networks with constant impedance loads is recalled.

2.4.1 Network model

Power lines in AC networks are typically modeled as the so-called π-model [1, 4, 5, 89], which consists of a series RL (resistance with inductance) element connected in parallel with R and C (resistance and capacitance) shunt-elements. For power networks with short power lines, e.g. microgrids, the shunt-elements can often be neglected [1, 4, 89]. Thus, a power line can be represented as a combination of resistance and inductance connected in series.

As this thesis is devoted to addressing control issues in microgrids with dominantly inductive lines (i.e., lossless lines), the line resistance is neglected. Let $X_{ij} \in \mathbb{R}_{>0}$ be the inductive reactance of a power line connecting two buses, say $i \in \mathcal{N}$ and $j \in \mathcal{N}$. Then,

$$X_{ij} = \omega L_{ij} \in \mathbb{R}_{>0},$$

where $\omega \in \mathbb{R}_{>0}$ denotes a frequency and $L_{ij} \in \mathbb{R}_{>0}$ is the inductance of the power line connecting bus i and bus j. The susceptance $B_{ij} \in \mathbb{R}_{<0}$ of the power line connecting bus i and bus j is then given by

$$B_{ij} = \frac{-1}{X_{ij}} \quad \in \mathbb{R}_{<0}. \tag{2.4.1}$$

The dynamics of the power lines are assumed to be negligible [1, 3]. Thereby, it is essential to note that a power line connecting bus i and bus j is denoted by (2.4.1) in the rest of this thesis.

2.4.2 Power flow

Consider a two-bus system, as shown in Figure 2.1. Let $V_1 : \mathbb{R}_{\geq 0} \to \mathbb{R}_{>0}$ and $V_2 : \mathbb{R}_{\geq 0} \to \mathbb{R}_{>0}$ be the voltage amplitudes at node 1 and node 2, respectively. Furthermore, let $\delta_1 : \mathbb{R}_{\geq 0} \to \mathbb{T}$ and $\delta_2 : \mathbb{R}_{\geq 0} \to \mathbb{T}$, respectively, be the phase angles at node 1 and 2. Then, the active and reactive power flows at node 1 are given respectively, by [5, Chapter 3] [1, Chapter 6]

$$\begin{aligned} P_1(V_1, V_2, \delta_1, \delta_2) &= |B_{12}| V_1(t) V_2(t) \sin(\delta_1(t) - \delta_2(t)), \\ Q_1(V_1, V_2, \delta_1, \delta_2) &= |B_{12}| V_1^2(t) - |B_{12}| V_1(t) V_2(t) \cos(\delta_1(t) - \delta_2(t)). \end{aligned} \tag{2.4.2}$$

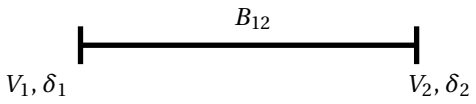

Figure 2.1. Schematic representation of a purely inductive power line connecting two buses.

Similar to a two-bus system, now let there be $n > 2$ nodes connected arbitrarily. The set of network nodes is denoted by $\mathcal{N} = \{1, ..., n\}$. Furthermore, the electrical network is assumed to be connected and the set of neighboring nodes of the i-th node is denoted by $\mathcal{N}_i = \{k \in \mathcal{N} \mid B_{ik} \neq 0\}$ where $B_{ik} \in \mathbb{R}_{<0}$ is the susceptance of the power line connecting node i and node k. The phase angle and voltage magnitude at each bus $i \in \mathcal{N}$ are denoted by $\delta_i : \mathbb{R}_{\geq 0} \to \mathbb{T}$, respectively $V_i : \mathbb{R}_{\geq 0} \to \mathbb{R}_{>0}$. Let $P_i : \mathbb{T}^n \times \mathbb{R}_{>0}^n \to \mathbb{R}$ and $Q_i : \mathbb{T}^n \times \mathbb{R}_{>0}^n \to \mathbb{R}$ represent the active and reactive power power injections at node i, respectively.

Then, the active and reactive power flows at node i are given respectively, by [1, 5]

$$P_i(\delta_1, \ldots, \delta_n, V_1, \ldots, V_n) = \sum_{k \in \mathcal{N}_i} |B_{ik}| V_i(t) V_k(t) \sin(\delta_i(t) - \delta_k(t)), \tag{2.4.3}$$

$$Q_i(\delta_1, \ldots, \delta_n, V_1, \ldots, V_n) = \sum_{k \in \mathcal{N}_i} |B_{ik}| V_i^2(t) - |B_{ik}| V_i(t) V_k(t) \cos(\delta_i - \delta_k). \tag{2.4.4}$$

2.4.3 Kron reduction

In general, a power network contains different kinds of buses where not only generators but also various types of loads are connected. Hence, writing down the system equations for such a network yields a set of differential algebraic equations (DAEs). If the loads connected in the network are constant impedance

loads, then using a commonly employed network reduction technique, termed as *Kron reduction*, such a system of DAEs can be represented as pure ordinary differential equations (ODEs) [1, 91]. In a Kron-reduced network, all the buses have a generator and a shunt admittance connected to them [1, 91].

For a Kron-reduced power network with inductive lines, active and reactive power flows at node i are given respectively by [1]

$$\begin{aligned} P_i(\delta_1,\ldots,\delta_n,V_1,\ldots,V_n) &= G_{ii}V_i^2(t) + \sum_{k\in\mathcal{N}_i}|B_{ik}|V_i(t)V_k(t)\sin(\delta_i(t)-\delta_k(t)),\\ Q_i(\delta_1,\ldots,\delta_n,V_1,\ldots,V_n) &= |B_{ii}|V_i^2(t) - \sum_{k\in\mathcal{N}_i}|B_{ik}|V_i(t)V_k(t)\cos(\delta_i(t)-\delta_k(t)), \end{aligned} \tag{2.4.5}$$

where $G_{ii}\in\mathbb{R}_{>0}$ is the shunt conductance and $B_{ii} = \bar{B}_{ii} + \sum_{k=1,k\neq i}^{n} B_{ik}$, where $\bar{B}_{ii}\in\mathbb{R}_{<0}$ is the shunt susceptance. In the sequel, the dependence of voltages and phase angles on time will not be displayed unless confusion arises.

2.5 Summary

In this chapter, the mathematical notation and preliminaries required for presenting the results in this thesis have been outlined. At first, the notation employed throughout this thesis has been introduced. Later some control theory basics and graph theory results have been recalled. Finally, some important power system basics, which are used extensively in this thesis, have been introduced.

Chapter 3

Problem statement

3.1 Introduction

As discussed in Chapter 1, the increasing integration of RESs into the modern power grid brings in various operational challenges. A possible remedy to tackle these challenges is to consider the whole grid as a set of locally controllable smaller networks, called *microgrids* [8, 17]. In this chapter, the concept of microgrid is introduced, and some exciting features are highlighted. Subsequently, control challenges in operating an islanded microgrid are recalled and, the hierarchical control architecture [63] advocated to address these challenges is discussed. Afterward, the common operating modes of inverters connected in a microgrid are described. Finally, based on the discussion thus far, control problems addressed in this thesis are precisely formulated.

3.2 Microgrids

To facilitate RES-integration, the concept of microgrids has been studied with increasing interest, both by the research community and by the industry [17–19, 23, 92, 93]. The concept of a microgrid is defined as below.

Definition 3.2.1. *[10, 17, 18, 23] An AC electrical network can be called an AC microgrid if the following conditions are satisfied.*

1. *It works as a connected subset of a low or medium voltage distribution system of an AC power network.*
2. *It has a single point of connection to the main power grid, which is called the point of common coupling (PCC).*

3. *It is a network consisting of generation units, loads and energy storage elements.*

4. *It can autonomously supply most of its loads using its own generation and storage units at least for some time.*

5. *It can work either connected to the main grid or disconnected from it. The former is called grid-tied or grid-connected mode, and the latter is called islanded or autonomous or stand-alone mode.*

6. *In grid-connected mode, it behaves as a single controllable generator or load with respect to the main grid.*

7. *In islanded mode, frequency, voltage, and power are actively controlled within the microgrid.*

Another concise definition of a microgrid that incorporates the points mentioned in Definition 3.2.1 is given below.

Definition 3.2.2. *[94] A microgrid is defined as a group of distributed generators, including RESs, ESSs, and loads, that operate together locally as a single controllable entity. Microgrids exist in various sizes and configurations; they can be large and complex networks with various generation resources and storage units serving multiple loads, or small and simple systems supplying a single customer.*

As per Definition 3.2.1 and Definition 3.2.2, the main components of a microgrid are RESs, loads and storage units. Predominantly, photovoltaic (PV) units, wind turbines, fuel cells, and conventional synchronous generators constitute the set of power generation units. Similar to conventional power systems, loads connected in a microgrid can be classified into residential, industrial, and commercial loads [10, 95]. Furthermore, the storage units play an important role in balancing the intermittent nature of power demand and supply [95, 96], thus actively contributing to network control tasks. Usually, storage units are batteries, flywheels or supercapacitors. A picture of an inverter-based microgrid is given in Figure 3.1.

In essence, the concept of microgrids facilitates various advantages to modern power systems. Some are listed below [10, 23, 38, 63].

1. The power quality can be significantly improved since the frequency and voltage are controlled locally.

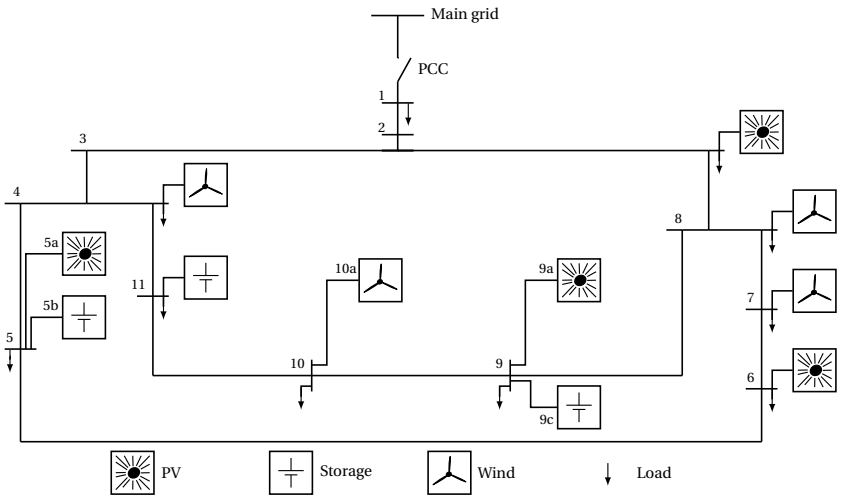

Figure 3.1. Pictorial representation of an inverter-based microgrid with various types of distributed generators, storage units and loads.

2. Losses are reduced due to localized power generation and consumption.

3. Similar to an islanded power system, an islanded microgrid also can provide reliable power supply during emergencies [1].

4. Clustering a huge power network into microgrids is essentially breaking down a bigger problem into smaller tasks, thereby reducing the complexity of the overall control problem.

3.2.1 Challenges in microgrids

As briefly mentioned in Chapter 1, in contrast to conventional power systems, a microgrid contains a large number of inverter-interfaced RESs. The physical characteristics of inverters differ from that of conventional generators [3, 16, 17]. Moreover, RESs are intermittent, heterogeneous, and small-sized (i.e., the power capacity is low). Hence, for stable and reliable operation of a low-inertia power network [26, 97, 98] like a microgrid, intelligent control techniques have to be employed [24, 26, 27, 32, 43].

According to Definition 3.2.1 and Definition 3.2.2, a microgrid can operate in islanded or grid-connected mode. In grid-connected mode, the utility grid can support the microgrid for control actions and power demand. However, in islanded mode, control capabilities have to be provided by the units connected

[1] In contrast to islanded power systems, islanded microgrids are composed mainly of RESs and ESSs.

within the microgrid [23]. Another crucial challenge in islanded power networks is that the system stability is negatively affected in the presence of a noticeable change in generation or load [99]. Therefore, this thesis focuses on *control of islanded inverter-based microgrids*.

3.2.2 Major control tasks in microgrids

As outlined briefly in Chapter 1, some important control tasks in an islanded microgrid are listed below.

1. Frequency stability [22, 62],
2. Voltage stability [24, 27, 100],
3. Network frequency restoration [13, 32, 36, 37, 51],
4. Voltage regulation at load bus [34, 35],
5. Desired power sharing [22, 23, 27, 62],
6. Optimal dispatch of resources [26, 61].

3.2.3 Hierarchical control architecture

Inspired by the conventional power systems, a hierarchical control structure [39, 40, 60, 63] is advocated to tackle control problems in an islanded microgrid. This control structure has three layers, namely

1. *Primary control* [22, 38, 62]: A decentralized proportional (droop) control; maintain frequency stability; achieve desired power sharing at steady-state.
2. *Secondary control* [13, 32, 37]: Usually a distributed integral control; correct steady-state deviations in network frequency.
3. *Tertiary control or energy management* [26, 61, 101]: Optimal dispatch of generation, storage and loads.

3.2.4 Class of microgrids studied in this work

Microgrids studied in this thesis are assumed to have purely inverter-based units (both RESs and storage units) as the power sources and dominantly inductive power lines (commonly known as *lossless power lines*.). Focusing on *inverter-based* microgrids can be justified due to the presence of a large number of distributed inverter-interfaced RESs present in a microgrid [8, 10], see also [24, 27].

The assumption of *lossless* power lines is explained below. Power lines in microgrids are relatively short because of closer electrical proximity between generators and loads. Furthermore, due to the lower power capacity of inverter-interfaced units, they are interfaced with each other through MV or LV networks. The line impedances of these networks are not purely inductive but have a non-negligible resistive part. Nevertheless, due to the presence of an output inductor and/or the possible presence of an output transformer, inverter output impedance is typically inductive [24, 27, 76]. Thus, the inductive parts dominate the resistive parts resulting in low resistance to inductive reactance (R/X) ratio.

In light of the above discussion, the class of microgrids considered in this thesis is solely *inverter-based lossless islanded microgrids*. Unless stated otherwise, such networks are simply referred to as *microgrids* from here on.

3.2.5 Inverter-interfaced units in a microgrid

The physical characteristics of inverters used in interfacing RESs to the AC grid widely differ from that of conventional generators [3, 102]. In conventional power grids, the task of network stabilization primarily depends on the rotational inertia and the synchronizing dynamics of synchronous machines [3]. However, in an inverter-based microgrid, inverters connected in the network are responsible for maintaining a stable operating point [15, 17]. In the sequel, a brief introduction to inverter models and the two operating modes in which an inverter can be operated are presented.

The output of RESs are mostly DC or variable frequency AC signals [103, 104]. Hence to integrate RESs into an AC network that operates at a frequency of 50 or 60 Hz, inverters are employed. The main components of an inverter are power semiconductor devices [102, 105]. The quality of the output AC signal, e.g., in terms of harmonic rejection, of an inverter-interfaced RES can be improved with the help of an output low pass filter with *RLC* elements[2].

[2] For further details about hardware design and inner control loops of an inverter, the reader is referred to [102, 105].

3.2.5.1 Common operating modes of an inverter

In general, there are two main operation modes for an inverter connected in a microgrid [14–16, 106, 107]:

1. Grid-forming mode[3]: In this mode, an inverter works with pre-defined voltage and frequency values, usually provided by the designer [15]. A grid-forming inverter can emulate a conventional generator's behavior, thus enabling voltage and frequency control in a microgrid [38].

2. Grid-feeding mode[4] : The inverter works as a power source, i.e., it supplies a pre-specified amount of active and reactive power. A higher-level control layer generally specifies the power injection set points of a grid-feeding inverter, see e.g. [61].

A grid-forming inverter can be represented as an ideal voltage source, and hence has a low-output impedance [14]. Therefore, it needs an extremely precise synchronization mechanism to operate it in parallel with other grid-forming inverters [14, 108]. Later in this thesis, the problem of synchronizing grid-forming inverters in the presence of clock drifts [43, 58] is investigated in detail. In industrial applications, grid-forming inverters are fed by constant DC voltage sources like batteries or flywheels [14].

Inverters operating in grid-feeding mode are usually controllable current sources and thus have a high parallel output impedance. As a consequence, they are suitable to operate in parallel with other grid-feeding inverters [14]. In practice, almost all inverter-interfaced RESs, such as PV or wind plants, are operated in grid-feeding mode [14, 107]. However, in the absence of grid-forming inverters, grid-feeding inverters cannot operate in an islanded microgrid. This is because grid-forming inverters are responsible for setting voltage levels and frequency in a microgrid [14]. A thorough investigation in the direction of *inverter modeling in microgrids* can be found in [23, Section 4.2].

From the above discussion, it is clear that grid-forming inverters are essential components in islanded inverter-based microgrids. In other words, similar to a conventional power network with synchronous generators, grid-forming capabilities in an inverter-based islanded microgrid are provided by grid-forming inverters [15, 19].

[3] Also referred as voltage source inverter (VSI) control [15].

[4] This mode is also called as PQ control or grid-following mode [15, 19].

3.3 Control objectives

This section formulates the control problems focused on in this thesis, starting with the required definitions.

The following definitions are required throughout this thesis.

Definition 3.3.1 (Accurate proportional active power sharing [22, 26, 27])**.** *Let $\mathscr{X}_i \in \mathbb{R}_{>0}$ denote a constant weighting factor, P_i^s the steady-state active power flow and P_i^d the desired active power set point at the i-th inverter, $i \in \mathscr{N}$. Then, two inverters, say inverter i and j, $j \in \mathscr{N}$, $j \neq i$, are said to share their active power flows accurately in proportion to $\mathscr{X}_i$ and $\mathscr{X}_j$ if*

$$\mathscr{X}_i(P_i^s - P_i^d) = \mathscr{X}_j(P_j^s - P_j^d). \tag{3.3.1}$$

Definition 3.3.2 (Accurate proportional reactive power sharing [22, 26, 27])**.** *Let $a_i \in \mathbb{R}_{>0}$ denote a constant weighting factor, Q_i^s the steady-state reactive power flow and Q_i^d the desired reactive power set point at the i-th inverter, $i \in \mathscr{N}$. Then, two inverters, say inverter i and j, $j \in \mathscr{N}$, $j \neq i$, are said to share their reactive power flows accurately in proportion to a_i and a_j if*

$$a_i(Q_i^s - Q_i^d) = a_j(Q_j^s - Q_j^d). \tag{3.3.2}$$

The parameters $\mathscr{X}_i$ and a_i are usually specified by the designer. A common choice would be to select $\mathscr{X}_i = a_i = 1/S_i^N$ where S_i^N is the nominal power rating (apparent power) of the i-th unit. Hence, achieving (3.3.1) and (3.3.2) ensure that the loads connected in the microgrid are shared among the generation units fairly, i.e., in proportion to their power ratings.

Definition 3.3.3 (Accurate network frequency restoration [13, 32, 37])**.** *Let $\omega^* \in \mathbb{R}_{>0}$ be the steady-state network frequency and $\omega^d \in \mathbb{R}_{>0}$ be the desired nominal frequency in a microgrid. Then, accurate frequency restoration means that*

$$\omega^* = \omega^d. \tag{3.3.3}$$

Definition 3.3.4 (PCC voltage restoration [34, 35])**.** *Let $V_{PCC} : \mathbb{R}_{\geq 0} \to \mathbb{R}_{>0}$ be the voltage amplitude at the PCC and $V_{PCC}^d \in \mathbb{R}_{>0}$ be the desired nominal voltage amplitude required at the PCC. Then, the objective of PCC voltage restoration is satisfied if*

$$V_{PCC}(t) \to V_{PCC}^d \quad as \quad t \to \infty. \tag{3.3.4}$$

3.3.1 Distributed secondary frequency control

This section explains in detail the motivation to focus on the two control objectives given by Definition 3.3.1 and Definition 3.3.3 in the presence of clock drifts.

3.3.1.1 The effect of clock drifts

Clock drifts are a non-negligible parameter uncertainty observed in inverter-based microgrids [43, 58]. Apart from sensor uncertainties, the presence of clock drifts are the main reason why grid-forming inverters fed with a fixed electrical frequency cannot operate in parallel [14, 43, 58, 108]. In [43, Section III], this problem is analytically investigated. The experimental output shown in [43, Figure 4] verifies that when two grid-forming inverters operate in parallel with a fixed electrical frequency, active power injections of the inverters diverge in the presence of clock drifts. Such an undesired active power divergence can eventually damage the inverters. A possible solution to this issue is to provide a common clock synchronization signal to all the grid-forming inverters [63]. Recall that a microgrid can have a large number of grid-forming inverters connected in it. Thus providing a clock signal to all these inverters would make the communication setup cumbersome.

3.3.1.2 Primary control layer: decentralized proportional control

In lossless microgrids, the *standard frequency droop control* yields a proportional relation between the active power flow and the frequency [38, Equation 13]. It has been shown in [43, 58] that the frequency droop control is robust towards clock drifts. The authors of [43, 58] confirm, both analytically and experimentally, that the frequency droop control alleviates the risk of operating grid-forming inverters in parallel in the presence of clock drifts. The property of robust stability is mainly due to the port Hamiltonian structure [50, 109] of the dynamical system corresponding to a droop-controlled microgrid [22]. Due to this robustness property, there is no need for providing a global clock synchronization signal to any of the inverters operating in a microgrid [43], thereby preserving one of the most important properties of frequency droop control, which is its *decentralized* nature. In light of the above discussion, the standard frequency droop control [38] is employed at the primary control layer throughout this thesis.

Despite the advantages mentioned above, in the presence of clock drifts, frequency droop control generate steady-state errors in active power injections, thereby disturbing the proportional active power sharing provided by the same [43, 58]. Furthermore, frequency droop control results in steady-state deviation in

the network frequency from the desired nominal value whenever there is a power imbalance in the network [63]. Thus, the next section focuses on addressing the problem of accurate proportional active power sharing and network frequency restoration in the presence of clock drifts.

3.3.1.3 Secondary control layer: distributed integral control

The proportional nature of the primary frequency droop control is the main reason for steady-state frequency deviation [63]. This steady-state frequency error is corrected using a secondary controller, which typically is a simple central integral controller [15, 39], where a central computing unit provides a control signal to all the grid-forming inverters connected in the microgrid. Another idea would be to design completely *decentralized* secondary frequency controllers, where at each grid-forming inverter the local frequency error[5] is numerically integrated and is provided to all the grid-forming inverters to regulate the network frequency.

However, a decentralized integral secondary control usually results in poor active power sharing and fails to achieve fast frequency regulation [26, Lemma 4.1]. Like primary droop control, decentralized secondary frequency control is also implemented at the grid-forming inverters connected in the network. Each grid-forming inverter corrects the local frequency error, which–due to the primary droop control–alters the local power injection. Such a change in local power injection, together with the aspect of maintaining overall power balance in the network, results in an enormous and unpredictable burden on the grid-forming inverters [26].

Based on the discussion thus far, *distributed consensus-based integral control* approaches are increasingly advocated to address secondary frequency control in microgrids, see e.g. [32, 37, 40, 51]. Compared to centralized control solutions, distributed control approaches improve system reliability and reduce the communication effort [40]. Besides, compared to decentralized secondary control, distributed secondary controllers achieve frequency regulation and active power sharing in a collective and fair manner, i.e., without putting any generator under undesired high load stress, see e.g., [26, 51, 110]. Nevertheless, since distributed control approaches require a communication network for their operation, there are various challenging aspects to be considered while designing such controllers, e.g., communication delays [36], denial-of-service [67, 68], optimal communication topology [64–66, 69].

[5] Local frequency error denotes the difference between the measured local frequency and the nominal desired frequency value of 50 or 60 Hz.

In addition to the above-mentioned issues, as mentioned in Section 1.3.2.1, the phenomenon of clock drifts is often neglected while designing distributed secondary controllers, see e.g. [13, 32, 36, 51, 64]. However, clock drift has an adverse on the performance of secondary frequency control [44–48]. Therefore, the chapter on *distributed secondary frequency control* presented in this thesis evaluates the robustness and performance of distributed frequency controllers in the presence of clock drifts. More precisely, the focus is to design distributed secondary frequency controllers in the presence of clock-drifts such that asymptotic stability [49, 50] of the closed-loop equilibrium point is guaranteed and, at the same time, the following two steady-state objectives are realized:

1. **Network frequency restoration as per Definition 3.3.3** and
2. **Accurate active power sharing according to Definition 3.3.1**.

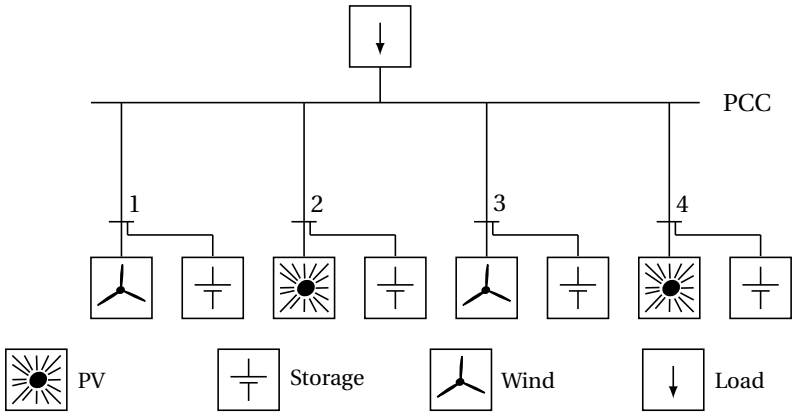

Figure 3.2. Schematic representation of a parallel microgrid with four generator buses and a load bus (PCC).

3.3.2 Distributed voltage control

Similar to primary frequency droop control, a primary *voltage droop control* is often used in microgrids [38]. But, when it comes to lossless microgrids, the use of voltage droop control is not preferred widely [27, 32, 111]. This is mainly because voltage droop control results in poor reactive power sharing in such networks. Further details about the under-performance of voltage droop control are mentioned briefly in Section 1.3.3 and is explained in detail later in this thesis.

As a result, distributed consensus-based voltage controllers to address the problem of accurate reactive power sharing and voltage stability in lossless microgrids

are increasingly used [27, 30]. Inspired by the works in [27, 30], this section focuses on a slightly different application of microgrids, where the generation units are connected in parallel [38]. With voltage stability and reactive power sharing, another important control objective in such a network is to restore the voltage amplitude at the common load bus (PCC) to the nominal value [34, 35].

As described in Section 1.3.3, a small electrical network where inverter-interfaced RESs and storage units are connected in parallel to a common load at the PCC is a typically encountered microgrid application [34, 35, 38, 77–83, 111], see Figure 3.2. Recall that such networks are termed as parallel microgrids. The task of controlling the network frequency and the voltage amplitudes in an inverter-based microgrid is the responsibility of grid-forming inverters, see Section 3.2.5.1. Hence, all the generator buses shown in Figure 3.2 are assumed to have at least one storage unit interfaced via a grid-forming inverter connected to them.

The second part of this thesis is devoted to addressing some practically important control objectives in a parallel microgrid by actively controlling the grid-forming inverters. More precisely, the idea is to design a distributed voltage controller for a lossless islanded parallel microgrid, which at steady-state yields a unique positive voltage solution having the following *desired* properties:

1. **PCC voltage restoration as per Definition 3.3.4**,
2. **Accurate reactive power sharing according to Definition 3.3.2** and
3. **Asymptotic stability in accordance to Definition 2.2.1.**

3.4 Summary

In this chapter, the concept of microgrid has been introduced and the control problems addressed in this work have been formalized. After presenting the definition of a microgrid, some interesting features of the same have been outlined. Later, some major control challenges in a microgrid and the commonly employed hierarchical control architecture have been described. The common operating modes of inverters connected in a microgrid have also been discussed. Finally, the control problems focused on in this thesis have been precisely formulated.

Chapter 4

Microgrid model and primary control

4.1 Introduction

In this chapter, the microgrid models are presented and the standard primary control laws are discussed. Recall that in this thesis, the section on *distributed secondary frequency control* focuses on meshed microgrids, and the section on *distributed voltage control* looks into the control aspects in parallel microgrids.

Nevertheless, both cases are dedicated to microgrids with inverter-based generation units, where grid-forming inverters are the main components responsible for controlling the network. Thus, the considered meshed and parallel microgrids differ only in terms of network and load models. Hence in this chapter, network and load models corresponding to meshed and, respectively parallel microgrids are discussed. Later, the model of a grid-forming inverter is presented. Finally, the primary droop control is described.

4.2 Network and load model: meshed microgrid

The loads connected in the meshed microgrid model is assumed to be constant impedance loads [1]. Thus by using the Kron-reduction technique mentioned in

[1] To the best of the author's knowledge, there is no standard model to represent all types of loads. For instance, constant power loads and dynamic loads [1, 5, 100]. Furthermore, the author of this thesis is aware that not all kinds of loads can be represented as constant impedance loads. Hence, considering different kinds of load models while designing controllers for microgrids is left out for future research, see e.g. [25, 110].

Section 2.4.3, every bus in the network can be represented as a generator bus with a shunt admittance connected to it. Furthermore, the power lines of the network are assumed to be lossless, i.e., inductive power lines. See Section 3.2.4 for a discussion justifying this assumption. In the case of a lossless Kron-reduced microgrid, active and reactive power flows at the i-th node $i \in \mathcal{N}$, has been given in (2.4.5).

4.3 Network and load model: parallel microgrid

In this section, network and load models used to model a lossless parallel microgrid are presented.

4.3.1 Network model

As explained in Section 3.3.2, it is assumed that each generator bus in the considered parallel microgrid has one storage unit interfaced via a grid-forming inverter connected to it; see also Figure 3.2. Therefore, in the context of parallel microgrids, the term *DG* or the word *inverter* represents a grid-forming inverter. Thus, the considered parallel microgrid has $n > 1$ DGs, which are all connected in parallel to the PCC, see Figure 4.1. The set of DGs connected to the PCC is denoted by $\mathcal{N} = \{1, 2, \dots, n\}$. Since the parallel microgrid is also assumed to have inductive lines, a power line connecting the i-th generator bus and the load bus (PCC) is represented by a susceptance $B_i \in \mathbb{R}_{<0}$.

Let $\delta_i : \mathbb{R}_{\geq 0} \to \mathbb{T}$ and $V_i : \mathbb{R}_{\geq 0} \to \mathbb{R}_{>0}$ represent the phase angle and the voltage magnitude at the i-th DGs, respectively. Furthermore, $\delta_{\text{PCC}} : \mathbb{R}_{\geq 0} \to \mathbb{T}$ and $V_{\text{PCC}} : \mathbb{R}_{\geq 0} \to \mathbb{R}_{>0}$, respectively, denote the phase angle and the voltage magnitude at the PCC. Then, based on (2.4.3), (2.4.4), the active and reactive power flows at the i-th DG are given respectively by

$$\begin{aligned} P_i(\delta_i, \delta_{\text{PCC}}, V_i, V_{\text{PCC}}) &= |B_i| V_i V_{\text{PCC}} \sin(\delta_i - \delta_{\text{PCC}}), \\ Q_i(\delta_i, \delta_{\text{PCC}}, V_i, V_{\text{PCC}}) &= |B_i| V_i^2 - |B_i| V_i V_{\text{PCC}} \cos(\delta_i - \delta_{\text{PCC}}). \end{aligned} \tag{4.3.1}$$

4.3.2 Load model

The load connected at the PCC is assumed to be a constant current load[2], represented by $I_L \in \mathbb{R}_{<0}$, see Figure 4.1. This thesis follows the *generator convention* [89], i.e., the injected active and reactive powers are counted positively, while the absorbed active and reactive powers are counted negatively. The load connected

[2] A study of a parallel microgrid with other types of loads, see e.g. [1, 5, 100], is planned as part of future research.

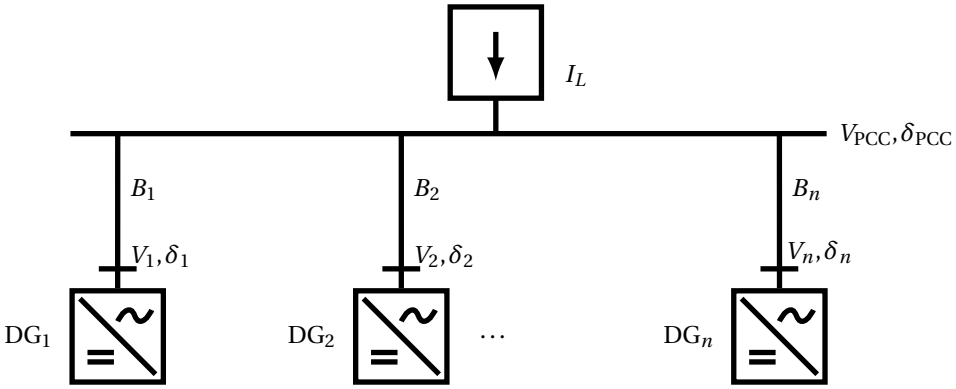

Figure 4.1. A detailed representation of a lossless parallel microgrid with n generators connected in parallel to the PCC. A constant current load I_L is connected at the PCC.

at the PCC in the parallel microgrid is assumed to be *inductive*. In the generator convention, $I_L < 0$ represents an inductive load. In practice, most electrical loads have inductive behavior [1, Chapter 7]. Thus the assumption that $I_L < 0$ is realistic.

By Kirchoff's current law, the current balance at the PCC is given by

$$I_L = \sum_{i=1}^{n} I_{\text{PCCi}}, \tag{4.3.2}$$

where $I_{\text{PCCi}} : \mathbb{R}_{\geq 0} \to \mathbb{R}$ is the current flow from the PCC to the i-th DG, which is given by [23, Section 4.4] [5]

$$I_{\text{PCCi}} = |B_i|(V_{\text{PCC}} - V_i). \tag{4.3.3}$$

By combining (4.3.3) and (4.3.2), it yields that

$$I_L = \sum_{i=1}^{n} |B_i|(V_{\text{PCC}} - V_i) = V_{\text{PCC}} \mathbb{1}_n^\top B \mathbb{1}_n - \mathbb{1}_n^\top B V, \tag{4.3.4}$$

where

$$B = \text{diag}(|B_i|) \in \mathbb{R}^{n \times n}, \tag{4.3.5}$$

and $V = \text{col}(V_i) \in \mathbb{R}^n_{>0}$. Note that the PCC voltage V_{PCC} implicitly depends on the bus voltages V_i. By using the current balance (4.3.4), this relation can be made explicit, i.e.,

$$V_{\text{PCC}}(V) = \frac{I_L + \mathbb{1}_n^\top B V}{\mathbb{1}_n^\top B \mathbb{1}_n}. \tag{4.3.6}$$

4.4 Inverter model

The standard model of a grid-forming inverter connected at the i-th node is given by [15, 23][3]

$$\begin{aligned} \dot{\delta}_i &= u_i^{\delta}, \\ V_i &= u_i^{V}, \end{aligned} \tag{4.4.1}$$

where $u_i^{\delta} : \mathbb{R}_{\geq 0} \to \mathbb{R}$ and $u_i^{V} : \mathbb{R}_{\geq 0} \to \mathbb{R}$ are frequency and voltage control inputs respectively. The inverter model (4.4.1) is used throughout this thesis.

4.5 Primary droop control

In this section, the standard practice of computing u_i^{δ} and u_i^{V} in (4.4.1) are recalled.

The control inputs u_i^{δ} and u_i^{V} in (4.4.1) are typically designed as the conventional primary droop control [38, 63], given by

$$u_i^{\delta} = \omega^d - k_{P_i}(P_i^m - P_i^d), \tag{4.5.1}$$

$$u_i^{V} = V_i^d - k_{Q_i}(Q_i^m - Q_i^d), \tag{4.5.2}$$

where $\omega^d \in \mathbb{R}_{>0}$ is the desired nominal frequency, $V_i^d \in \mathbb{R}_{>0}$ is the desired voltage amplitude, $k_{P_i} \in \mathbb{R}_{>0}$, respectively $k_{Q_i} \in \mathbb{R}_{>0}$ are the frequency, respectively voltage droop coefficients and $P_i^d \in \mathbb{R}$ and $Q_i^d \in \mathbb{R}$ are the desired power set points. Furthermore, $P_i^m : \mathbb{R}_{\geq 0} \to \mathbb{R}$ and $Q_i^m : \mathbb{R}_{\geq 0} \to \mathbb{R}$ are the active and reactive powers measured through a low pass filter with time constant $\tau_i \in \mathbb{R}_{>0}$. The dynamics of the low pass filter is given by [83, 92]

$$\begin{aligned} \tau_i \dot{P}_i^m &= -P_i^m + P_i, \\ \tau_i \dot{Q}_i^m &= -Q_i^m + Q_i, \end{aligned} \tag{4.5.3}$$

where P_i and Q_i are given by (2.4.5) for a meshed microgrid and by (4.3.1) in case of a parallel microgrid.

Recalling (2.4.5) and (4.3.1), combining (4.4.1), (4.5.1), (4.5.2) and (4.5.3) gives the closed-loop system corresponding to a primary droop-controlled inverter as

$$\begin{aligned} \dot{\delta}_i &= \omega^d - k_{P_i}(P_i^m - P_i^d), \\ \tau_i \dot{P}_i^m &= -P_i^m + P_i, \\ V_i &= V_i^d - k_{Q_i}(Q_i^m - Q_i^d), \\ \tau_i \dot{Q}_i^m &= -Q_i^m + Q_i. \end{aligned} \tag{4.5.4}$$

[3] An underlying assumption to the model (4.4.1) is that whenever an inverter connects to a RES, it is equipped with a storage unit.

A tuning criterion guaranteeing asymptotic stability of the equilibrium point of (4.5.4) has been presented in [22]. However, it is important to note that in contrast to the frequency droop control (4.5.1), the voltage droop control (4.5.2) has to be tuned in a heuristic fashion [22, 24, 27, 112]. Moreover, it has been shown in the literature, see e.g. [32], that the decentralized nature of (4.5.2) results in poor reactive power sharing. Consequently, the rest of this thesis assume that the phase angles of the grid-forming inverters are controlled using the frequency droop control (4.5.1).

For presenting the contributions coming under the section *distributed secondary frequency control*, in the sequel, the model of a primary droop-controlled inverter (4.5.4) in the presence of clock drifts is presented. In addition, the steady-state performance regarding

- frequency droop control (under explicit consideration of clock drifts) and
- voltage droop control

are also discussed later in this chapter.

4.5.1 Primary droop control with inaccurate clock

In practice, (4.5.4) is implemented on a digital processor employing numerical integration. In such a setup, the phase angle δ_i is obtained after numerically integrating $\dot{\delta}_i$. The time signal generated by the local clock of each grid-forming inverter is used to determine the sampling interval used in the numerical integration employed to calculate δ_i.

It is a well-known fact that the clocks used to generate these local time signals are not synchronized [41, 42], hence resulting in clock inaccuracies or simply *clock drifts* amongst the inverters. An immediate effect of clock drifts is that the sampling interval of the numerical integration differs between inverters. The impact of the difference in sampling intervals on the dynamics (4.5.4) is investigated next.

In the following, an equivalent model of (4.5.4) considering clock inaccuracies is presented. The local time signal $t_i \in \mathbb{R}$ of the i-th inverter expressed in terms of the global time signal $t \in \mathbb{R}$ is given by [43, 58, 113–115]

$$t_i = \left(\frac{1}{1+\mu_i}\right) t + \zeta_i, \tag{4.5.5}$$

where $\mu_i \in \mathbb{R}$ is the relative drift of the clock at the i-th inverter and $\zeta_i \in \mathbb{R}$ is the local clock offset. From (4.5.5),

$$\frac{d(\cdot)}{dt_i} = (1+\mu_i)\frac{d(\cdot)}{dt}. \tag{4.5.6}$$

Suppose that the numerical integration in (4.5.4) is expressed in terms of the local time signal t_i. Inserting (4.5.6) in (4.5.4) gives

$$\begin{aligned}
(1+\mu_i)\frac{d\delta_i}{dt} &= \omega^d - k_{P_i}(P_i^m - P_i^d),\\
(1+\mu_i)\tau_i\frac{dP_i^m}{dt} &= -P_i^m + P_i,\\
V_i &= V_i^d - k_{Q_i}(Q_i^m - Q_i^d),\\
(1+\mu_i)\tau_i\frac{dQ_i^m}{dt} &= -Q_i^m + Q_i,
\end{aligned} \tag{4.5.7}$$

where now, the time derivatives are expressed with respect to the global time t. Without loss of generality, the offset value ζ_i can be included in the initial conditions of the system (4.5.7).

Following [43, 58], to investigate the effect of clock drifts, it is convenient to introduce the *internal* frequency $\bar{\omega}_i : \mathbb{R}_{\geq 0} \to \mathbb{R}$ of the inverter at the i-th node which is related to the actual *electrical* frequency $\omega_i = \dot{\delta}_i$ by

$$\bar{\omega}_i = (1+\mu_i)\dot{\delta}_i = (1+\mu_i)\omega_i, \quad \forall\, i \in \mathcal{N}. \tag{4.5.8}$$

In the literature, the effect of clock drifts is often neglected, i.e., $\mu_i = 0$ and assume that $\bar{\omega}_i = \omega_i$, see e.g., [13, 32, 36, 51, 64]. However, it has been shown in [43, 58] that clock drifts disturb synchronization and power sharing in microgrids, depending upon the clock drift value μ_i at each inverter. This problem is explained in the sequel.

4.5.1.1 Steady-state performance

In practice, $\mu_i \neq \mu_j$ where $i, j \in \mathcal{N}$, $j \neq i$, i.e., the clock drifts values of different inverters are different. Furthermore, clock drift values observed in commercial inverters can vary from 10^{-6} [42, 43] to 10^{-3} [71, Table I] depending on the quality of the micro-controller used. Considering this fact, the system (4.5.7) at steady-state yields

$$\begin{aligned}
(1+\mu_i)\omega_i^s = \bar{\omega}_i^s &= \omega^d - k_{P_i}(P_i^s - P_i^d),\\
V_i^s &= V_i^d - k_{Q_i}(Q_i^s - Q_i^d),
\end{aligned} \tag{4.5.9}$$

where the superscript s denotes the steady-state value and $\bar{\omega}_i$ is given by (4.5.8). Note that

$$\omega_i^s = \omega_j^s = \omega^*,$$

where $\omega_i^s \in \mathbb{R}_{>0}$ and $\omega_j^s \in \mathbb{R}_{>0}$ are the electrical frequencies at inverters $i \in \mathcal{N}$ and $j \in \mathcal{N}$ at steady-state respectively and $\omega^* \in \mathbb{R}_{>0}$ is the synchronized electrical frequency. Thus, the steady-state equations (4.5.9) become

$$\begin{aligned} \bar{\omega}_i^s &= (1+\mu_i)\omega_i^s = (1+\mu_i)\omega^* = \omega^d - k_{P_i}(P_i^s - P_i^d), \\ V_i^s &= V_i^d - k_{Q_i}(Q_i^s - Q_i^d). \end{aligned} \tag{4.5.10}$$

It is a common practice to select the frequency droop gain as $k_{P_i} = 1/S_i^N$ where $S_i^N \in \mathbb{R}_{>0}$ is the power rating of the i-th inverter, see [62, Theorem 7], [22, Lemma 6.2]. Hence, (4.5.10) can be expressed as

$$\begin{aligned} \omega^d - (1+\mu_i)\omega^* &= \frac{P_i^s - P_i^d}{S_i^N}, \\ V_i^s &= V_i^d - k_{Q_i}(Q_i^s - Q_i^d). \end{aligned} \tag{4.5.11}$$

Recall that $\mu_i \neq \mu_j, j \in \mathcal{N}, j \neq i$. Thus from (4.5.11),

$$\frac{P_i^s - P_i^d}{S_i^N} \neq \frac{P_j^s - P_j^d}{S_j^N},$$

which as per Definition 3.3.1, disturbs steady-state active power sharing.

Next, looking at the steady-state equation corresponding to voltage droop control in (4.5.11), i.e.,

$$V_i^d - V_i^s = k_{Q_i}(Q_i^s - Q_i^d), \tag{4.5.12}$$

where it can be seen that the effect of clock drifts is negligible. Again, to understand the aspect of reactive power sharing, let the voltage droop gain in (4.5.12) be selected as $k_{Q_i} = 1/S_i^N$, which gives

$$V_i^d - V_i^s = \frac{Q_i^s - Q_i^d}{S_i^N}. \tag{4.5.13}$$

In contrast to the concept of synchronized electrical frequency, typically the voltage amplitudes at steady-state are different for different buses. Hence, $V_i^s \neq V_j^s, j \in \mathcal{N}, j \neq i$. Thus, it yields from (4.5.13) that

$$\frac{Q_i^s - Q_i^d}{S_i^N} \neq \frac{Q_j^s - Q_j^d}{S_j^N},$$

which denotes poor reactive power sharing according to Definition 3.3.2, see also [22, Remark 6.6], [32, Section III].

4.6 Summary

In this chapter, the microgrid model and the commonly used primary droop control law [38] have been introduced. At first, network and load models of meshed and parallel microgrids considered in this thesis have been presented. Furthermore, since this thesis focuses upon inverter-based microgrids, the model of a grid-forming inverter has been presented.

After introducing the concept of clock drifts, the model of a droop-controlled inverter in the presence of clock drifts has been derived. Additionally, the steady-state performance of frequency droop control with explicit consideration of clock drifts has been investigated. The effect of clock drifts on voltage droop control was found to be negligible. Nevertheless, voltage droop control renders poor steady-state reactive power sharing. The above observation has also been explained in this chapter.

Chapter 5

Distributed secondary frequency control

5.1 Introduction

In the previous chapter, the model of an inverter-based meshed microgrid has been presented. Later, based on [43, 58], the model of a droop-controlled inverter under explicit consideration of clock drifts has been derived. As shown in Chapter 4, clock drift disturb steady-state active power sharing provided by frequency droop control. In this context, the contributions of this chapter can be organized as sections:

1. **Steady-state performance of distributed secondary frequency control** The idea behind this section is to compare the steady-state performance of distributed secondary frequency controllers, e.g. [13, 32, 36, 51, 64] in the presence of clock drifts. The performance is compared in terms of steady-state network frequency restoration (Definition 3.3.3) and active power sharing (Definition 3.3.1). For this purpose, the model of a frequency droop-controlled microgrid in the presence of clock drifts is recalled from Chapter 4. Then, a *general distributed frequency control representation* is proposed, which can be parametrized into the control approaches presented in [13, 32, 36, 51, 64], and many more. Based on the proposed general distributed controller representation, necessary and sufficient conditions for accurate steady-state network frequency restoration (Definition 3.3.3) and active power sharing (Definition 3.3.1) are derived. The approaches presented in [13, 32, 36, 51, 64] were found to be not satisfying these conditions. Thus, a particular parameterization of the above-mentioned general

distributed controller representation is proposed, which satisfies the conditions required for achieving the control objectives focused on in this chapter. This controller parametrization is termed as the GDAI (generalized distributed averaging integral) control.

2. **Stability analysis and tuning criterion** In this section, a tuning criterion that guarantees local asymptotic stability of the closed-loop equilibrium point in the presence of uncertain clock drift values is derived. The presented tuning criterion can be cast as a set of LMIs which can be easily solved to find the stabilizing parameters of the GDAI controller.

The results presented in this chapter are based on the author's publications [116–118].

5.2 Primary frequency (droop) control: Effect of clock drifts

As mentioned in Chapter 3, the proportional nature of primary frequency droop control results in steady-state network frequency deviation from the nominal value. In the presence of clock drifts, proportional active power sharing provided by the frequency droop control is also disturbed, see Section 4.5.1. However, the effect of clock drifts on voltage control is negligible. Hence, this chapter focuses on designing distributed secondary frequency controllers such that the network frequency is restored to a desired nominal value and active power sharing is maintained at steady-state in the presence of clock drifts. The task of voltage control is neglected in this chapter and is addressed in the next chapter for a different microgrid application. For mathematical simplicity, the voltage amplitudes are assumed to be constant, see e.g. [36, 62]. For an analysis considering varying voltage amplitudes, the reader is referred to [22, 30].

Based on (4.5.7), the model of a primary-frequency droop-controlled unit in the presence of clock drifts is given as

$$\begin{aligned}(1+\mu_i)\dot{\delta}_i = \bar{\omega}_i &= \omega^d - k_{P_i}(P_i^m - P_i^d),\\ (1+\mu_i)\tau_i \dot{P}_i^m &= -P_i^m + P_i,\end{aligned} \tag{5.2.1}$$

where P_i is given by (2.4.5) which–under the standing assumption that voltage amplitudes are constant–can be expressed as

$$P_i(\delta) = G_{ii}V_i^2 + \hat{P}_i, \tag{5.2.2}$$

where $\delta := \mathrm{col}(\delta_1, \ldots, \delta_n) \in \mathbb{T}^n$ and

$$\hat{P}_i(\delta) = \sum_{k \in \mathcal{N}_i} |B_{ik}| V_i V_k \sin(\delta_i - \delta_k). \tag{5.2.3}$$

Furthermore, it is convenient to rewrite the dynamics (5.2.1) as follows. Differentiating the first equation in (5.2.1) with respect to time yields

$$(1+\mu_i)\ddot{\delta}_i = \dot{\tilde{\omega}}_i = -k_{P_i}\dot{P}_i^m = -k_{P_i}\frac{1}{(1+\mu_i)\tau_i}\left(-P_i^m + \hat{P}_i(\delta) + G_{ii}V_i^2\right), \tag{5.2.4}$$

where to write the latter equality, the second equation in (5.2.1) has been used. Next, from the first equation in (5.2.1), the measured power P_i^m can be expressed as

$$P_i^m = \frac{1}{k_{P_i}}\left(-\tilde{\omega}_i + \omega^d\right) + P_i^d. \tag{5.2.5}$$

Substituting (5.2.5) in (5.2.4) and multiplying the result with $1/k_{P_i}$ yields

$$(1+\mu_i)M_i\dot{\tilde{\omega}}_i = -D_i(\tilde{\omega}_i - \omega^d) - \left(\hat{P}_i(\delta) + G_{ii}V_i^2 - P_i^d\right), \tag{5.2.6}$$

where $M_i = \tau_i / k_{P_i} \in \mathbb{R}_{>0}$ is the virtual inertia coefficient and $D_i = 1/k_{P_i} \in \mathbb{R}_{>0}$ is the damping coefficient.

Combining (5.2.6) with (4.5.8) yields

$$\begin{aligned} (1+\mu_i)\dot{\delta}_i &= \tilde{\omega}_i, \\ (1+\mu_i)M_i\dot{\tilde{\omega}}_i &= -D_i(\tilde{\omega}_i - \omega^d) - \left(\hat{P}_i(\delta) + G_{ii}V_i^2 - P_i^d\right), \end{aligned} \tag{5.2.7}$$

which is an equivalent representation of (5.2.1). See also [119].

To derive a compact model representation of the microgrid, it is convenient to introduce the matrices

$$M = \mathrm{diag}(M_i) \in \mathbb{R}^{n\times n}, \quad D = \mathrm{diag}(D_i) \in \mathbb{R}^{n\times n}, \quad \mu = \mathrm{diag}(\mu_i) \in \mathbb{R}^{n\times n}, \tag{5.2.8}$$

and the vectors

$$\omega = \mathrm{col}(\omega_i) \in \mathbb{R}^n, \quad \tilde{\omega} = \mathrm{col}(\tilde{\omega}_i) \in \mathbb{R}^n, \quad P^{\mathrm{net}} = \mathrm{col}(P_i^d - G_{ii}V_i^2) \in \mathbb{R}^n. \tag{5.2.9}$$

Inspired by [36, 110], a *potential function* $U : \mathbb{R}^n \to \mathbb{R}$ is defined in the following:

$$U(\delta) = -\sum_{\{i,k\} \in [\mathcal{N}]^2} |B_{ik}| V_i V_k \cos(\delta_i - \delta_k). \tag{5.2.10}$$

Let $\hat{P}(\delta) = \mathrm{col}(\hat{P}_i(\delta)) \in \mathbb{R}^n$ where $\hat{P}_i$ is defined in (5.2.3). With $U(\delta)$ given by (5.2.10), note that

$$\nabla_\delta U(\delta) = \hat{P}(\delta).$$

Then, the dynamics (5.2.7) for the whole microgrid can be expressed as

$$\begin{aligned} (I_n + \mu)\dot{\delta} &= \bar{\omega}, \\ (I_n + \mu)M\dot{\bar{\omega}} &= -D(\bar{\omega} - \mathbb{1}_n \omega^d) - \left(\nabla_\delta U(\delta) - P^{\mathrm{net}}\right), \end{aligned} \tag{5.2.11}$$

where the matrices and the vectors used in (5.2.11) are defined in (5.2.8) and (5.2.9), respectively.

Observe that due to the skew symmetry of the power flows,

$$\mathbb{1}_n^\top \hat{P}(\delta) = \mathbb{1}_n^\top \nabla_\delta U(\delta) = 0. \tag{5.2.12}$$

Next, for better clarity of the results presented in this chapter, the notion of active power sharing given in Definition 3.3.1 is expressed for the whole network as

$$\mathscr{X}\left(\nabla_\delta U(\delta^s) - P^{\mathrm{net}}\right) = \alpha \mathbb{1}_n, \tag{5.2.13}$$

where $\alpha \in \mathbb{R}$, $\mathscr{X} = \mathrm{diag}(\mathscr{X}_i) \in \mathbb{R}^{n\times n}$ is a weighting matrix with $\mathscr{X}_i \in \mathbb{R}_{>0}$, $\nabla_\delta U(\delta^s) = \nabla_\delta U(\delta)|_{\delta=\delta^s} = \mathrm{col}(\hat{P}_i(\delta^s))$ where $\hat{P}_i$ is given by (5.2.3) and P^{net} is defined in (5.2.9).

For the purpose of attaining steady-state active power sharing using frequency droop control, it has been shown in [62, Theorem 7], [22, Lemma 6.2] that the entries of the damping matrix D in (5.2.11) shall be chosen according to

$$\mathscr{X} D = \kappa I_n, \tag{5.2.14}$$

where $\kappa \in \mathbb{R}_{>0}$. Recall that D is the inverse droop coefficient matrix. Therefore, if $\mathscr{X}_i$ is chosen as $\mathscr{X}_i = 1/S_i^N$, then the condition (5.2.14) can be understood as an inversely proportional choice of droop coefficients[1] in correspondence to the power ratings[2].

5.3 Secondary frequency control: Effect of clock drifts

Like any power network, a microgrid is also designed to work very close to the nominal frequency value of 50 or 60 Hz [1, 3]. However, the proportional nature

[1] The condition (5.2.14) for two inverters has been briefly recalled in Section 4.5.1.

[2] Recall that S_i^N is the power rating of the i-th unit.

of primary droop control results in steady-state frequency deviation. Therefore, following the standard practice [26, 36, 51], a secondary control input $u = \mathrm{col}(u_i) : \mathbb{R}_{\geq 0} \to \mathbb{R}^n$ is introduced to the model (5.2.11) with the aim of correcting the steady-state frequency deviation. Thus, (5.2.11) becomes

$$\begin{aligned} (I_n + \mu)\dot{\delta} &= \bar{\omega}, \\ (I_n + \mu)M\dot{\bar{\omega}} &= -D(\bar{\omega} - \mathbb{1}_n\omega^d) - \left(\nabla_\delta U(\delta) - P^{\mathrm{net}}\right) + u. \end{aligned} \tag{5.3.1}$$

Along any synchronized motion (i.e., a motion with constant electrical frequencies $\omega^s = \omega^* \mathbb{1}_n$ for $\omega^* \in \mathbb{R}_{>0}$, constant phase angle differences $\delta_i^s - \delta_k^s$ and constant secondary control input u^s) of the system (5.3.1), it yields

$$\begin{aligned} \mathbb{1}_n^\top M(I_n + \mu)\dot{\bar{\omega}} = 0 = &-\mathbb{1}_n^\top D(\bar{\omega}^s - \mathbb{1}_n\omega^d) \\ &- \mathbb{1}_n^\top \left(\nabla_\delta U(\delta^s) - P^{\mathrm{net}}\right) + \mathbb{1}_n^\top u^s. \end{aligned} \tag{5.3.2}$$

Note that in the presence of clock drifts, internal frequencies of inverters are not uniform, i.e., from (4.5.8), $\omega^s = \omega^* \mathbb{1}_n$ implies that

$$\bar{\omega}^s = (I_n + \mu)\omega^s = \omega^*(I_n + \mu)\mathbb{1}_n. \tag{5.3.3}$$

Moreover with (5.2.12) and by inserting (5.3.3) into (5.3.2), the scalar ω^* can be obtained from (5.3.2) as

$$\omega^* = \omega^d \frac{\mathbb{1}_n^\top D \mathbb{1}_n}{\mathbb{1}_n^\top D(I_n + \mu)\mathbb{1}_n} + \frac{\mathbb{1}_n^\top (P^{\mathrm{net}} + u^s)}{\mathbb{1}_n^\top D(I_n + \mu)\mathbb{1}_n}. \tag{5.3.4}$$

From (5.3.4), it is obvious that $\omega^* = \omega^d$ if and only if u^s satisfies

$$\boxed{\mathbb{1}_n^\top (P^{\mathrm{net}} + u^s) = \omega^d \mathbb{1}_n^\top D\mu \mathbb{1}_n.} \tag{5.3.5}$$

In the case of ideal clocks, i.e., if $\mu = \mathbb{0}_{n\times n}$, from (5.3.4), it is clear that $\omega^* = \omega^d$ if and only if $\mathbb{1}_n^\top (P^{\mathrm{net}} + u^s) = 0$. Similar results assuming ideal inverter clocks have been presented in [36, 51]. However from (5.3.4), in the presence of clock drifts (i.e., $\mu_i \neq 0$), satisfying $\mathbb{1}_n^\top (P^{\mathrm{net}} + u^s) = 0$ does not guarantee $\omega^* = \omega^d$.

5.3.1 General distributed control representation

In this section, a control law for the input is designed. The following *general distributed control representation* is proposed:

$$\boxed{\begin{aligned} u &= p, \\ (I_n + \mu)\dot{p} &= -(\mathbf{B} + \beta \mathscr{X}\mathbf{D}\mathscr{L})(\bar{\omega} - \mathbb{1}_n\omega^d) - \mathbf{D}\mathscr{X}\mathscr{L}\mathscr{X}p, \end{aligned}} \tag{5.3.6}$$

where $p : \mathbb{R}_{\geq 0} \to \mathbb{R}^n$ is a new variable. Furthermore, $\mathbf{B} \in \mathbb{R}^{n\times n}$ and $\mathbf{D} \in \mathbb{R}^{n\times n}$ are diagonal controller matrices, $\beta \in \mathbb{R}$ is a controller parameter, $\mathscr{L} \in \mathbb{R}^{n\times n}$ is the Laplacian matrix of a connected and undirected graph representing the communication network. Finally, $\mathscr{X}$ is the design parameter defined in (5.2.13). The matrix $\mathbf{B}$ is commonly called the *pinning gain matrix*, see e.g. [13].

It is customary to use the internal frequency $\bar{\omega}$ of the inverters to implement a distributed control law like (5.3.6), since it obviates the requirement for extra frequency measurement. This is mainly because new measurement devices can potentially increase the complexity and can bring in further measurement errors into the system, see e.g. [13, 32, 36, 51, 110]. Therefore, it is essential to note that in the control law (5.3.6), the internal frequency $\bar{\omega}$ is used. However, in the works mentioned above, the effect of clock drifts is not considered, and thus, the authors assume that the internal frequency and the electrical frequency are the same, i.e., $\bar{\omega} = \omega$. Yet, when explicitly considering clock drifts, from (4.5.8), it is important to note that $\bar{\omega} = (I_n + \mu)\omega$.

The control law (5.3.6) represents a generalized version of various distributed secondary frequency controllers and can be parametrized into

1. the DAI control presented/studied in [32, 36, 51, 110] if the control parameters in (5.3.6) are chosen such that
$$\mathbf{B} > 0, \beta = 0, \mathbf{D} > 0 \quad \text{and} \tag{5.3.7}$$
2. the *pinning* control law proposed in [13] if the control parameters in (5.3.6) are chosen such that
$$\mathbf{B} \geq 0, \mathbf{B} \not> 0, \beta = 0, \mathbf{D} > 0. \tag{5.3.8}$$

Applying the parametrization (5.3.7) in the general controller representation (5.3.6), results in the DAI controller [32, 36, 51, 110] given by

$$\begin{aligned} u &= p, \\ (I_n + \mu)\dot{p} &= -\mathbf{B}(\bar{\omega} - \mathbb{1}_n \omega^d) - \mathbf{D}\mathscr{X}\mathscr{L}\mathscr{X} p \\ \mathbf{B} &> 0. \end{aligned} \tag{5.3.9}$$

Similarly, applying the parametrization (5.3.8) (5.3.6) gives the pinning controller [13]

$$\begin{aligned} u &= p, \\ (I_n + \mu)\dot{p} &= -\mathbf{B}(\bar{\omega} - \mathbb{1}_n \omega^d) - \mathbf{D}\mathscr{X}\mathscr{L}\mathscr{X} p \\ \mathbf{B} &\geq 0, \mathbf{B} \not> 0. \end{aligned} \tag{5.3.10}$$

The correspondence of (5.3.10) with the control law presented in [13] is detailed in the following remark.

Remark 5.3.1. *The primary frequency droop control [13, Equation 47] for the whole microgrid expressed in the notation followed in this thesis is given by*

$$\omega = -D^{-1}\left(\nabla U(\delta) - P^{net}\right) + u^{sec}, \tag{5.3.11}$$

where $u^{sec}: \mathbb{R}_{\geq 0} \to \mathbb{R}^n$ is the secondary control input. Note that (5.3.11) *is equivalent to* (5.3.1) *if*

- $\mu = \mathbb{0}_{n\times n}$ *(yielding $\bar{\omega} = \omega$, see* (4.5.8)*),*
- $\tau_i = 0 \quad \Rightarrow \quad M = diag(\tau_i / k_{P_i}) = \mathbb{0}_{n\times n}$,
- $\omega^d = 0$ *and*
- $u^{sec} = D^{-1}u$.

Furthermore, the secondary frequency control law proposed in [13, Equations 52,53] for the whole network can be expressed as

$$\begin{aligned} u &= p, \\ \dot{p} &= -C_F\left[(\mathscr{B}+\mathscr{L})(\omega - \mathbb{1}_n\omega^d) + \mathscr{L}D^{-1}\left(\nabla U(\delta) - P^{net}\right)\right], \end{aligned}$$

where $C_F > 0$ and $\mathscr{B} \geq 0$ are diagonal controller matrices and $\mathscr{L} \in \mathbb{R}^{n\times n}$ is the Laplacian matrix of the communication graph. Inserting $D^{-1}\left(\nabla U(\delta) - P^{net}\right)$ from (5.3.11) *in the above control law yields*

$$\begin{aligned} \dot{p} &= -C_F\mathscr{B}(\omega - \mathbb{1}_n\omega^d) - C_F\mathscr{L}u^{sec}, \\ &= -C_F\mathscr{B}(\omega - \mathbb{1}_n\omega^d) - C_F\mathscr{L}D^{-1}p, \\ &= -C_F\mathscr{B}(\omega - \mathbb{1}_n\omega^d) - \frac{1}{\kappa}C_F\mathscr{L}\mathscr{X}p, \end{aligned}$$

where $u^{sec} = D^{-1}u = D^{-1}p$ and $D^{-1} = \frac{1}{\kappa}\mathscr{X}$, see (5.2.14)*. Considering non-zero clock drift values as well as for $C_F = \kappa\mathbf{D}\mathscr{X} > 0$ and $C_F\mathscr{B} = \mathbf{B} \geq 0$, the control law described above is the same as* (5.3.10)*.*

In the remainder of this thesis, DAI and pinning control represent (5.3.9) and (5.3.10), respectively.

For the subsequent analysis, it is convenient to introduce the notion below.

Definition 5.3.2 (Synchronized motion)**.** *The closed-loop system* (5.3.1), (5.3.6) *admits a synchronized motion if it has a solution for all* $t \geq 0$ *of the form*

$$\delta^s(t) = \delta_0^s + \omega^s t, \quad \omega^s = \omega^* \mathbb{1}_n, \quad p^s \in \mathbb{R}^n,$$

where $\omega^* \in \mathbb{R}_{>0}$ *is the synchronized electrical frequency and* $\delta_0^s \in \mathbb{R}^n$ *such that*

$$|\delta_{0,i}^s - \delta_{0,k}^s| < \frac{\pi}{2} \quad \forall\, i \in \mathcal{N},\ \forall\, k \in \mathcal{N}_i.$$

With constant phase angle differences $\delta_i^s(t) - \delta_j^s(t)$ for all $t \geq 0$, $i, j \in \mathcal{N}$ in the system (5.3.1), (5.3.6) imply that the frequencies of all the units have converged to a common value, i.e., $\dot{\delta}_i^s = \dot{\delta}_i^s = \omega^*$, $\omega^* \in \mathbb{R}_{>0}$, thus the terminology *synchronized motion*, see e.g., [110, Lemma 4.2] for further details about synchronized motions in power system models similar to (5.3.1), (5.3.6).

Next, the standard assumption of power flow feasibility is recalled.

Assumption 5.3.3. *The closed-loop system* (5.3.1), (5.3.6) *possesses a synchronized motion.* □

In practice, clock drift values observed in commercial inverters can vary from 10^{-6} [42, 43] to 10^{-3} [71, Table I] depending on the quality of the micro-controller used. Therefore as outlined in [43, 58], for secondary frequency control, it is reasonable to assume that the clock drifts are bounded. This is formalized in the assumption below.

Assumption 5.3.4. $\|\mu\|_2 \leq \epsilon, \quad 0 \leq \epsilon < 1.$

5.4 Problem statement

In light of the discussion thus far, this chapter focuses on the following problem.

Problem 5.4.1 (**Secondary control objectives**)**.** *Consider the closed-loop system* (5.3.1), (5.3.6) *with Assumption 5.3.4 and Assumption 5.3.3. Design the parameters* $\mathbf{B}$, β, $\mathbf{D}$ *and the edge-weights of* $\mathcal{L}$ *in* (5.3.1), (5.3.6) *such that the following control objectives are satisfied:*

1. *Accurate frequency restoration as per Definition 3.3.3.*
2. *Accurate active power sharing according to Definition 3.3.1.*
3. *Asymptotic convergence of the solutions of* (5.3.1), (5.3.6) *to the synchronized motion given in Definition 5.3.2.*

5.5 Steady-state performance

In this section, the first two points in Problem 5.4.1 are addressed. At first, a necessary and sufficient condition for accomplishing the first objective in Problem 5.4.1 is presented.

Lemma 5.5.1 (Accurate frequency restoration)**.** *Consider the closed-loop system* (5.3.1), (5.3.6) *with Assumption 5.3.3. Let* $\mathbf{D} > 0$. *Suppose that the diagonal matrix* $\mathbf{B}$ *has at least one positive entry. Then, the synchronized electrical frequency* ω^* *of the system* (5.3.1), (5.3.6) *is given by*

$$\omega^* = \frac{\mathbb{1}_n^\top \mathbf{D}^{-1}\mathscr{X}^{-1}\mathbf{B}\mathbb{1}_n}{\mathbb{1}_n^\top \mathbf{D}^{-1}\mathscr{X}^{-1}\mathbf{B}(I_n+\mu)\mathbb{1}_n}\omega^d. \tag{5.5.1}$$

Furthermore, accurate network frequency restoration, i.e., (3.3.3), *is achieved if and only if*

$$\mathbb{1}_n^\top \mathbf{D}^{-1}\mathscr{X}^{-1}\mathbf{B}\mu\mathbb{1}_n = 0. \tag{5.5.2}$$

Proof. Along any synchronized motion, the electrical frequencies at all nodes of (5.3.1), (5.3.6) have to be identical, i.e.,

$$\dot{\delta}^s = \omega^s = \mathbb{1}_n\omega^*, \tag{5.5.3}$$

which yields (5.3.3). Furthermore, at steady-state, $\dot{p}^s = \mathbb{0}_n$. Hence, (5.3.6) becomes

$$-(I_n+\mu)\dot{p}^s = \mathbb{0}_n = (\mathbf{B}+\beta\mathscr{X}\mathbf{D}\mathscr{L})(\bar{\omega}^s - \mathbb{1}_n\omega^d) + \mathbf{D}\mathscr{X}\mathscr{L}\mathscr{X}p^s. \tag{5.5.4}$$

Multiplying (5.5.4) from the left with $\mathbb{1}_n^\top\mathbf{D}^{-1}\mathscr{X}^{-1}$ and recalling the fact that $\mathbb{1}_n^\top\mathscr{L} = \mathbb{0}_n^\top$, yields

$$0 = \mathbb{1}_n^\top \mathbf{D}^{-1}\mathscr{X}^{-1}\mathbf{B}(\bar{\omega}^s - \mathbb{1}_n\omega^d).$$

Using (5.3.3) in the above equation leads to

$$0 = \mathbb{1}_n^\top \mathbf{D}^{-1}\mathscr{X}^{-1}\mathbf{B}\Big((I_n+\mu)\mathbb{1}_n\omega^* - \mathbb{1}_n\omega^d\Big). \tag{5.5.5}$$

Under the standing assumption that at least one entry of the diagonal matrix $\mathbf{B}$ is positive, ω^* can be solved from (5.5.5) resulting in (5.5.1).

Note that from (5.5.1), $\omega^* = \omega^d$ if and only if

$$\mathbb{1}_n^\top \mathbf{D}^{-1}\mathscr{X}^{-1}\mathbf{B}(I_n+\mu)\mathbb{1}_n = \mathbb{1}_n^\top \mathbf{D}^{-1}\mathscr{X}^{-1}\mathbf{B}\mathbb{1}_n,$$

which is equivalent to (5.5.2), completing the proof. □

In the following lemma, a necessary and sufficient condition for fulfilling the second objective in Problem 5.4.1 is derived.

Lemma 5.5.2 (Active power sharing)**.** *Consider the closed-loop system* (5.3.1), (5.3.6) *with Assumption 5.3.3. Let* $\mathbf{D} > 0$. *Suppose that the diagonal matrix* $\mathbf{B}$ *has at least one positive entry and* D *is chosen as per* (5.2.14). *Then, active power sharing according to Definition 3.3.1 along the synchronized motion is achieved if and only if* $\mathbf{B}$, β, $\mathbf{D}$ *and* $\mathscr{L}$ *are chosen such that*

$$\left[\mathbf{D}^{-1}\mathscr{X}^{-1}\mathbf{B} + (\beta+\kappa)\mathscr{L}\right]\mathbf{F}\mathbb{1}_n\omega^d = \mathbb{0}_n, \tag{5.5.6}$$

where

$$\mathbf{F} = \frac{\mathbb{1}_n^\top\mathbf{D}^{-1}\mathscr{X}^{-1}\mathbf{B}\mathbb{1}_n}{\mathbb{1}_n^\top\mathbf{D}^{-1}\mathscr{X}^{-1}\mathbf{B}(I_n+\mu)\mathbb{1}_n}(I_n+\mu) - I_n. \tag{5.5.7}$$

Proof. Along a synchronized motion, the primary control dynamics (5.3.1) with $u^s = p^s$ (see (5.3.6)) becomes

$$\mathbb{0}_n = -D(\bar{\omega}^s - \mathbb{1}_n\omega^d) - \left(\nabla_\delta U(\delta^s) - P^{\text{net}}\right) + p^s, \tag{5.5.8}$$

which can be rearranged as

$$p^s = D(\bar{\omega}^s - \mathbb{1}_n\omega^d) + \left(\nabla_\delta U(\delta^s) - P^{\text{net}}\right). \tag{5.5.9}$$

Next, consider (5.3.6) at steady-state given by

$$\mathbb{0}_n = (\mathbf{B} + \beta\mathscr{X}\mathbf{D}\mathscr{L})(\bar{\omega}^s - \mathbb{1}_n\omega^d) + \mathbf{D}\mathscr{X}\mathscr{L}\mathscr{X}p^s. \tag{5.5.10}$$

Inserting p^s obtained from (5.5.9) in (5.5.10) results in

$$\begin{aligned}\mathbb{0}_n = &\left(\mathbf{B} + \beta\mathscr{X}\mathbf{D}\mathscr{L}\right)(\bar{\omega}^s - \mathbb{1}_n\omega^d) + \mathbf{D}\mathscr{X}\mathscr{L}\mathscr{X}D(\bar{\omega}^s - \mathbb{1}_n\omega^d)\\ &+ \mathbf{D}\mathscr{X}\mathscr{L}\mathscr{X}\left(\nabla_\delta U(\delta^s) - P^{\text{net}}\right).\end{aligned}$$

Under the standing assumption that (5.2.14) is satisfied, the above equation becomes

$$\mathbb{0}_n = \left(\mathbf{B} + \beta\mathscr{X}\mathbf{D}\mathscr{L} + \kappa\mathbf{D}\mathscr{X}\mathscr{L}\right)(\bar{\omega}^s - \mathbb{1}_n\omega^d) + \mathbf{D}\mathscr{X}\mathscr{L}\mathscr{X}\left(\nabla_\delta U(\delta^s) - P^{\text{net}}\right),$$

which, when left-multiplied with $\mathbf{D}^{-1}\mathscr{X}^{-1} > 0$, yields

$$\mathbb{0}_n = \left(\mathbf{D}^{-1}\mathscr{X}^{-1}\mathbf{B} + \beta\mathscr{L} + \kappa\mathscr{L}\right)(\bar{\omega}^s - \mathbb{1}_n\omega^d) + \mathscr{L}\mathscr{X}\left(\nabla_\delta U(\delta^s) - P^{\text{net}}\right). \tag{5.5.11}$$

Recall that $\mathscr{L}$ is the Laplacian matrix of a connected undirected graph. Hence,

$$\mathscr{L}\mathscr{X}\left(\nabla_\delta U(\delta^s) - P^{\text{net}}\right) = \mathbb{0}_n$$

if and only if (5.2.13) is satisfied, i.e., active power sharing. From (5.5.11),

$$\mathscr{L}\mathscr{X}\left(\nabla_\delta U(\delta^s) - P^{\text{net}}\right) = \mathbb{0}_n$$

if and only if

$$\left(\mathbf{D}^{-1}\mathscr{X}^{-1}\mathbf{B} + (\beta+\kappa)\mathscr{L}\right)(\bar{\omega}^s - \mathbb{1}_n\omega^d) = \mathbb{0}_n. \tag{5.5.12}$$

Finally, with (5.3.3) and ω^* given by (5.5.1), the condition (5.5.12) holds if and only if (5.5.6) is satisfied. This completes the proof. □

5.5.1 DAI and pinning control

In this section, the steady-state behavior of the DAI control and the pinning control are evaluated based on Lemma 5.5.1 and Lemma 5.5.2.

1. **DAI control**: Consider Lemma 5.5.1 and the DAI-parametrization (5.3.7). With (5.3.7), the condition (5.5.2) is not satisfied. Hence, the objective of network frequency restoration is not satisfied, i.e., $\omega^* \neq \omega^d$. Next, consider Lemma 5.5.2. It can be directly verified that (5.3.7) does not satisfy (5.5.6) and thus steady-state active power sharing is also not achieved.

2. **Pinning control**: Consider Lemma 5.5.1. It can be seen that the pinning-parametrization (5.3.8) satisfies (5.5.2) if the structure of the pinning gain matrix $\mathbf{B} \geq 0$ is chosen such that $\mathbf{B}\mu = \mathbb{0}_{n\times n}$, resulting in $\omega^* = \omega^d$. However, (5.3.8) does not satisfy the conditions of Lemma 5.5.2. Thus in the presence of clock drifts, active power sharing is not achieved using the pinning control.

5.6 GDAI control

In light of the discussion thus far, a parametrization of (5.3.6) which satisfy both Lemma 5.5.1 and Lemma 5.5.2 is yet to be presented. Since the coefficients μ_i are unknown and different for different units, Lemma 5.5.2 reveals that unlike in the case of ideal clocks [13, 32, 36, 64], when taking clock drifts explicitly into account, it is hard to determine $\mathbf{B}$, β and $\mathbf{D}$ directly from the conditions presented in Lemmata 5.5.1 and 5.5.2. Therefore, instead below, a sufficient condition for the control parameters $\mathbf{B}$, β and $\mathbf{D}$ satisfying Lemmata 5.5.1 and 5.5.2 is presented.

Lemma 5.6.1 (Accurate frequency restoration and active power sharing)**.** *Consider the closed-loop system* (5.3.1), (5.3.6) *with Assumption 5.3.3. Let* $\mathbf{D} > 0$. *Suppose that the diagonal matrix* $\mathbf{B}$ *has at least one positive entry and* D *is chosen as*

per (5.2.14). *Then, the first two objectives in Problem 5.4.1 along a synchronized motion are achieved if the control parameters* $\mathbf{B}$ *and* β *are chosen such that*

$$\boxed{\mathbf{B}\mu = \mathbb{0}_{n\times n} \quad \textit{and} \quad \beta = -\kappa.} \tag{5.6.1}$$

Proof. Consider Lemma 5.5.1. For $\mathbf{B}\mu = \mathbb{0}_{n\times n}$, (5.5.2) holds. Thus, accurate network frequency restoration is assured, i.e., $\omega^* = \omega^d$.

Next, consider Lemma 5.5.2. With $\mathbf{B}\mu = \mathbb{0}_{n\times n}$, (5.5.6) becomes

$$\left[(\beta+\kappa)\mathscr{L}\right]\mu\mathbb{1}_n\omega^d = \mathbb{0}_n,$$

which holds when $\beta = -\kappa$. Hence, Lemma 5.5.2 is satisfied, yielding proportional active power sharing, completing the proof. □

Applying the parameters (5.6.1) to the general distributed controller representation (5.3.6) yields

$$\boxed{\begin{aligned} u &= p, \\ (I_n+\mu)\dot{p} &= (-\mathbf{B}+\kappa\mathscr{X}\mathbf{D}\mathscr{L})(\bar{\omega}-\mathbb{1}_n\omega^d) - \mathbf{D}\mathscr{X}\mathscr{L}\mathscr{X}p, \\ \mathbf{B}\mu &= \mathbb{0}_{n\times n}, \quad \mathbf{B}\geq 0. \end{aligned}} \tag{5.6.2}$$

The condition $\mathbf{B}\mu = \mathbb{0}_{n\times n}$ can be interpreted as follows. Define the clock of one of the inverters in the network as master clock, say the k-th inverter, $k \geq 1$. Then, $\mu_k = 0$ and the drifts $\mu_i, i \neq k$, of all other clocks in the microgrid are expressed with respect to the master clock of the k-th inverter. Furthermore, the diagonal pinning gain matrix $\mathbf{B} \geq 0$ will have a non-zero positive entry only at the (k,k)-th position, resulting in $\mathbf{B}\mu = \mathbb{0}_{n\times n}$.

The control law (5.6.2) is termed as generalized distributed averaging integral (GDAI) control in the remainder of this thesis.

5.7 Robust GDAI control design

The GDAI controller (5.6.2) has been identified as a solution to address the first two objectives mentioned in Problem 5.4.1. In this section, the third point in Problem 5.4.1 is addressed. More precisely, a sufficient tuning criterion with which the solutions of the system (5.3.1), (5.6.2) asymptotically converge to the synchronized motion given in Definition 5.3.2 is presented. Here, the terminology *robust* denotes that the presented tuning criterion considers that the clock drift matrix μ has uncertain entries.

5.7.1 Closed-loop system

Combining (5.3.1) and (5.6.2) yields the closed-loop system

$$\begin{aligned}(I_n+\mu)\dot{\delta} &= \bar{\omega},\\ (I_n+\mu)M\dot{\bar{\omega}} &= -D(\bar{\omega}-\mathbb{1}_n\omega^d)-\left(\nabla_\delta U(\delta)-P^{\text{net}}\right)+p,\\ (I_n+\mu)\dot{p} &= (-\mathbf{B}+\kappa\mathscr{X}\mathbf{D}\mathscr{L})(\bar{\omega}-\mathbb{1}_n\omega^d)-\mathbf{D}\mathscr{X}\mathscr{L}\mathscr{X}p.\end{aligned} \tag{5.7.1}$$

5.7.1.1 Coordinate reduction and error states

As the power flow $\nabla_\delta U(\delta) = \text{col}(\hat{P}_i(\delta))$ only depends on angle differences (see (5.2.3)), following [22] and choosing an arbitrary node, say node n, all angles can be expressed relative to that node, i.e.,

$$\theta = \mathscr{R}^\top\delta, \quad \theta:\mathbb{R}_{\geq 0}\to\mathbb{T}^{n-1}, \quad \mathscr{R} = \begin{bmatrix} I_{n-1} \\ -\mathbb{1}_{n-1}^\top \end{bmatrix} \in \mathbb{R}^{n\times(n-1)}.$$

Note that the matrix $\mathscr{R}$ has the property

$$\mathbb{1}_n^\top\mathscr{R} = \mathbb{0}_{n-1}^\top.$$

With Assumption 5.3.3 for the system (5.7.1), the following error states are defined.

$$\begin{aligned}\tilde{\omega} &:= \bar{\omega}-\bar{\omega}^s = \bar{\omega}-(I_n+\mu)\mathbb{1}_n\omega^d,\\ \tilde{\theta} &:= \theta-\theta^s, \quad \tilde{p} := p-p^s, \quad x := \text{col}\left(\tilde{\theta},\tilde{\omega},\tilde{p}\right),\end{aligned}$$

where $\theta^s = \mathscr{R}^\top\delta^s$ with δ^s and p^s given in Definition 5.3.2. Furthermore, (5.3.3) and (3.3.3) were used to express $\bar{\omega}^s$.

Thus, the resulting error dynamics of the system (5.7.1) is given by

$$\begin{aligned}\dot{\tilde{\theta}} &= \mathscr{R}^\top(I_n+\mu)^{-1}\tilde{\omega},\\ (I_n+\mu)M\dot{\tilde{\omega}} &= -D\tilde{\omega}-\mathscr{R}\left[\nabla_{\tilde{\theta}}U(\delta(\tilde{\theta}+\theta^s))-\nabla_{\tilde{\theta}}U(\delta(\theta^s))\right]+\tilde{p},\\ (I_n+\mu)\dot{\tilde{p}} &= (-\mathbf{B}+\kappa\mathscr{X}\mathbf{D}\mathscr{L})\tilde{\omega}-\mathbf{D}\mathscr{X}\mathscr{L}\mathscr{X}\tilde{p},\end{aligned} \tag{5.7.2}$$

where

$$\begin{aligned}\nabla_{\tilde{\theta}}U(\delta(\tilde{\theta}+\theta^s)) &= \frac{\partial U(\delta(\tilde{\theta}+\theta^s))}{\partial\tilde{\theta}},\\ \nabla_{\tilde{\theta}}U(\delta(\theta^s)) &= \frac{\partial U(\delta(\theta+\theta^s))}{\partial\tilde{\theta}}\Big|_{\tilde{\theta}=\mathbb{0}_{n-1}}.\end{aligned}$$

Note that $x^* = \mathbb{0}_{3n-1}$ is an equilibrium point of (5.7.2). Furthermore, asymptotic stability of $x^* = \mathbb{0}_{3n-1}$ implies asymptotic convergence of the solutions of the system (5.7.1) to the synchronized motion given in Definition 5.3.2 up to a uniform shift of all angles [22].

5.7.2 Stability criterion

For presenting the main result of this section, it is convenient to define the following. Since μ is a diagonal matrix, with Assumption 5.3.4,

$$\begin{aligned} \|\mu(I_n+\mu)^{-1}\|_2 &\le g_1(\epsilon), \quad g_1(\epsilon) = \tfrac{\epsilon}{1-\epsilon} > 0, \\ \|(\mu^2+2\mu)(I_n+\mu)^{-2}\|_2 &\le g_2(\epsilon), \quad g_2(\epsilon) = \tfrac{\epsilon^2+2\epsilon}{(1-\epsilon)^2} > 0. \end{aligned} \tag{5.7.3}$$

Some matrices useful for presenting the stability result are defined in the following.

$$\begin{aligned} T &:= \begin{bmatrix} T_{11} & \frac{1}{2}\left(-\varsigma I_n - \sigma D \mathbb{1}_n \mathbb{1}_n^\top \mathbf{D}^{-1}\mathscr{X}^{-1} + \tilde{\mathbf{B}} - \kappa \mathscr{L}\mathscr{X}\right) \\ * & T_{22} \end{bmatrix}, \\ \hat{T}_2 &:= \begin{bmatrix} \sigma M \mathbb{1}_n \mathbb{1}_n^\top \tilde{\mathbf{B}} \mathscr{X}^{-1} & \sigma \mathbf{D}^{-1}\mathscr{X}^{-1}\mathbb{1}_n\mathbb{1}_n^\top D \\ \mathbb{0}_{n\times n} & -\sigma \mathbf{D}^{-1}\mathscr{X}^{-1}\mathbb{1}_n\mathbb{1}_n^\top \end{bmatrix}, \\ H_\mu &:= \begin{bmatrix} \varsigma g_2(\epsilon) M & \mathbb{0}_{n\times n} \\ \mathbb{0}_{n\times n} & g_1(\epsilon)\mathbf{D}^{-1} \end{bmatrix}, \end{aligned} \tag{5.7.4}$$

where $g_1(\epsilon)$ and $g_2(\epsilon)$ are defined in (5.7.3). Furthermore, $\sigma \in \mathbb{R}_{>0}$, $\tilde{\mathbf{B}} = \mathbf{D}^{-1}\mathbf{B} \ge 0$ and

$$\begin{aligned} T_{11} &= \varsigma D - \frac{\sigma}{2}\left(M\mathbb{1}_n\mathbb{1}_n^\top\tilde{\mathbf{B}}\mathscr{X}^{-1} + \mathscr{X}^{-1}\tilde{\mathbf{B}}\mathbb{1}_n\mathbb{1}_n^\top M\right), \\ T_{22} &= \mathscr{X}\mathscr{L}\mathscr{X} + \frac{\sigma}{2}\left(\mathbf{D}^{-1}\mathscr{X}^{-1}\mathbb{1}_n\mathbb{1}_n^\top + \mathbb{1}_n\mathbb{1}_n^\top\mathscr{X}^{-1}\mathbf{D}^{-1}\right). \end{aligned}$$

The stability result is as follows.

Proposition 5.7.1. *Consider the system* (5.7.2) *with Assumption 5.3.3. Recall* $g_1(\epsilon)$ *and* $g_2(\epsilon)$ *defined in* (5.7.3)*. Suppose that there exist* $\varsigma \in \mathbb{R}_{>0}$ *and* $\sigma \in \mathbb{R}_{>0}$*, such that*

$$H_{nom} := \begin{bmatrix} \varsigma M & -\sigma M \mathbb{1}_n \mathbb{1}_n^\top \mathbf{D}^{-1}\mathscr{X}^{-1} \\ * & \mathbf{D}^{-1} \end{bmatrix} > H_\mu, \tag{5.7.5}$$

and

$$\begin{aligned} T &> \left(\epsilon\zeta + \varsigma g_1(\epsilon)\sqrt{\lambda_{\max}(D^2)+1}\right) I_{2n}, \\ 0 &\ge \begin{bmatrix} -\zeta I_{2n} & \hat{T}_2 \\ * & -\zeta I_{2n} \end{bmatrix}, \end{aligned} \tag{5.7.6}$$

where $\zeta \in \mathbb{R}_{>0}$ *and the matrices* H_μ*,* T *and* $\hat{T}_2$ *are defined in* (5.7.4)*. Then, local asymptotic stability of* $x^* = \mathbb{0}_{3n-1}$ *is guaranteed for all unknown clock drifts satisfying Assumption 5.3.4.*

Proof. Consider the Lyapunov function candidate

$$\begin{aligned}\mathcal{V} = &\frac{\varsigma}{2}\tilde{\omega}^\top M\tilde{\omega} + \varsigma U(\delta(\tilde{\theta}+\theta^s)) - \varsigma\nabla_{\tilde{\theta}}U(\delta(\theta^s))^\top\tilde{\theta}\\ &+\frac{1}{2}\tilde{p}^\top\mathbf{D}^{-1}(I_n+\mu)\tilde{p}\\ &-\sigma\tilde{p}^\top(I_n+\mu)\mathbf{D}^{-1}\mathscr{X}^{-1}\mathbb{1}_n\mathbb{1}_n^\top M(I_n+\mu)\tilde{\omega},\end{aligned} \tag{5.7.7}$$

where $\varsigma > 0$ and $\sigma > 0$ are design parameters. The Lyapunov function $\mathcal{V}$ contains kinetic and potential energy terms $\tilde{\omega}^\top M\tilde{\omega}$, respectively $U(\delta)$ [59], a quadratic term in secondary control input $\tilde{p}$ and a cross term between $\tilde{\omega}$ and $\tilde{p}$ which facilitates that $\mathcal{V}$ is decreasing along the trajectories of (5.7.2).

First, it is shown that $\mathcal{V}$ is indeed positive definite under the premises of Proposition 5.7.1. For this purpose, observe that $\nabla_x\mathcal{V}\big|_{x=x^*} = \mathbb{0}_{3n-1}$ which confirms that x^* is a critical point of $\mathcal{V}$. Moreover, the Hessian of $\mathcal{V}$ at x^* is given by

$$\nabla_x^2\mathcal{V}|_{x=x*} = \begin{bmatrix}\varsigma\nabla_{\tilde{\theta}}^2U(\delta(\tilde{\theta}+\theta^s))|_{\tilde{\theta}=\mathbb{0}_{n-1}} & \mathbb{0}_{(n-1)\times n} & \mathbb{0}_{(n-1)\times n}\\ * & \varsigma M & -\sigma(I_n+\mu)M\mathbb{1}_n\mathbb{1}_n^\top\mathbf{D}^{-1}\mathscr{X}^{-1}(I_n+\mu)\\ * & * & \mathbf{D}^{-1}(I_n+\mu)\end{bmatrix}. \tag{5.7.8}$$

From [22, Lemma 5.8],

$$\nabla_{\tilde{\theta}}^2U(\delta(\tilde{\theta}+\theta^s))|_{\tilde{\theta}=\mathbb{0}_{n-1}} > 0.$$

Therefore, the Hessian $\nabla_x^2\mathcal{V}|_{x=x*}$ is positive definite if and only if

$$\begin{bmatrix}\varsigma M & -\sigma(I_n+\mu)M\mathbb{1}_n\mathbb{1}_n^\top\mathbf{D}^{-1}\mathscr{X}^{-1}(I_n+\mu)\\ * & \mathbf{D}^{-1}(I_n+\mu)\end{bmatrix} > 0. \tag{5.7.9}$$

By performing a congruence transformation using the positive definite matrix $S = \text{blkdiag}\big((I_n+\mu)^{-1},(I_n+\mu)^{-1}\big)$ and by invoking Sylvester's law of inertia [84], it is clear that the matrix on the left hand side of (5.7.9) is positive definite if and only if the following matrix inequality is satisfied

$$\begin{bmatrix}\varsigma(I_n+\mu)^{-2}M & -\sigma M\mathbb{1}_n\mathbb{1}_n^\top\mathbf{D}^{-1}\mathscr{X}^{-1}\\ * & (I_n+\mu)^{-1}\mathbf{D}^{-1}\end{bmatrix} > 0. \tag{5.7.10}$$

Inequality (5.7.10) can be equivalently written as

$$H_{\text{nom}} - \begin{bmatrix}\varsigma(\mu^2+2\mu)(I_n+\mu)^{-2}M & \mathbb{0}_{n\times n}\\ \mathbb{0}_{n\times n} & \mu(I_n+\mu)^{-1}\mathbf{D}^{-1}\end{bmatrix} > 0,$$

where H_{nom} is defined in (5.7.5). Furthermore, since μ, M and $\mathbf{D}$ are all diagonal matrices,

$$\begin{bmatrix} \varsigma(\mu^2+2\mu)(I_n+\mu)^{-2}M & \mathbb{0}_{n\times n} \\ \mathbb{0}_{n\times n} & \mu(I_n+\mu)^{-1}\mathbf{D}^{-1} \end{bmatrix} \leq H_\mu,$$

where H_μ is defined in (5.7.4). Consequently, under the premises of Proposition 5.7.1, $\nabla_x^2 \mathcal{V}|_{x=x*} > 0$, confirming positive definiteness of $\mathcal{V}$. Note that $\nabla_x \mathcal{V}\big|_{x=x^*} = \mathbb{0}_{3n-1}$ and $\nabla_x^2 \mathcal{V}|_{x=x*} > 0$ implies that x^* is a strict local minimum of $\mathcal{V}$ [50].

Next, calculating the time derivative of $\mathcal{V}$ along the solutions of (5.7.2) gives

$$\begin{aligned} \dot{\mathcal{V}} &= -\varsigma\tilde{\omega}^\top (I_n+\mu)^{-1} D\tilde{\omega} + \varsigma\tilde{\omega}^\top (I_n+\mu)^{-1}\tilde{p} \\ &\quad + \tilde{p}^\top \left(-\mathbf{D}^{-1}\mathbf{B} + \kappa\mathscr{X}\mathscr{L}\right)\tilde{\omega} - \tilde{p}^\top \mathscr{X}\mathscr{L}\mathscr{X}\tilde{p} \\ &\quad + \sigma\tilde{p}^\top (I_n+\mu)\mathbf{D}^{-1}\mathscr{X}^{-1}\mathbb{1}_n\mathbb{1}_n^\top D\tilde{\omega} \\ &\quad - \sigma\tilde{p}^\top (I_n+\mu)\mathbf{D}^{-1}\mathscr{X}^{-1}\mathbb{1}_n\mathbb{1}_n^\top \tilde{p} \\ &\quad + \sigma\tilde{\omega}^\top (I_n+\mu)M\mathbb{1}_n\mathbb{1}_n^\top \mathscr{X}^{-1}\mathbf{D}^{-1}\mathbf{B}\tilde{\omega} \\ &= -\eta^\top \begin{bmatrix} \tilde{\mathbf{T}}_{11} & \tilde{\mathbf{T}}_{12} \\ \tilde{\mathbf{T}}_{21} & \tilde{\mathbf{T}}_{22} \end{bmatrix} \eta, \end{aligned} \tag{5.7.11}$$

where

$$\eta := \text{col}(\tilde{\omega}, \tilde{p}), \tag{5.7.12}$$

and

$$\begin{aligned} \tilde{\mathbf{T}}_{11} &= \varsigma(I_n+\mu)^{-1}D - \sigma(I_n+\mu)M\mathbb{1}_n\mathbb{1}_n^\top\mathscr{X}^{-1}\mathbf{D}^{-1}\mathbf{B}, \\ \tilde{\mathbf{T}}_{22} &= \mathscr{X}\mathscr{L}\mathscr{X} + \sigma(I_n+\mu)\mathbf{D}^{-1}\mathscr{X}^{-1}\mathbb{1}_n\mathbb{1}_n^\top, \\ \tilde{\mathbf{T}}_{12} &= -\varsigma(I_n+\mu)^{-1}, \\ \tilde{\mathbf{T}}_{21} &= -\sigma(I_n+\mu)\mathbf{D}^{-1}\mathscr{X}^{-1}\mathbb{1}_n\mathbb{1}_n^\top D + \mathbf{D}^{-1}\mathbf{B} - \kappa\mathscr{X}\mathscr{L}. \end{aligned}$$

Note that the scalar $\dot{\mathcal{V}}$ can be equivalently expressed as

$$\begin{aligned} \dot{\mathcal{V}} &= -\eta^\top \begin{bmatrix} \tilde{\mathbf{T}}_{11} & \tilde{\mathbf{T}}_{12} \\ \tilde{\mathbf{T}}_{21} & \tilde{\mathbf{T}}_{22} \end{bmatrix} \eta = -\frac{1}{2}\eta^\top \begin{bmatrix} \tilde{\mathbf{T}}_{11}+\tilde{\mathbf{T}}_{11}^\top & \tilde{\mathbf{T}}_{12}+\tilde{\mathbf{T}}_{21}^\top \\ * & \tilde{\mathbf{T}}_{22}+\tilde{\mathbf{T}}_{22}^\top \end{bmatrix} \eta, \\ &:= -\eta^\top \begin{bmatrix} \mathbf{T}_{11} & \mathbf{T}_{12} \\ * & \mathbf{T}_{22} \end{bmatrix} \eta := -\eta^\top \mathbf{T}\eta, \end{aligned} \tag{5.7.13}$$

where

$$
\begin{aligned}
\mathbf{T}_{11} &= \frac{1}{2}\left(\tilde{\mathbf{T}}_{11} + \tilde{\mathbf{T}}_{11}^{\top}\right) \\
&= \varsigma(I_n + \mu)^{-1} D \\
&\quad - \tfrac{\sigma}{2}\left((I_n + \mu) M \mathbb{1}_n \mathbb{1}_n^{\top} \mathbf{D}^{-1} \mathbf{B} \mathscr{X}^{-1} + \mathbf{D}^{-1} \mathbf{B} \mathscr{X}^{-1} \mathbb{1}_n \mathbb{1}_n^{\top} M (I_n + \mu)\right), \\
\mathbf{T}_{22} &= \frac{1}{2}\left(\tilde{\mathbf{T}}_{22} + \tilde{\mathbf{T}}_{22}^{\top}\right) \\
&= \mathscr{X} \mathscr{L} \mathscr{X} + \tfrac{\sigma}{2}\left((I_n + \mu) \mathbf{D}^{-1} \mathscr{X}^{-1} \mathbb{1}_n \mathbb{1}_n^{\top} + \mathbb{1}_n \mathbb{1}_n^{\top} \mathbf{D}^{-1} \mathscr{X}^{-1} (I_n + \mu)\right), \\
\mathbf{T}_{12} &= \frac{1}{2}\left(\tilde{\mathbf{T}}_{12} + \tilde{\mathbf{T}}_{21}^{\top}\right) \\
&= \frac{1}{2}\left(-\varsigma(I_n + \mu)^{-1} - \sigma D \mathbb{1}_n \mathbb{1}_n^{\top} (I_n + \mu) \mathbf{D}^{-1} \mathscr{X}^{-1} + \mathbf{D}^{-1} \mathbf{B} - \kappa \mathscr{L} \mathscr{X}\right).
\end{aligned}
$$

Note that the entries of the matrix $\mathbf{T}$ defined in (5.7.13) are uncertain, because the clock drift matrix μ is uncertain. Hence, to obtain verifiable conditions that ensure $\mathbf{T} > 0$ and, thus, $\dot{\mathscr{V}}(\eta)$ being negative definite, observe that $\mathbf{T}$ can be decomposed as

$$
\mathbf{T} = T - \frac{1}{2}\left(\Gamma_1 \hat{T}_1 + \hat{T}_1^{\top} \Gamma_1\right) - \frac{1}{2}\left(\Gamma_2 \hat{T}_2 + \hat{T}_2^{\top} \Gamma_2\right), \tag{5.7.14}
$$

where T and $\hat{T}_2$ are defined in (5.7.4) and

$$
\begin{aligned}
&\Gamma_1 = \operatorname{blkdiag}\left(\mu(I_n + \mu)^{-1}, \mu(I_n + \mu)^{-1}\right), \\
&\Gamma_2 = \operatorname{blkdiag}\left(\mu, \mu\right), \quad \hat{T}_1 = \begin{bmatrix} \varsigma D & -\varsigma I_n \\ \mathbb{0}_{n\times n} & \mathbb{0}_{n\times n} \end{bmatrix}.
\end{aligned} \tag{5.7.15}
$$

For any matrices $A \in \mathbb{R}^{n\times n}$ and $B \in \mathbb{R}^{n\times n}$, it holds that [84]

$$
AB + B^{\top} A^{\top} \leq 2\|A\|_2 \|B\|_2 I_n.
$$

Thus (5.7.14) can be expressed as

$$
\mathbf{T} \geq T - \left(\|\hat{T}_1\|_2 \|\Gamma_1\|_2 + \|\hat{T}_2\|_2 \|\Gamma_2\|_2\right) I_{2n}. \tag{5.7.16}
$$

Assumption 5.3.4 together with (5.7.3), implies that

$$
\|\Gamma_1\|_2 \leq g_1(\epsilon), \quad \|\Gamma_2\|_2 \leq \epsilon,
$$

where Γ_1 and Γ_2 are defined in (5.7.15). Therefore, (5.7.16) becomes

$$
\mathbf{T} \geq T - \left(g_1(\epsilon)\|\hat{T}_1\|_2 + \epsilon \|\hat{T}_2\|_2\right) I_{2n}. \tag{5.7.17}
$$

Furthermore, from (5.7.15), $\|\hat{T}_1\|_2$ can be calculated as

$$\|\hat{T}_1\|_2 = \sqrt{\lambda_{\max}(\hat{T}_1\hat{T}_1^\top)} = \varsigma\sqrt{\lambda_{\max}(D^2)+1}.$$

Turning to $\hat{T}_2$ defined in (5.7.4), see that $\hat{T}_2$ depends on the control parameters $\mathbf{B}$ and $\mathbf{D}$. Therefore, to obtain $\|\hat{T}_2\|_2$ required in (5.7.17), the following technique is employed.

Let $\zeta \in \mathbb{R}_{>0}$ be an upper bound for $\|\hat{T}_2\|_2$, i.e.,

$$\begin{aligned}
&\|\hat{T}_2\|_2 = \sqrt{\lambda_{\max}(\hat{T}_2\hat{T}_2^\top)} \leq \zeta \\
\Leftrightarrow\quad &\lambda_{\max}(\hat{T}_2\hat{T}_2^\top) \leq \zeta^2, \\
\Leftrightarrow\quad &\hat{T}_2\hat{T}_2^\top \leq \zeta^2 I_{2n}, \\
\Leftrightarrow\quad &\frac{1}{\zeta}\hat{T}_2\hat{T}_2^\top - \zeta I_{2n} \leq 0.
\end{aligned}$$

By using the Schur complement [84], the last inequality above is equivalent to the second inequality in (5.7.6). Thus, from (5.7.17), it can be concluded that $\mathbf{T} > 0$ if

$$T - \left(\varsigma g_1(\epsilon)\sqrt{\lambda_{\max}(D^2)+1} + \epsilon\zeta\right) I_{2n} > 0,$$

where ζ satisfies the second inequality in (5.7.6). Thus, with the made assumptions, $\mathbf{T} > 0$ implies that

$$\dot{\mathcal{V}}(\eta) < 0 \quad \text{for} \quad \eta(t) \neq \mathbb{0}_{2n}. \tag{5.7.18}$$

This shows that x^* is stable. Recall $\eta(t)$ defined in (5.7.12), which means that $\dot{\mathcal{V}}(\eta)$ does not depend on $\tilde{\theta}$.

Hence, to conclude local asymptotic stability of x^*, one needs to show that the following implication holds along solutions of the system (5.7.2):

$$\eta(t) \equiv \mathbb{0}_{2n} \quad \Rightarrow \quad x(t) = x^*. \tag{5.7.19}$$

From (5.7.12), $\eta(t) = \mathbb{0}_{2n}$ is equivalent to $\tilde{\omega} = \mathbb{0}_n$ and $\tilde{p} = \mathbb{0}_n$. Furthermore, from (5.7.2), $\tilde{\omega} = \mathbb{0}_n$ implies that $\tilde{\theta}$ is constant. Moreover at $\eta(t) = \mathbb{0}_{2n}$, from the second equation in (5.7.2), this yields

$$\mathbb{0}_n = -\mathscr{R}\left[\nabla_{\tilde{\theta}} U(\delta(\tilde{\theta}+\theta^s)) - \nabla_{\tilde{\theta}} U(\delta(\theta^s))\right],$$

which by multiplying from the left with $\mathscr{R}^\top$ and rearranging terms is equivalent to

$$\mathscr{R}^\top\mathscr{R}\nabla_{\tilde{\theta}} U(\delta(\tilde{\theta}+\theta^s)) = \mathscr{R}^\top\mathscr{R}\nabla_{\tilde{\theta}} U(\delta(\theta^s)). \tag{5.7.20}$$

Note that $\mathscr{R}^\top\mathscr{R}$ is invertible and recall that $\nabla^2_{\tilde{\theta}} U(\delta(\tilde{\theta}+\theta^s))|_{\tilde{\theta}=\mathbb{0}_{n-1}} > 0$ [22, Lemma 5.8]. Therefore, in a neighborhood of the origin, (5.7.20) only holds for $\tilde{\theta} = \mathbb{0}_{n-1}$, which shows that the implication (5.7.19) holds. Hence, x^* is locally asymptotically stable, completing the proof. □

Remark 5.7.2. *By fixing the tuning parameter σ, the design conditions* (5.7.5) *and* (5.7.6) *are a set of LMIs in $\varsigma, \zeta, \tilde{\mathbf{B}}, \mathbf{D}^{-1}$ and $\mathscr{L}$ that can be solved efficiently by using standard softwares like Yalmip [120] within MATLAB®. Furthermore, the control parameters $\mathbf{B}$ and $\mathbf{D}$ can be easily recovered from $\tilde{\mathbf{B}} = \mathbf{D}^{-1}\mathbf{B}$ and $\mathbf{D}^{-1}$.*

5.8 Summary

In this chapter, the steady-state performance of various distributed frequency controllers in the presence of clock drifts has been compared. Based on the comparison, some common approaches in the literature, see e.g. [13,32,36,51,64], were found to be not fulfilling the objectives of steady-state accurate network frequency restoration and active power sharing in the presence of clock drifts. In this regard, a control approach termed as GDAI control has been proposed, which achieves the objectives mentioned above. Later, a sufficient condition that guarantees local asymptotic stability of the equilibrium point with primary frequency droop control and secondary GDAI control has been derived.

Chapter 6

Distributed voltage control

6.1 Introduction

As described in Chapter 4, in contrast to frequency droop control, the usage of voltage droop control in microgrids with inductive power lines leads to poor reactive power sharing [32]. Moreover, achieving accurate reactive power sharing at steady-state in the sense Definition 3.3.2 without disturbing voltage stability can also be very challenging [25, 27]. Recently, works like [25, 27] has investigated the problem of reactive power sharing and voltage stability in lossless AC microgrids. In a similar setting, a detailed study on addressing accurate power sharing and voltage stability in DC microgrids has been presented in [121].

Inspired by [25, 27, 121], on top of reactive power sharing and voltage stability, regulating the voltage amplitude at a joint load is also considered in this chapter. The above-mentioned control objectives are quintessential in a microgrid with parallel-connected inverters, i.e., a parallel microgrid, where the load is connected at the PCC [24, 34, 35].

In this regard, this chapter focuses on voltage control in lossless parallel AC microgrids and is organized as follows.

1. At first, the model of a lossless parallel microgrid is recalled from Chapter 4 with required assumptions.
2. Then, existence and uniqueness properties of a stationary positive voltage solution to the algebraic equations corresponding to steady-state accurate reactive power sharing and PCC voltage restoration are established.

3. Later, a distributed voltage control law is proposed, which at equilibrium yields the desired unique voltage solution mentioned above.

4. Finally, a stability criterion is derived by using Lyapunov theory, which guarantees asymptotic convergence of the closed-loop system trajectories to the desired equilibrium point. As it turned out to be the case that the stability criterion depends on the unknown voltage equilibrium, a sufficient condition in the form of an LMI is presented. This LMI requires only the knowledge about an upper bound of the voltage equilibrium.

The results presented in this chapter is partly based on the author's work [122].

6.2 Model of a parallel microgrid

In this section, the model of a parallel microgrid described in Chapter 4 is briefly recalled and the assumptions required for the rest of this chapter are formalized. Starting with the decoupled reactive power flow equation, model of an inverter employed for voltage control is described.

6.2.1 Decoupled reactive power flow

Consider the power flow equations in a parallel microgrid given by (4.3.1). The study presented in this chapter makes use of the standard decoupling assumption [1], which is formalized below[1].

Assumption 6.2.1. $|\delta_i(t) - \delta_{PCC}(t)| < \epsilon \quad \forall\, t \geq 0, \quad i \in \mathcal{N}, \epsilon \in \mathbb{R}_{>0}, \epsilon \ll 1.$

Under Assumption 6.2.1, $\cos(\delta_i - \delta_{\text{PCC}}) \approx 1$ and thus the reactive power flow Q_i given in (4.3.1) becomes independent of $\delta_i - \delta_{\text{PCC}}$, i.e.,

$$Q_i(V_i, V_{\text{PCC}}) = |B_i| V_i (V_i - V_{\text{PCC}}). \tag{6.2.1}$$

[1] Recall that the considered parallel microgrid is assumed to have $n > 1$ inverters connected in parallel to the PCC, where a common load is present. Furthermore, the set of inverters is denoted by $\mathcal{N} = \{1, \ldots, n\}$, see Chapter 4.

6.2.2 Inverter model for voltage control

Under Assumption 6.2.1, the reactive power injection depends only on the voltage amplitudes, see (6.2.1). Hence, in the rest of this chapter, angle dynamics in the inverter model (4.4.1) is neglected, yielding [27]

$$\begin{aligned} V_i &= u_i^V, \\ \tau_i \dot{Q}_i^m &= -Q_i^m + Q_i, \end{aligned} \tag{6.2.2}$$

where Q_i is the decoupled reactive power injection given by (6.2.1) and $u_i^V : \mathbb{R}_{\geq 0} \to \mathbb{R}$ is the voltage control input. The second equality in (6.2.2) is the power measurement dynamics corresponding to reactive power, obtained from (4.5.3).

Remark 6.2.2. *Note that in the inverter model* (6.2.2)*, the effect of clock drifts is neglected. This is explained below. Consider the model* (6.2.2) *with clock drifts, i.e.,*

$$\begin{aligned} V_i &= u_i^V, \\ \tau_i (1+\mu_i) \dot{Q}_i^m &= -Q_i^m + Q_i. \end{aligned} \tag{6.2.3}$$

Even though the clock drift value μ_i has an effect on the numerical integration of the power measurement filter in (6.2.3)*, the steady-state performance is not affected. In other words, the injected reactive power and the measured reactive power at steady-state are equal, i.e.,* $0 = -Q_i^{m^s} + Q_i^s$.

The model (6.2.2) for the whole parallel microgrid can be expressed as

$$\begin{aligned} V &= u^V, \\ \tau_Q \dot{Q}^m &= -Q^m + Q_I, \end{aligned} \tag{6.2.4}$$

where $u^V = \mathrm{col}(u_i^V) \in \mathbb{R}^n$, $Q^m = \mathrm{col}(Q_i^m) \in \mathbb{R}^n$ and $\tau_Q = \mathrm{diag}(\tau_i) \in \mathbb{R}^{n \times n}$. Furthermore,

$$Q_I(V, V_{\mathrm{PCC}}) = \mathrm{col}(Q_i(V_i, V_{\mathrm{PCC}})) = [V]BV - V_{\mathrm{PCC}}BV, \tag{6.2.5}$$

where Q_i is given by (6.2.1), $B > 0$ is defined in (4.3.5) and $[V] = \mathrm{diag}(V_i) \in \mathbb{R}^{n \times n}$. The expression for $V_{\mathrm{PCC}} = V_{\mathrm{PCC}}(V)$ is given by (4.3.6). Finally, recall that the load connected at the PCC is represented by a constant current load $I_L \in \mathbb{R}_{<0}$, see Section 4.3.2.

6.3 Problem statement

Recall the definition of accurate proportional reactive power sharing, i.e., Definition 3.3.2. Let $A = \text{diag}(a_i)$ and $Q_i^d = Q_j^d = 0$ where $i, j \in \mathcal{N}$. In practice, the desired reactive power injections are provided by a higher-level control, for example, the one proposed in [123]. Thus the assumption of $Q_i^d = Q_j^d = 0$ is for the sake of simplicity and does not affect the results presented in this chapter.

The control problems investigated in this chapter are precisely described below.

Problem 6.3.1. *Consider the system* (6.2.4), (6.2.5), (4.3.6). *Compute a control law for the control input u^V, such that the solutions of the system* (6.2.4), (6.2.5), (4.3.6) *converge asymptotically to a unique stationary voltage solution $V^* \in \mathbb{R}^n_{>0}$ with the following two properties:*

1. *Voltage regulation at the PCC, i.e.,*

$$V_{PCC}(V^*) = V_{PCC}^d \quad \textit{and} \tag{6.3.1}$$

2. *Reactive power sharing among DGs, i.e.,*

$$AQ_I(V^*, V_{PCC}(V^*)) = \alpha \mathbb{1}_n, \textit{ for some } \alpha \in \mathbb{R}. \tag{6.3.2}$$

Note that (6.3.1) is precisely (3.3.4) and (6.3.2) is (3.3.2) written for the whole network.

In comparison to some related works on voltage control [27,30,32], the consideration of a parallel microgrid topology results in a clear voltage regulation objective, i.e., 1) in Problem 6.3.1. Besides, as shown in the sequel, this type of voltage regulation objective does not conflict with that of reactive power sharing.

6.4 Existence of a unique stationary solution

Before proceeding to the controller design, existence and uniqueness properties of stationary solutions to the network equations (6.2.5), (4.3.6) under the requirements of Problem 6.3.1 has to be investigated. More precisely, this is equivalent to investigating solutions to the set of equations (6.3.1), (6.3.2). Note that (6.3.1), (6.3.2) is a system of $n+1$ equations in n unknowns, i.e., $V^* \in \mathbb{R}^n_{>0}$, hence is an

overdetermined system of nonlinear equations. Explicitly solving such an overdetermined system of nonlinear equations can be difficult. Yet, the following result shows that for any $A > 0$ and $I_L < 0$ there is exactly one $V^* \in \mathbb{R}^n_{>0}$, which satisfies (6.3.2) and (6.3.1) simultaneously.

Lemma 6.4.1. *For any given $V^d_{PCC} > 0$, $A > 0$, and $I_L < 0$, there exists a unique vector $V^* = col(V^*_i) \in \mathbb{R}^n_{>0}$ that satisfies both* (6.3.1) *and* (6.3.2).

Proof. Consider (6.3.1) and (6.3.2). Note that any $V^* \in \mathbb{R}^n_{>0}$ satisfying (6.3.1) and (6.3.2) simultaneously has to satisfy

$$AQ_I(V^*, V^d_{\mathrm{PCC}}) = \alpha \mathbb{1}_n, \tag{6.4.1}$$

which by (6.2.1) can be written as

$$a_i|B_i|(V^*_i)^2 - a_i|B_i|V^d_{\mathrm{PCC}}V^*_i - \alpha = 0, \quad i \in \mathcal{N}. \tag{6.4.2}$$

Furthermore, left-multiplying (6.4.1) with $\mathbb{1}^\top_n A^{-1}[V^*]^{-1}$ yields

$$\mathbb{1}^\top_n [V^*]^{-1} Q_I(V^*, V^d_{\mathrm{PCC}}) = -I_L = \alpha \mathbb{1}^\top_n [V^*]^{-1} A^{-1} \mathbb{1}_n, \tag{6.4.3}$$

where (6.2.5) and (4.3.4) were used to obtain the first equality. From (6.4.3) and the fact that $I_L < 0$, it is easy to see that necessarily $\alpha > 0$, which means that (6.4.2) has one negative and one positive solution for V^*_i. Denoting the latter by V^+_i, which can be calculated as

$$V^+_i = \frac{a_i|B_i|V^d_{\mathrm{PCC}} + \sqrt{(a_i|B_i|V^d_{\mathrm{PCC}})^2 + 4a_i|B_i|\alpha}}{2a_i|B_i|} := f_i(\alpha). \tag{6.4.4}$$

Now, bearing in mind (6.4.4), it remains to show that there exists a unique $\alpha > 0$ that satisfies (6.4.3), which in terms of α can be written as

$$|I_L| = \alpha \sum_{i \in \mathcal{N}} \frac{1}{a_i f_i(\alpha)} := g(\alpha). \tag{6.4.5}$$

Note that, if such α exists and is unique, then $V^* = \mathrm{col}(V^*_i) = \mathrm{col}(V^+_i)$ is the unique solution to the algebraic equations (6.3.1)-(6.3.2).

From (6.4.5), it is obvious that

$$\lim_{\alpha \to 0} g(\alpha) = 0, \qquad \lim_{\alpha \to +\infty} g(\alpha) = +\infty.$$

Hence, by continuity of g, there exists $\alpha > 0$ that satisfies (6.4.5). To prove uniqueness, it is enough to show that g is a strictly increasing function. For this purpose, differentiating $g(\alpha)$ with respect to α gives

$$g'(\alpha) = \sum_{i\in\mathcal{N}} \frac{1}{a_i f_i(\alpha)} - \alpha \sum_{i\in\mathcal{N}} \frac{f_i'(\alpha)}{a_i f_i^2(\alpha)} = \sum_{i\in\mathcal{N}} \frac{f_i(\alpha) - \alpha f_i'(\alpha)}{a_i f_i^2(\alpha)}.$$

Hence, g is strictly increasing if

$$f_i(\alpha) - \alpha f_i'(\alpha) > 0, \tag{6.4.6}$$

for each $i \in \mathcal{N}$. Observe that $f_i(\alpha)$ given by (6.4.4) is concave in $\mathbb{R}_{\geq 0}$, thereby

$$f_i(0) \leq f_i(\alpha) + f'(\alpha)(0-\alpha).$$

Noting that $f_i(0) = V_{\text{PCC}}^d > 0$, the latter inequality implies (6.4.6), hence confirming the uniqueness of $\alpha > 0$ which satisfies (6.4.5). Therefore, as discussed before, corresponding to this unique $\alpha > 0$, there exists a unique $V_i^* = f_i(\alpha)$, see (6.4.4). This yields that there exists a unique voltage vector $V^* = \text{col}(V_i^*)$ satisfying (6.3.1)-(6.3.2), completing the proof.

□

6.5 A distributed voltage control law for reactive power sharing and PCC voltage regulation

In this section, a distributed voltage control law to address Problem 6.3.1 is proposed.

6.5.1 Control law

Consider the parallel microgrid model (6.2.4), (6.2.5), (4.3.6). The control input u^V is computed such that

$$\begin{aligned} u^V &= V^d + \nu, \\ \dot{\nu} &= -K\mathscr{L}AQ^m - \left(V_{\text{PCC}}(V) - V_{\text{PCC}}^d\right) E\mathbb{1}_n, \end{aligned} \tag{6.5.1}$$

where $V^d = \text{col}(V_i^d) \in \mathbb{R}_{>0}^n$ is the vector of desired voltage amplitudes at each inverter and $\nu : \mathbb{R}_{\geq 0} \to \mathbb{R}^n$ is a new variable. Furthermore, $K = \text{diag}(k_i) \in \mathbb{R}^{n\times n}$

where $k_i \in \mathbb{R}_{>0}$ is a controller parameter, $\mathscr{L} \in \mathbb{R}^{n\times n}$ is the Laplacian matrix of a connected undirected graph and $E \in \mathbb{R}^{n\times n}$ is a diagonal *pinning gain matrix* which has positive entries only for the units which have access to the quantity $V_{\mathrm{PCC}} - V^d_{\mathrm{PCC}}$. This implies that $V_{\mathrm{PCC}} - V^d_{\mathrm{PCC}}$ is not required at all the inverters to implement (6.5.1), hence significantly relaxing the communication requirements. Obviously, the matrix E has at least one nonzero element, i.e., $E \geq 0$.

Remark 6.5.1. *Similar to the inverter model* (6.2.2)*, the effect of clock drifts on the numerical integration performed in the controller* (6.5.1) *is neglected. This is because the steady-state performance of* (6.5.1) *is not disturbed in the presence of clock drifts, which is further clarified in Lemma 6.5.3.*

6.5.2 Closed-loop system

By combining (6.2.4) and (6.5.1), the following closed-loop dynamics is obtained:

$$\begin{aligned} \dot{V} &= -K\mathscr{L}AQ^m - \left(V_{\mathrm{PCC}}(V) - V^d_{\mathrm{PCC}}\right)E\mathbb{1}_n, \\ \tau_Q \dot{Q}^m &= -Q^m + Q_I(V, V_{\mathrm{PCC}}), \end{aligned} \tag{6.5.2}$$

where $V(0) = V^d$.

Remark 6.5.2. *In practice, the voltage amplitude of a grid-forming inverter is provided by the operator. This also applies to the initial conditions of the voltages $V(0) = V^d$ in* (6.5.2)*. See also [14, 27].*

The following vectors are essential for presenting the main results of this section.

$$\begin{aligned} z &:= \mathrm{col}(V, Q^m) \in \mathbb{R}^{2n}, \\ z^* &:= \mathrm{col}(V^*, Q_I(V^*, V^d_{\mathrm{PCC}})) = \mathrm{col}(V^*, \alpha A^{-1}\mathbb{1}_n), \\ \alpha &= \frac{-I_L}{\mathbb{1}_n^\top [V^*]^{-1} A^{-1}\mathbb{1}_n} \in \mathbb{R}_{>0}, \end{aligned} \tag{6.5.3}$$

where (6.4.1) and (6.4.3) were used to write the last two equalities. The lemma below presents an important property about the point z^*.

Lemma 6.5.3. *The vector z^* given by* (6.5.3) *is the unique equilibrium point of the closed-loop system* (6.5.2)*.*

Proof. In the proof of Lemma 6.4.1, it has been shown that satisfying (6.3.1) and (6.3.2) yields a unique solution V^*. In addition, since $\mathscr{L}$ is the Laplacian matrix of

a connected undirected graph, recall that $\mathscr{L}\mathbb{1}_n = \mathbb{0}_n$. As a consequence, at $z = z^*$, the system (6.5.2) is at equilibrium.

Next, to show that z^* is the only equilibrium point of the system (6.5.2), the concept of contradiction is used. Suppose that for the system (6.5.2), there exists another equilibrium solution $z^s := \text{col}(V^s, Q^{ms}) \in \mathbb{R}^{2n}$, i.e.,

$$\begin{aligned} \mathbb{0}_n &= -K\mathscr{L}AQ^{ms} - \left(V_{\text{PCC}}(V^s) - V^d_{\text{PCC}}\right) E\mathbb{1}_n, \\ \mathbb{0}_n &= -Q^{ms} + Q_I(V^s, V_{\text{PCC}}(V^s)), \end{aligned} \tag{6.5.4}$$

which readily yields

$$\mathbb{0}_n = K\mathscr{L}AQ_I\left(V^s, V_{\text{PCC}}(V^s)\right) + \left(V_{\text{PCC}}(V^s) - V^d_{\text{PCC}}\right) E\mathbb{1}_n. \tag{6.5.5}$$

Since $K = \text{diag}(k_i) > 0$, left-multiplying (6.5.5) with $\mathbb{1}_n^\top K^{-1}$ yields

$$\left(V_{\text{PCC}}(V^s) - V^d_{\text{PCC}}\right) \text{trace}(K^{-1}E) = 0. \tag{6.5.6}$$

Recall that E is a diagonal positive semidefinite matrix. Hence $\text{trace}(K^{-1}E) > 0$, which implies that (6.5.6) is satisfied if and only if $V_{\text{PCC}}(V^s) = V^d_{\text{PCC}}$. But this implies that V^s also has to satisfy

$$\mathscr{L}AQ_I(V^s, V_{\text{PCC}}(V^s)) = \mathbb{0}_n. \tag{6.5.7}$$

Since $\mathscr{L}$ is the Laplacian matrix of an undirected connected graph, (6.5.7) is equivalent to

$$Q_I(V^s, V_{\text{PCC}}(V^s)) = \beta A^{-1}\mathbb{1}_n, \tag{6.5.8}$$

for some $\beta \in \mathbb{R}$. From Lemma 6.4.1, it follows that there is only one solution, which is V^*, that satisfies $V_{\text{PCC}}(V^s) = V^d_{\text{PCC}}$ and (6.5.8) simultaneously. Consequently, $V^s = V^*$ and (6.5.8) becomes $Q_I(V^*, V_{\text{PCC}}(V^*)) = \alpha A^{-1}\mathbb{1}_n$ where α is given by (6.5.3). From the second equation in (6.5.4), this yields $Q^{ms} = \alpha A^{-1}\mathbb{1}_n$. In essence, $z^s := \text{col}(V^s, Q^{ms}) = \text{col}(V^*, \alpha A^{-1}\mathbb{1}_n) = z^*$. This completes the proof. □

Remark 6.5.4. *The distributed voltage controller (DVC) proposed in [27] to address the problem of reactive power sharing in lossless meshed microgrids is given by by [27, Equation 12]*

$$\begin{aligned} \dot{V} &= -K\mathscr{L}AQ^m, \\ \tau_Q\dot{Q}^m &= -Q^m + Q_I^{meshed}(V), \end{aligned} \tag{6.5.9}$$

where $Q_I^{meshed}(V) = col(Q_i) \in \mathbb{R}^n$ with Q_i given by (2.4.5)*. Note that* (6.5.2) *is similar to* (6.5.9)*, but has a noticeable difference. More precisely,* (6.5.2) *is designed for a lossless parallel microgrid where the objective of PCC voltage regulation is also considered.*

6.5.3 Error states

In the sequel, the vector $z = \mathrm{col}(V, Q^m)$ is expressed with respect to the unique equilibrium point $z^* = \mathrm{col}(V^*, \alpha A^{-1}\mathbb{1}_n)$, i.e.,

$$\begin{aligned} \tilde{Q}^m &:= Q^m - \alpha A^{-1}\mathbb{1}_n, \\ \tilde{V} &:= V - V^*, \\ x &:= \mathrm{col}(\tilde{V}, \tilde{Q}^m) \in \mathbb{R}^{2n}. \end{aligned} \tag{6.5.10}$$

Thus, the closed-loop system (6.5.2) in error states x can be expressed as

$$\begin{aligned} \dot{\tilde{V}} &= -K\mathscr{L}A\tilde{Q}^m - \left(V_{\mathrm{PCC}}(\tilde{V} + V^*) - V_{\mathrm{PCC}}(V^*)\right) E\mathbb{1}_n, \\ \tau_Q \dot{\tilde{Q}}^m &= -\tilde{Q}^m + \left(Q_I\left(\tilde{V} + V^*, V_{\mathrm{PCC}}(\tilde{V} + V^*)\right) - Q_I\left(V^*, V_{\mathrm{PCC}}(V^*)\right)\right). \end{aligned} \tag{6.5.11}$$

Note that with Q_I given in (6.2.5),

$$\begin{aligned} Q_I\left(\tilde{V} + V^*, V_{\mathrm{PCC}}(\tilde{V} + V^*)\right) - Q_I\left(V^*, V_{\mathrm{PCC}}(V^*)\right) &= [\tilde{V} + V^*]B(\tilde{V} + V^*) \\ &\quad - V_{\mathrm{PCC}}(\tilde{V} + V^*)B(\tilde{V} + V^*) \\ &\quad - [V^*]BV^* + V_{\mathrm{PCC}}(V^*)BV^*, \\ &= [\tilde{V} + 2V^*]B\tilde{V} - V_{\mathrm{PCC}}(\tilde{V} + V^*)B\tilde{V} \\ &\quad - \left(V_{\mathrm{PCC}}(\tilde{V} + V^*) - V_{\mathrm{PCC}}(V^*)\right)BV^*, \\ &= \left([\tilde{V} + 2V^*] - V_{\mathrm{PCC}}(\tilde{V} + V^*)I_n\right)B\tilde{V} \\ &\quad - \left(V_{\mathrm{PCC}}(\tilde{V} + V^*) - V_{\mathrm{PCC}}(V^*)\right)BV^*. \end{aligned} \tag{6.5.12}$$

By using (6.5.12), the closed-loop system (6.5.11) becomes

$$\begin{aligned} \dot{\tilde{V}} &= -K\mathscr{L}A\tilde{Q}^m - \left(V_{\mathrm{PCC}}(\tilde{V} + V^*) - V_{\mathrm{PCC}}(V^*)\right) E\mathbb{1}_n, \\ \tau_Q \dot{\tilde{Q}}^m &= -\tilde{Q}^m + \left([\tilde{V} + 2V^*] - V_{\mathrm{PCC}}(\tilde{V} + V^*)I_n\right)B\tilde{V} \\ &\quad - \left(V_{\mathrm{PCC}}(\tilde{V} + V^*) - V_{\mathrm{PCC}}(V^*)\right)B[V^*]\mathbb{1}_n, \end{aligned} \tag{6.5.13}$$

where

$$x^* := \mathbb{0}_{2n} \tag{6.5.14}$$

is the equilibrium point of (6.5.13). Note that x^* is just a shift of coordinates from the unique equilibrium point z^* defined in (6.5.3). Hence, asymptotic stability of x^* implies that the trajectories of the closed-loop system (6.5.2) converge asymptotically to z^*.

6.5.4 A condition for asymptotic stability

For presenting the stability results, it is convenient to define the following matrix.

$$\Phi(V^*) := \begin{bmatrix} \Phi_{11} & \Phi_{12} & \Phi_{13} \\ * & \Phi_{22} & \Phi_{23} \\ * & * & \text{trace}(BE) \end{bmatrix} \in \mathbb{R}^{(2n+1)\times(2n+1)}, \tag{6.5.15}$$

where

$$\begin{aligned}
\Phi_{11}(V^*) &= \sigma R \tau_Q^{-1} \left(2[V^*] - V_{\text{PCC}}^d I_n\right) B, \\
\Phi_{12}(V^*) &= \frac{1}{2}\left(\xi M K \mathscr{L} A - \zeta \left(2[V^*] - V_{\text{PCC}}^d I_n\right) B - \sigma R \tau_Q^{-1}\right), \\
\Phi_{13}(V^*) &= \frac{1}{2}\left(\xi M E \mathbb{1}_n - \sigma R \tau_Q^{-1} B[V^*]\mathbb{1}_n\right), \\
\Phi_{22} &= \zeta I_n - \frac{\sigma}{2}\left(RK\mathscr{L}A + A\mathscr{L}KR\right), \\
\Phi_{23}(V^*) &= \frac{1}{2}\left(A\mathscr{L}KB\mathbb{1}_n - \sigma R E \mathbb{1}_n + \zeta B[V^*]\mathbb{1}_n\right),
\end{aligned}$$

where $\xi \in \mathbb{R}_{>0}$, $\sigma \in \mathbb{R}_{>0}$, $\zeta \in \mathbb{R}_{>0}$, and $R \in \mathbb{R}^{n\times n}$, $M \in \mathbb{R}^{n\times n}$ are two positive definite diagonal matrices.

The stability result is as follows.

Proposition 6.5.5. *Consider the closed-loop system* (6.5.13). *Suppose that there exist* $\xi \in \mathbb{R}_{>0}$, $\sigma \in \mathbb{R}_{>0}$, $\zeta \in \mathbb{R}_{>0}$ *and positive definite diagonal matrices* $R \in \mathbb{R}^{n\times n}$ *and* $M \in \mathbb{R}^{n\times n}$. *Then,* x^* *is locally asymptotically stable if* K, E *and* $\mathscr{L}$ *are chosen such that*

$$\begin{aligned}
\begin{bmatrix} \xi M + \frac{1}{\text{trace}(B)} B\mathbb{1}_n\mathbb{1}_n^\top B & -\sigma R \\ -\sigma R & \zeta \tau_Q \end{bmatrix} > 0, \\
\Phi(V^*) > 0,
\end{aligned} \tag{6.5.16}$$

where $\Phi(V^*)$ *is given by* (6.5.15).

Proof. Consider the Lyapunov function candidate

$$\begin{aligned}
\mathscr{F}(x) = \frac{\xi}{2}\tilde{V}^\top M \tilde{V} + \frac{1}{2}\left(V_{\text{PCC}}(\tilde{V} + V^*) - V_{\text{PCC}}(V^*)\right)^2 \text{trace}(B) \\
+ \frac{\zeta}{2}\tilde{Q}^{m\top}\tau_Q \tilde{Q}^m - \sigma \tilde{Q}^{m\top} R \tilde{V},
\end{aligned} \tag{6.5.17}$$

where $\xi \in \mathbb{R}_{>0}$, $\zeta \in \mathbb{R}_{>0}$ and $\sigma \in \mathbb{R}_{>0}$. Furthermore $R \in \mathbb{R}^{n\times n}$ and $M \in \mathbb{R}^{n\times n}$ are positive definite diagonal matrices. The function (6.5.17) has three quadratic

terms in $\tilde{V}$, V_{PCC} (in error states) and $\tilde{Q}^m$ respectively. A cross term between $\tilde{V}$ and $\tilde{Q}^m$ is also included in $\mathscr{F}$, since it facilitates that the function $\mathscr{F}$ is decreasing along the solutions of (6.5.13).

Observe that $\mathscr{F}(x^*) = 0$. Moreover with V_{PCC} given by (4.3.6), the gradient of $\mathscr{F}$ with respect to x can be calculated as

$$\nabla_x \mathscr{F} = \begin{bmatrix} \xi M\tilde{V} + \big(V_{\mathrm{PCC}}(\tilde{V}+V^*) - V_{\mathrm{PCC}}(V^*)\big) B\mathbb{1}_n - \sigma R\tilde{Q}^m \\ \zeta\tau_Q\tilde{Q}^m - \sigma R\tilde{V} \end{bmatrix}. \tag{6.5.18}$$

Evaluating the gradient at $x = x^*$, it can be seen that $\nabla_x \mathscr{F}|_{x^*} = \mathbb{0}_{2n}$. Therefore, x^* is a critical point of $\mathscr{F}$ [49, 50].

The Hessian of $\mathscr{F}$ at $x = x^*$ is given by

$$\nabla_x^2 \mathscr{F}|_{x^*} = \begin{bmatrix} \xi M + \frac{1}{\mathrm{trace}(B)} B\mathbb{1}_n\mathbb{1}_n^\top B & -\sigma R \\ -\sigma R & \zeta\tau_Q \end{bmatrix}. \tag{6.5.19}$$

Recall that $M > 0$, $\xi > 0$ and $\tau_Q > 0$. Furthermore since $B > 0$, the matrix $B\mathbb{1}_n\mathbb{1}_n^\top B$ is positive semidefinite. Thus, both block-diagonal matrices of $\nabla_x^2 \mathscr{F}|_{x^*}$ are positive definite. Therefore, under the standing assumption that the first condition in (6.5.16) is satisfied, the LHS of (6.5.19) is positive definite, confirming that x^* is an isolated minimum of $\mathscr{F}$. Hence, $\mathscr{F}$ qualifies as a potential Lyapunov function to study stability of x^* [49, 50].

Calculating the time derivative of $\mathscr{F}$ along the solutions of (6.5.13) yields

$$\begin{aligned} \dot{\mathscr{F}} = &-\xi\tilde{V}^\top MK\mathscr{L}A\tilde{Q}^m \\ &-\xi\tilde{V}^\top ME\mathbb{1}_n\big(V_{\mathrm{PCC}}(\tilde{V}+V^*) - V_{\mathrm{PCC}}(V^*)\big) \\ &-\big(V_{\mathrm{PCC}}(\tilde{V}+V^*) - V_{\mathrm{PCC}}(V^*)\big)\mathbb{1}_n^\top BK\mathscr{L}A\tilde{Q}^m \\ &-\mathbb{1}_n^\top BE\mathbb{1}_n\big(V_{\mathrm{PCC}}(\tilde{V}+V^*) - V_{\mathrm{PCC}}(V^*)\big)^2 \\ &+\sigma\tilde{Q}^{m\top}RK\mathscr{L}A\tilde{Q}^m \\ &+\sigma\tilde{Q}^{m\top}RE\mathbb{1}_n\big(V_{\mathrm{PCC}}(\tilde{V}+V^*) - V_{\mathrm{PCC}}(V^*)\big) \\ &-\zeta\tilde{Q}^{m\top}\tilde{Q}^m \\ &+\zeta\tilde{Q}^{m\top}\big([\tilde{V}+2V^*] - V_{\mathrm{PCC}}(\tilde{V}+V^*)I_n\big)B\tilde{V} \\ &-\zeta\tilde{Q}^{m\top}B[V^*]\mathbb{1}_n\big(V_{\mathrm{PCC}}(\tilde{V}+V^*) - V_{\mathrm{PCC}}(V^*)\big) \\ &+\sigma\tilde{V}^\top R\tau_Q^{-1}\tilde{Q}^m \\ &-\sigma\tilde{V}^\top R\tau_Q^{-1}\big([\tilde{V}+2V^*] - V_{\mathrm{PCC}}(\tilde{V}+V^*)I_n\big)B\tilde{V} \\ &+\sigma\tilde{V}^\top R\tau_Q^{-1}B[V^*]\mathbb{1}_n\big(V_{\mathrm{PCC}}(\tilde{V}+V^*) - V_{\mathrm{PCC}}(V^*)\big) \\ = &-\eta^\top\Phi(\tilde{V})\eta, \end{aligned} \tag{6.5.20}$$

where

$$\eta := \begin{bmatrix} \tilde{V} \\ \tilde{Q}^m \\ \left(V_{\mathrm{PCC}}(\tilde{V}+V^*) - V_{\mathrm{PCC}}(V^*)\right) \end{bmatrix} \in \mathbb{R}^{2n+1}, \tag{6.5.21}$$

and

$$\Phi(\tilde{V}) := \begin{bmatrix} \Phi_{11} & \Phi_{12} & \Phi_{13} \\ * & \Phi_{22} & \Phi_{23} \\ * & * & \mathrm{trace}(BE) \end{bmatrix} \in \mathbb{R}^{(2n+1)\times(2n+1)}, \tag{6.5.22}$$

with

$$\begin{aligned}
\Phi_{11}(\tilde{V}) &= \sigma R \tau_Q^{-1} \left([\tilde{V} + 2V^*] - V_{\mathrm{PCC}}(\tilde{V}+V^*) I_n \right) B, \\
\Phi_{12}(\tilde{V}) &= \frac{1}{2} \left(\xi M K \mathscr{L} A - \sigma R \tau_Q^{-1} - \zeta B \left([\tilde{V} + 2V^*] - V_{\mathrm{PCC}}(\tilde{V}+V^*) I_n \right) \right), \\
\Phi_{13}(V^*) &= \frac{1}{2} \left(\xi M E \mathbb{1}_n - \sigma R \tau_Q^{-1} B [V^*] \mathbb{1}_n \right), \\
\Phi_{22} &= \zeta I_n - \frac{\sigma}{2} \left(R K \mathscr{L} A + A \mathscr{L} K R \right), \\
\Phi_{23}(V^*) &= \frac{1}{2} \left(A \mathscr{L} K B \mathbb{1}_n - \sigma R E \mathbb{1}_n + \zeta B [V^*] \mathbb{1}_n \right).
\end{aligned}$$

Note that

$$\Phi(\tilde{V})|_{\tilde{V}=\mathbb{0}_n} = \Phi(V^*),$$

where $\Phi(V^*)$ is defined in (6.5.15). Under the premises of Proposition 6.5.5, see (6.5.16),

$$\Phi(\tilde{V})|_{\tilde{V}=\mathbb{0}_n} > 0.$$

Thus by continuity, there exists a (small) neighborhood around $\tilde{V} = \mathbb{0}_n$ such that $\Phi(\tilde{V}) > 0$, and, thus, $\dot{\mathscr{F}} \leq 0$. Hence, x^* is a stable equilibrium point.

To establish asymptotic stability of x^*, the following implication has to hold along the solutions of the system (6.5.13):

$$\eta = \mathbb{0}_{2n+1} \quad \Rightarrow \quad x(t) = x^* \tag{6.5.23}$$

Since $\Phi(\tilde{V}) > 0$, and with η defined in (6.5.21), $\eta = \mathbb{0}_{2n+1}$ directly implies that $\tilde{V} = \mathbb{0}_n$ and $\tilde{Q}^m = \mathbb{0}_n$. By using the definition of x and x^* given respectively by (6.5.10) and (6.5.14), $\tilde{V} = \mathbb{0}_n$ and $\tilde{Q}^m = \mathbb{0}_n$ means that $x = \mathbb{0}_{2n} = x^*$. As a consequence, the implication (6.5.23) holds, ensuring that x^* is locally asymptotically stable. This completes the proof. □

The stability condition $\Phi(V^*) > 0$ given in (6.5.16) depends on the equilibrium voltage vector V^*. As mentioned earlier in Lemma 6.4.1, solving for V^* explicitly from the set of algebraic equations (6.3.1), (6.3.2) is difficult. Hence, unfortunately, to verify $\Phi(V^*) > 0$, an expression for V^* in terms of the system parameters is missing. Thus in the sequel, a tuning criterion in the form of an LMI in K and E is presented, which if feasible, guarantees $\Phi(V^*) > 0$. This LMI requires only the knowledge about an upper bound of V^*, i.e.,

$$\|[V^*]\|_2 \leq \varrho, \quad \varrho \in \mathbb{R}_{>0}. \tag{6.5.24}$$

A possible practical choice for ϱ would be to select it as the maximum admissible voltage amplitude in the network, see e.g., [124].

The following matrices are required for presenting the next result.

$$\begin{aligned} U_1(V^*) &:= \text{blockdiag}([V^*] - V^d_{\text{PCC}} I_n, \mathbb{0}_{n\times n}, 0), \\ U_2 &:= \begin{bmatrix} -2\sigma R\tau_Q^{-1} B & 2\zeta B & \mathbb{0}_{n\times 1} \\ \mathbb{0}_{n\times n} & \mathbb{0}_{n\times n} & \mathbb{0}_{n\times 1} \\ \mathbb{0}_{1\times n} & \mathbb{0}_{1\times n} & 0 \end{bmatrix}, \\ J_1(V^*) &:= \text{blockdiag}([V^*], [V^*], 0), \\ J_2 &:= \begin{bmatrix} \mathbb{0}_{n\times n} & \mathbb{0}_{n\times n} & \sigma R\tau_Q^{-1} B\mathbb{1}_n \\ \mathbb{0}_{n\times n} & \mathbb{0}_{n\times n} & -\zeta B\mathbb{1}_n \\ \mathbb{0}_{1\times n} & \mathbb{0}_{1\times n} & 0 \end{bmatrix}, \end{aligned} \tag{6.5.25}$$

where $U_1, U_2, J_1, J_2 \in \mathbb{R}^{(2n+1)\times(2n+1)}$. Furthermore, $\Psi \in \mathbb{R}^{(2n+1)\times(2n+1)}$ is defined as

$$\Psi := \begin{bmatrix} \sigma V^d_{\text{PCC}} R\tau_Q^{-1} B & \frac{1}{2}\left(\xi MK\mathscr{L}A - \sigma R\tau_Q^{-1} - \zeta V^d_{\text{PCC}} B\right) & \frac{1}{2}\xi ME\mathbb{1}_n \\ * & \zeta I_n - \frac{\sigma}{2}(RK\mathscr{L}A + A\mathscr{L}KR) & \frac{1}{2}(A\mathscr{L}KB\mathbb{1}_n - \sigma RE\mathbb{1}_n) \\ * & * & \text{trace}(BE) \end{bmatrix}. \tag{6.5.26}$$

A sufficient condition which guarantees $\Phi(V^*) > 0$ is as follows.

Corollary 6.5.6. *Consider the closed-loop system* (6.5.13) *and the Lyapunov function* (6.5.17). *Suppose that ξ, σ, ζ, M and R are fixed such that the first condition in* (6.5.16) *is satisfied. Then, x^* is locally asymptotically stable if the controller parameters K and E are chosen such that*

$$\Psi > \left((\varrho - V^d_{PCC})\|U_2\|_2 + \varrho\|J_2\|_2\right) I_{2n+1}, \tag{6.5.27}$$

where U_2 and J_2 are defined in (6.5.25), *Ψ in* (6.5.26) *and ϱ is the upper bound of V^* mentioned in* (6.5.24).

Proof. Consider the system (6.5.13). Choosing the same Lyapunov function (6.5.17) and following similar steps as in the proof of Proposition 6.5.5, it can be observed that a sufficient condition for x^* to be an isolated minimum of $\mathscr{F}$ is given by the first condition in (6.5.16). Therefore, under the premises of Corollary 6.5.6, local asymptotic stability of x^* can be ensured if $\Phi(V^*) > 0$, i.e., the second condition in (6.5.16).

Consider $\Phi(V^*)$ given by (6.5.15), which can be equivalently expressed as

$$\Phi(V^*) = \Psi - \frac{1}{2}\left(U_1(V^*)U_2 + U_2^\top U_1(V^*)\right) - \frac{1}{2}\left(J_1(V^*)J_2 + J_2^\top J_1(V^*)\right), \tag{6.5.28}$$

where U_1, U_2, J_1, J_2 are defined in (6.5.25) and Ψ is defined in (6.5.26). The intension behind expressing $\Phi(V^*)$ as in (6.5.28) is to derive a sufficient condition that ensures $\Phi(V^*) > 0$.

For any two square matrices, say $X \in \mathbb{R}^{n\times n}$ and $Y \in \mathbb{R}^{n\times n}$, it follows that [84]

$$\frac{1}{2}\left(XY + Y^\top X^\top\right) \leq \|X\|_2 \|Y\|_2 I_n.$$

Thus, a sufficient condition for $\Phi(V^*) > 0$ is given by

$$\Psi > \left(\|U_1(V^*)\|_2 \|U_2\|_2 + \|J_1(V^*)\|_2 \|J_2\|_2\right) I_{2n+1}. \tag{6.5.29}$$

Since U_1 and J_1 defined in (6.5.25) are block diagonal matrices with diagonal block entries, $\|U_1\|_2$ and $\|J_1\|_2$ can be calculated as

$$\|U_1\|_2 = \sqrt{\lambda_{\max}\left(([V^*] - V^d_{\mathrm{PCC}} I_n)^2\right)} \leq \varrho - V^d_{\mathrm{PCC}},$$
$$\|J_1\|_2 = \sqrt{\lambda_{\max}\left([V^*]^2\right)} \leq \varrho,$$

where in the inequality above, the fact that $[V^*]$ is a diagonal matrix upper-bounded by ϱ (see (6.5.24)) has been used. As a consequence, the RHS of (6.5.29) can be lower bounded by the RHS of (6.5.27), completing the proof. □

Remark 6.5.7. *Note that the matrices U_2 and J_2 defined in* (6.5.25) *contain only the system parameters τ_Q, B and the tuning parameters σ, ζ and R, which stem from the Lyapunov function* (6.5.17). *Hence, $\|U_2\|_2$ and $\|J_2\|_2$ required in* (6.5.27) *can be computed directly. Thus,* (6.5.27) *is an LMI in K and E, which can be solved by using a standard software package like Yalmip [120] within MATLAB®.*

6.6 Summary

The problems of voltage stability, reactive power sharing, and PCC voltage restoration in a lossless parallel microgrid have been addressed in this chapter. Starting with the proof about the existence of a unique voltage equilibrium, a distributed voltage controller which drives the closed-loop system solutions asymptotically to the desired equilibrium has been presented. Alas, the derived stability criterion depends on the voltage equilibrium. Thus, a sufficient condition that ensures the feasibility of the stability criterion has been derived. This sufficient condition requires only the knowledge about an upper bound of the voltage equilibrium and is in the form of an LMI, which can be solved numerically to obtain stabilizing controller parameters.

Chapter 7

Case study

7.1 Introduction

This chapter is dedicated to validate, via simulation, robustness of the approaches presented in Chapter 5 and Chapter 6 towards typical modeling uncertainties and some exogenous disturbances observed in microgrids.

At first, the performance and robustness of the GDAI controller proposed in Chapter 5 towards modeling uncertainties are investigated. The controller parameters are chosen based on the tuning criterion presented in Chapter 5. Furthermore, the results are compared with other distributed secondary frequency controllers in the literature; for example, the DAI control [32, 51] and the pinning control [40].

The second part of this chapter focusses on investigating whether the distributed voltage controller proposed in Chapter 6 is robust towards load disturbances and modeling errors like small line resistances. The operational compatibility of the proposed voltage controller with the standard frequency droop control [38] is also examined.

Throughout this chapter, the terms *weighted active power*, respectively *weighted reactive power* represent the fraction $(P_i - P_i^d)/S_i^N$, respectively Q_i/S_i^N where P_i, respectively Q_i are the active, respectively reactive power injections. Furthermore, $S_i^N \in \mathbb{R}_{>0}$ is the nominal power rating and $P_i^d \in \mathbb{R}$ is the desired active power set point at the i-th inverter, $i \in \mathcal{N}$.

7.2 Distributed secondary frequency control

In this section, via simulation, steady-state performance of the GDAI-controlled system (5.3.1), (5.6.2), the DAI-controlled system (5.3.1), (5.3.9) and the pinning-controlled system (5.3.1), (5.3.10) are compared in the presence of clock drifts.

The microgrid used in the case study is depicted in Figure 7.1, which is simulated using MATLAB®/Simulink® and PLECS [125]. Power lines are modelled as dynamic π-models [1, 4, 89]. Since the microgrids under consideration are assumed to have short power lines, shunt elements in the π-model are neglected [1, 4, 89]. See also [23, Section 2.4.4]. Small positive line resistance is considered in the power lines to evaluate robustness towards typical uncertainties. Furthermore, a constant impedance load of 500 kVA (unity power factor) is connected to all grid-forming inverters (GFIs). The time constant of the low pass filter used in the power measurement is 0.2 sec. To measure the synchronized electrical frequency ω^* (given by (5.5.1)) of the considered microgrid accurately, a conventional three-phase synchronous reference frame phase locked loop (SRF-PLL) [126] is connected at the PCC.

The weighting matrix $\mathscr{X}$ for the microgrid is selected as (in pu)

$$\mathscr{X} = \text{diag}(0.48, 0.46, 0.52, 0.53, 0.51, 0.53, 0.45, 0.54), \tag{7.2.1}$$

and the vector of desired active power set points as (in pu)

$$P^d = \text{col}(0.25, 0.35, 0.45, 0.55, 0.65, 0.75, 0.80, 0.85). \tag{7.2.2}$$

The damping matrix D required in (5.3.1) is chosen according to (5.2.14) with $\kappa = 0.5$. Furthermore, the incidence matrix $\mathscr{B}$ of the communication graph is calculated from the topology shown in Figure 7.2. It is worth mentioning that there might be other choices of $\mathscr{B}$ to construct the Laplacian matrix $\mathscr{L}$. See, e.g. [64, 65] for a comprehensive study on topology identification to implement similar distributed frequency control laws in power systems. Finding a suitable communication topology to implement distributed secondary frequency controllers is beyond the scope of this thesis. In this section, the intention is to calculate the controller parameters $\mathbf{D}$, $\mathbf{B}$ and the edge weight matrix $\mathbf{W}$ yielding $\mathscr{L} = \mathscr{B}\mathbf{W}\mathscr{B}^\top$ which satisfy the LMIs (5.7.5) and (5.7.6).

The clock of the GFI connected at node 1 in Figure 7.1 is chosen as the master clock, i.e., $\mu_1 = 0$. The relative clock drift values of the other GFIs considered in the simulation are

$$\mu = 10^{-4}\text{diag}(0, 10, 20, -10, 25, 15, -15, 5) \in \mathbb{R}^{8\times 8}. \tag{7.2.3}$$

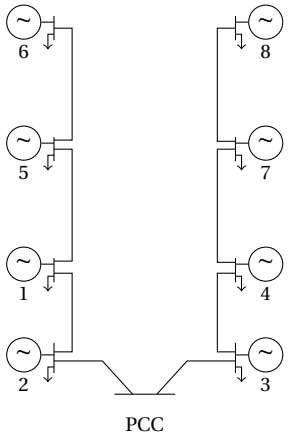

Figure 7.1. Microgrid used to simulate distributed frequency controllers. There are eight grid-forming inverters (GFIs), all of them having a constant impedance load connected to them. At the PCC, a phase locked loop (PLL) is connected to measure the synchronized electrical frequency of the network (i.e., ω^* given by (5.5.1)) accurately. GFI1 is chosen as the master clock, see (7.2.3).

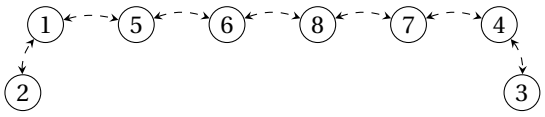

Figure 7.2. Topology of the communication network used to simulate distributed frequency controllers.

Hence, with the considered clock drift factors, $\epsilon = 0.003$ in Assumption 5.3.4.

The tuning criterion (5.7.5), (5.7.6) presented in Proposition 5.7.1 is verified using the optimization toolbox Yalmip [120] in MATLAB®/Simulink®. The conditions (5.7.5), (5.7.6) were solved with $\sigma = 0.12$, where the tuning parameter ς and the controller parameters **D**, **B** and **W** were the free parameters in the LMIs. Feasibility of (5.7.5), (5.7.6) ensures that the trajectories of the system (5.3.1), (5.6.2) asymptotically converge to a desired synchronized motion given in Definition 5.3.2.

The controller parameters satisfying (5.7.5), (5.7.6) were obtained as

$$\begin{aligned} \mathbf{D} &= \mathrm{diag}(0.10, 0.40, 0.07, 0.10, 0.10, 0.31, 0.38, 0.20), \\ \mathbf{B} &= \mathrm{diag}(0.16, 0, 0, 0, 0, 0, 0, 0), \\ \mathbf{W} &= \mathrm{diag}(1.23, 0.42, 0.53, 0.59, 0.68, 0.38, 0.52). \end{aligned} \tag{7.2.4}$$

Next, the microgrid shown in Figure 7.1 is simulated using the parameters (7.2.4).

7.2.1 GDAI control

The GDAI-controlled system (5.3.1), (5.6.2) is simulated using the control parameters (7.2.4). The simulation output is given in Figure 7.3 where until 10 sec, only the frequency droop control is under operation, i.e., (5.3.1) with $u = \mathbb{0}_8$.

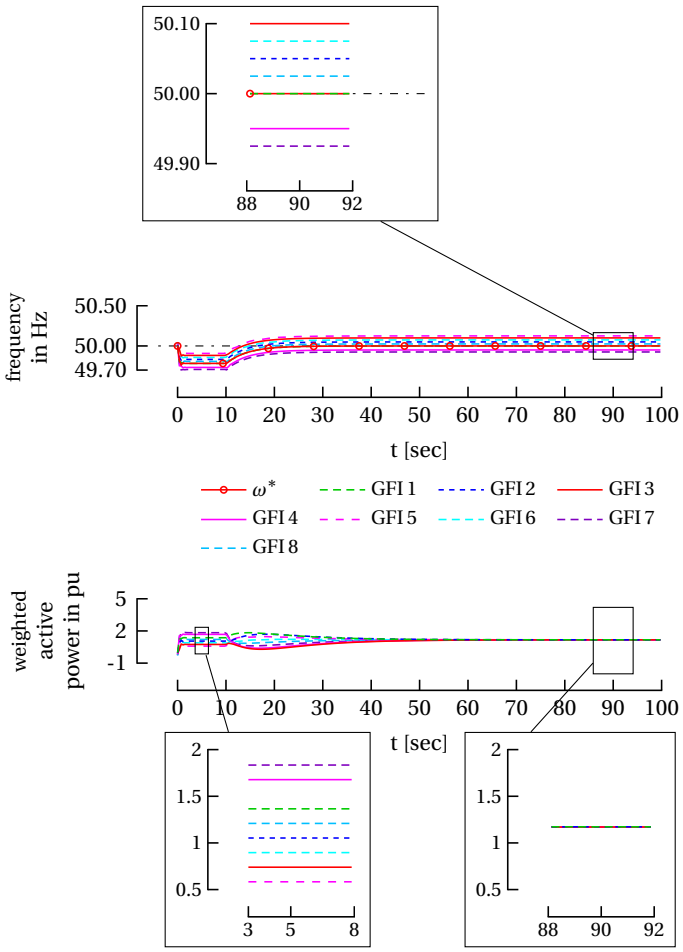

Figure 7.3. Simulation result with droop control (5.3.1) (active from 0 sec) and GDAI control (5.6.2) (activated at 10 sec). Note that ω^* converges exactly to 50 Hz and the weighted active powers reach consensus, see the zoom plots at 90 sec.

The GDAI control (5.6.2) is activated at 10 sec. Recall that (5.6.2) satisfies the conditions of Lemma 5.5.1. Hence, $\omega^* = \omega^d$. See the enlarged frequency plot at 90 sec in Figure 7.3 where it can be seen that $\omega^* = 50\text{Hz} = \omega^d$. Furthermore, since the GDAI control also satisfies the conditions of Lemma 5.6.1, steady-state active power sharing is guaranteed in the presence of clock drifts. This can be confirmed by observing the enlarged weighted active power plot in Figure 7.3 at

90 sec, where, it is clear that the weighted active powers of all the inverters have converged to a common value. For better clarity, compare the enlarged weighted active power plots at 5 sec (droop control only: maximum relative deviation of approximately 42%) and 90 sec (droop and GDAI control: 0% relative deviation) in Figure 7.3. This confirms that the GDAI controller can correct steady-state errors in active power sharing.

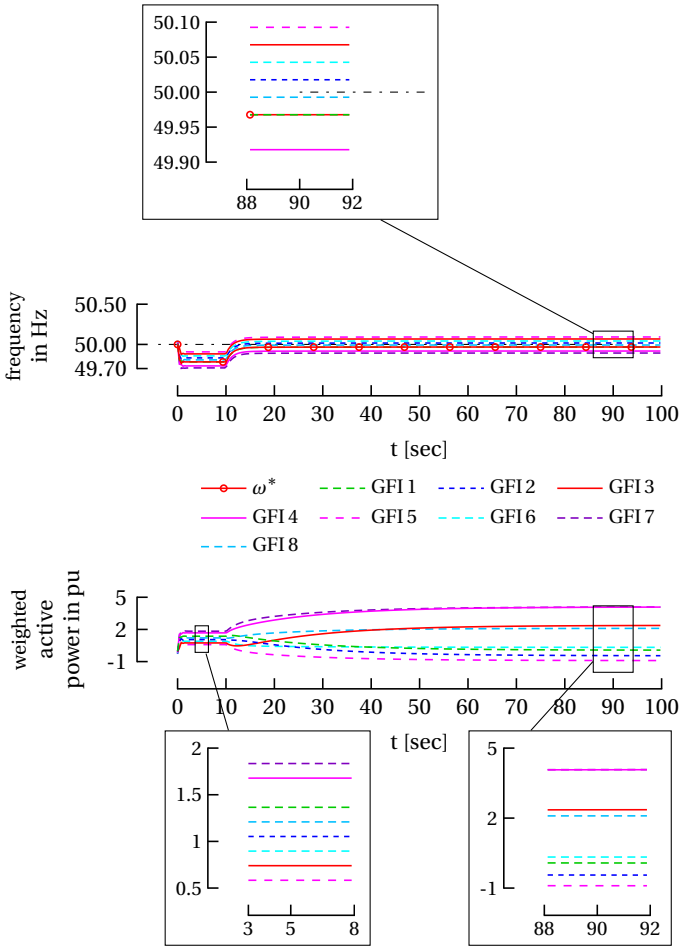

Figure 7.4. Simulation result with droop control (5.3.1) (active from 0 sec) and DAI control (5.3.9) (activated at 10 sec). Note that ω^* does not converge to 50 Hz and the the weighted active powers do not reach consensus. See the zoom plots at 90 sec.

For comparing the steady-state behavior of the GDAI control with other distributed control approaches, the DAI control and the pinning control are also simulated using the same microgrid shown in Figure 7.1. For this purpose, communication topology shown in Figure 7.2 is used.

7.2.2 DAI control

In this section the DAI-controlled system (5.3.1), (5.3.9) is simulated. The same parameters as in (7.2.4) are used, with the only exception that

$$\mathbf{B} = (0.16) \cdot I_8.$$

See also (5.3.9). The corresponding simulation output is given in Figure 7.4, where until 10 sec, only the frequency droop control (5.3.1) is under operation. The DAI controller (5.3.9) is activated at 10 sec. In Figure 7.4, it can be seen that the inverters' internal frequencies have converged close to the nominal value of $\omega^d = 50$ Hz, but not exactly to 50 Hz in the presence of clock drifts. The enlarged frequency plot in Figure 7.4 at 90 sec shows that $\omega^* \approx 49.97 \neq 50$ Hz, hence resulting in a non-negligible steady-state network frequency error of approximately 30 mHz.

Considering the aspect of active power sharing, at 10 sec, when the DAI controller is activated on top of the droop controller, it can be observed that the weighted active powers diverge a bit. See the weighted active power plot in Figure 7.4 at 5 sec (droop control: maximum relative deviation of approximately 42%) and 90 sec (droop and DAI control: maximum relative deviation of approximately 80%) respectively. An observation from Figure 7.4 is that the steady-state performance in terms of active power sharing in the presence of clock drifts is relatively better with frequency droop control than a combination of droop and DAI controllers.

7.2.3 Pinning control

In this section, the pinning-controlled system (5.3.1), (5.3.10) is simulated. The controller parameters used are the same as in (7.2.4). The simulation output is given in Figure 7.5, where until 10 sec, only the frequency droop control is under operation. The pinning controller is activated at 10 sec. Recall that $\mathbf{B} \geq 0$, see (5.3.10). Moreover from (7.2.4) and (7.2.3), observe that $\mathbf{B}$ satisfies $\mathbf{B}\mu = \mathbb{0}_{8\times 8}$. Hence, with ω^* defined in (5.5.1) and with $\mathbf{C} = \mathbb{0}_{8\times 8}$, $\omega^* = \omega^d$. This can be confirmed by observing the enlarged frequency plot at 90 sec in Figure 7.5, where it is clear that $\omega^* = \omega^d = 50$ Hz.

However, concerning active power sharing, the pinning control (5.3.10) is not able to correct deviations in active power sharing ratios, confirming the results presented in Section 5.5.1. Nevertheless, in contrast to the DAI controller, the weighted active powers do not diverge. See the weighted active power plot in Figure 7.5 at 5 sec (droop control only) and 90 sec (droop and pinning controller), wherein both the cases, an approximate maximum relative deviation of 42% can be observed.

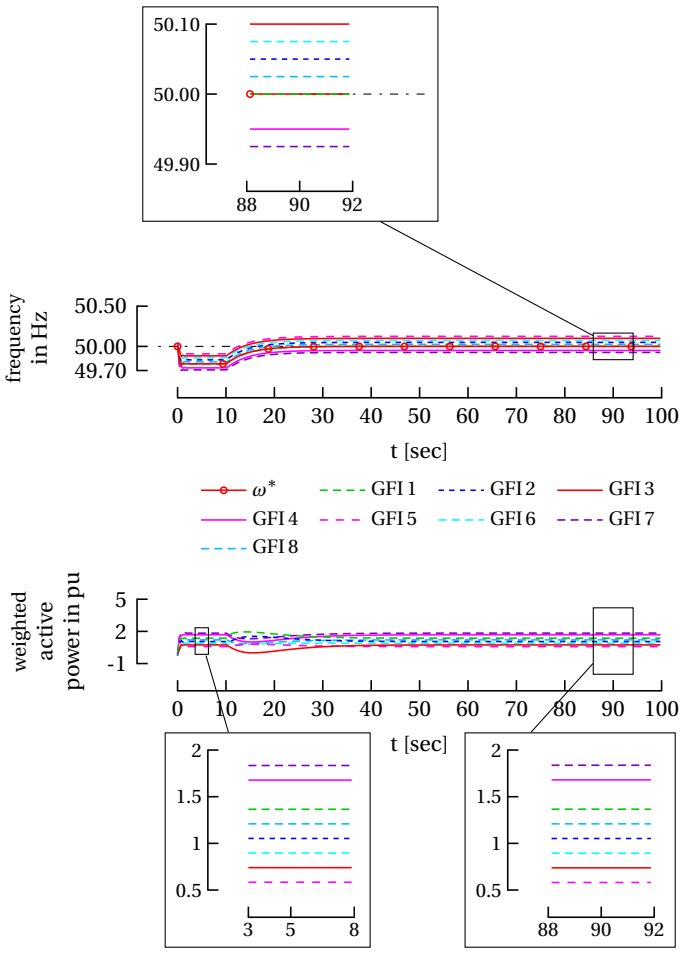

Figure 7.5. Simulation result with droop control (5.3.1) (active from 0 sec) and pinning control (5.3.10) (activated at 10 sec). Note that ω^* converges exactly to 50 Hz. However, the the weighted active powers do not attain consensus. See the zoom plots at 90 sec.

7.3 Distributed voltage control

In this section, the performance of the distributed voltage control (6.5.1) and its operational compatibility with frequency droop control (4.5.1) is illustrated via simulation. In essence, the system (4.4.1), (6.5.1), (4.5.1) is simulated.

The parallel microgrid used in the case study is shown in Figure 7.6, which was simulated using MATLAB®/Simulink® and PLECS [125]. The parameters of the simulated microgrid are given in Table 7.1. The power line connecting each DG to the PCC is modeled as a dynamic π-model [1, 4, 89]. A small positive resistance is also considered in the power line, see Table 7.1.

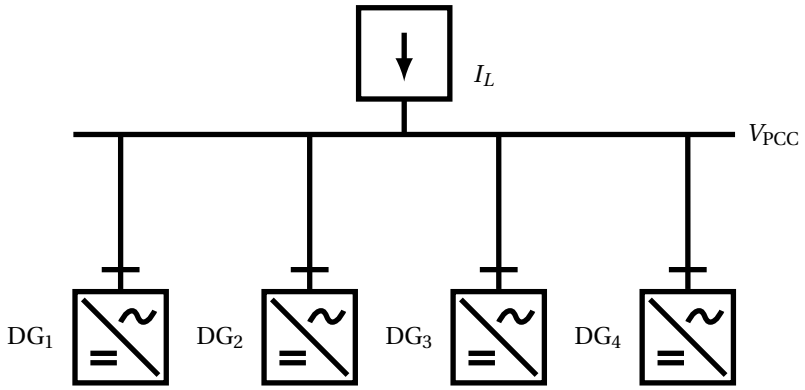

Figure 7.6. Parallel microgrid used in the simulation.

The frequency droop control (4.5.1) is employed at each inverter to control the frequencies. For achieving steady-state active power sharing, droop coefficients are selected as $k_{P_i} = \frac{1}{S_i^N}$, $i = 1,2,3,4$ where S_i^N is the nominal power rating given in Table 7.1. Furthermore, the entries of the weighting matrix $A = \text{diag}(a_i)$ required in (6.5.1) are chosen as per $a_i = \frac{1}{S_i^N}$, for more details see the discussion below Definition 3.3.2.

The communication topology used in the simulation is shown in Figure 7.7. Since the PCC voltage is communicated only to DG_1, the pinning gain matrix E takes the form $E = \text{diag}(e_1, 0, 0, 0)$ where $e_1 \in \mathbb{R}_{>0}$ is a controller parameter. Furthermore, the incidence matrix of the communication graph is fixed to

$$\mathscr{B} = \begin{bmatrix} 1 & 0 & 0 \\ -1 & 1 & 0 \\ 0 & -1 & 1 \\ 0 & 0 & -1 \end{bmatrix},$$

see Figure 7.7. For simplicity, it is assumed that the edge weights of the communication graph are equal to one, i.e., the edge weight matrix corresponding to

Table 7.1. Parameters of the simulated parallel MG.

Line parameters				
Resistance = 1.2 mΩ/km, Reactance = 9.5 mΩ/km				
DG number	1	2	3	4
Power rating S_i^N (in pu)	1	0.5	0.33	0.25
Line length (km) to PCC	2	5	7	3

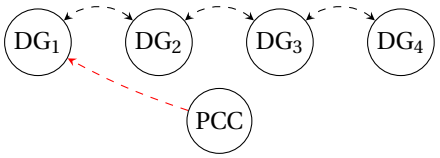

Figure 7.7. Communication topology used to implement the distributed voltage control (6.5.1).

Figure 7.7 reads $\mathbf{W} = I_3$. Thus, the Laplacian matrix $\mathscr{L} = \mathscr{B}\mathbf{W}\mathscr{B}^\top$ used in (6.5.1) writes as

$$\mathscr{L} = \begin{bmatrix} 1 & -1 & 0 & 0 \\ -1 & 2 & -1 & 0 \\ 0 & -1 & 2 & -1 \\ 0 & 0 & -1 & 1 \end{bmatrix}.$$

One of the main objectives of this section is to find the controller parameters K and E in (6.5.1) such that the conditions presented in Proposition 6.5.5 are satisfied. However, the conditions presented in Proposition 6.5.5 depend on the equilibrium voltage vector V^*, which–unfortunately–is unknown. Nonetheless, Corollary 6.5.6 presents a sufficient condition for the feasibility of Proposition 6.5.5, provided that an upper bound of V^* is known. The conditions presented in Corollary 6.5.6 are solved using the optimization toolbox Yalmip [120] and the solver Mosek [127] in MATLAB®/Simulink®. The tuning parameters σ, ζ, ξ, M and R are selected such that the first condition in (6.5.16) is satisfied. Note that the scalar ϱ required in (6.5.27) is the upper bound of V^*, i.e., (6.5.24). For solving (6.5.27), ϱ is set to $\varrho = 1.10$ pu. The LMI (6.5.27) is solved with K and E as the free parameters.

The LMI (6.5.27) was found to be feasible, yielding

$$\begin{aligned} K &= \mathrm{diag}(0.05, 0.12, 0.17, 0.07), \\ E &= \mathrm{diag}(e_1, 0, 0, 0) \quad \text{with} \quad e_1 = 0.08. \end{aligned} \tag{7.3.1}$$

7.3.1 Case 1: Load jumps

In this section, I_L connected at the PCC is simulated with load jumps. The corresponding simulation result of the distributed voltage control (4.4.1), (6.5.1) with the frequency droop control (4.4.1), (4.5.1) is shown in Figure 7.8. Between 0 to 5 sec, DG voltages are set to $V^d = 1$pu, see Remark 6.5.2. As a consequence, before 5 sec, PCC voltage is deviated from $V^d_{\mathrm{PCC}} = 1$pu. See the enlarged voltage

plot in Figure 7.8 before 5 sec. Furthermore, before 5 sec, it can be seen from the weighted reactive power plot in Figure 7.8 that reactive power sharing is poor.

The distributed voltage controller (6.5.1) is activated at 5 sec. After this, the PCC voltage converges quickly to 1pu, see the enlarged plot in Figure 7.8 at 15 sec. Hence, (6.3.1), i.e., PCC voltage restoration. Furthermore, the weighted reactive powers reach consensus, thereby confirming that the inverters share the load I_L in a proportional fashion, i.e., (6.3.2). Observe that the load jump starts at around 45 sec. After the load jump, PCC voltage regulation (see the enlarged plot at 70 sec) and reactive power sharing are re-established.

Furthermore, achieving PCC voltage regulation and reactive power sharing using (6.5.2) does not disturb the active power sharing provided by the frequency droop control (4.5.1), see the weighted active power plot in Figure 7.8, thus confirming the operational compatibility of the distributed voltage controller with frequency droop control.

7.3.2 Case 2: Continuously fluctuating load demand

In this section, a more realistic load profile provided by an industrial partner is used to simulate variations in I_L. The simulation output is given in Figure 7.9.

Similar to the previous case, frequency droop control (4.5.1) is active from 0 sec and the distributed voltage controller (6.5.1) is activated at 5 sec. From the enlarged voltage plots (at 15 sec and 70 sec) in Figure 7.9, it can be seen that the PCC voltage has converged to $V^d_{\text{PCC}} = 1\text{pu}$. Furthermore, the weighted reactive powers reach a consensus soon after 5 sec and are undisturbed throughout the simulation time of 100 sec. Similar to the case of load jumps, the distributed voltage controller does not affect active power sharing provided by frequency droop control. See the weighted active power plot in Figure 7.9.

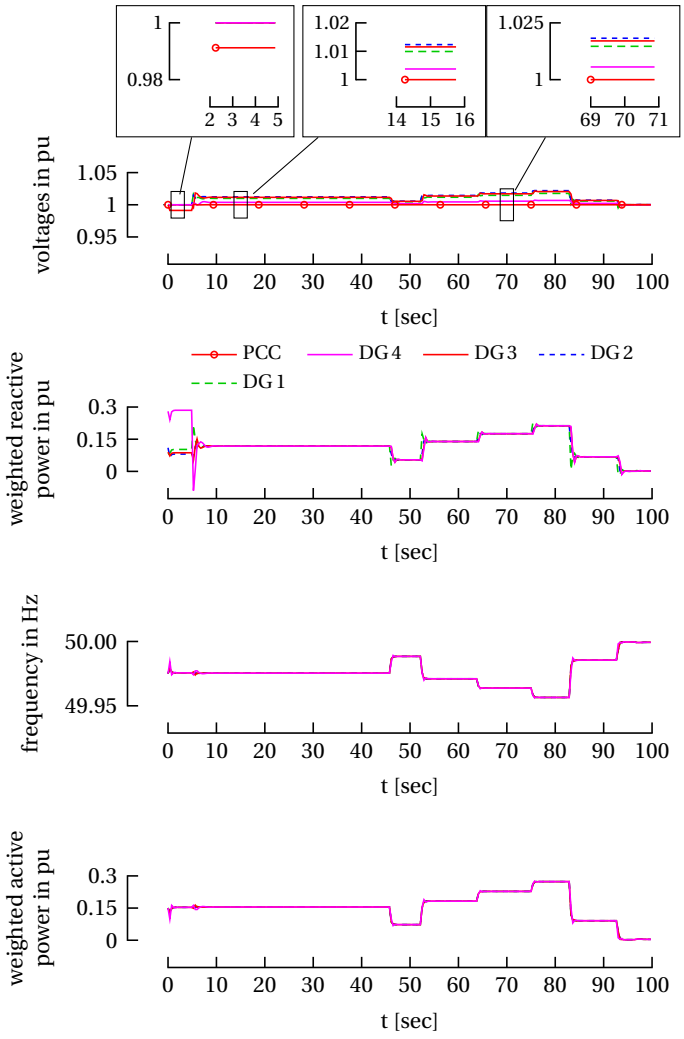

Figure 7.8. Load steps: Simulation output with the frequency droop control (4.4.1), (4.5.1) (active from 0 sec) and the distributed voltage control (4.4.1), (6.5.1)(activated at 5 sec). The PCC voltage is restored to $V^d_{\mathrm{PCC}} = 1$ pu, see the enlarged voltage plots at 15 sec and 70 sec. The weighted reactive powers achieve consensus soon after 5 sec, without disturbing the active power sharing provided by the frequency droop control.

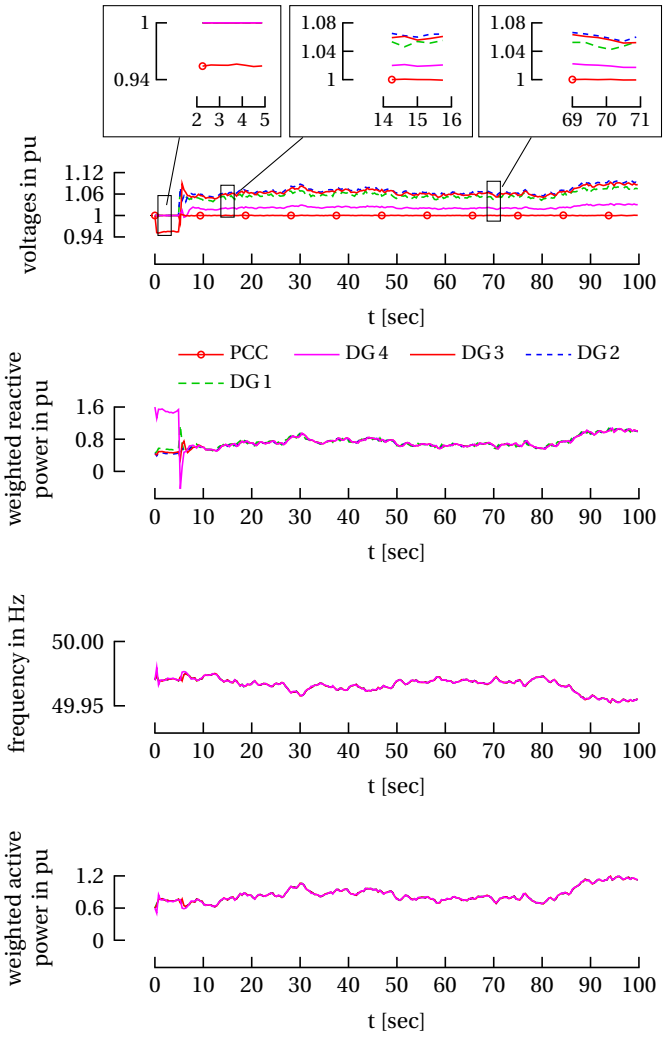

Figure 7.9. Continuously fluctuating load demand: Simulation output with the frequency droop control (4.4.1), (4.5.1) (active from 0 sec) and the distributed voltage control (4.4.1), (6.5.1) (activated at 5 sec). The PCC voltage is restored to $V^d_{\text{PCC}} = 1$ pu, see the enlarged voltage plots at 15 sec and 70 sec. The weighted reactive powers achieve consensus soon after 5 sec, without disturbing the active power sharing provided by the frequency droop control.

7.4 Summary

In this chapter, via simulation, robustness and performance of the control approaches presented in Chapter 5 and Chapter 6 towards modeling errors and disturbances have been studied.

For the considered case, the tuning criterion presented in Chapter 5 was found to be feasible, confirming asymptotic convergence of the closed-loop system's trajectories with the GDAI control to a desired synchronized motion. Furthermore, the GDAI control performance has been compared with that of the DAI and the pinning control, confirming the results from Chapter 5 regarding steady-state performance of distributed frequency controllers in the presence of clock drifts.

In the second part of this chapter, the distributed voltage controller proposed in Chapter 6 has been simulated together with the frequency droop control. The tuning criterion presented in Chapter 6 has been used to select the parameters of the distributed voltage controller. The proposed controller's performance has been tested in the presence of small line resistances and load disturbances. The simulation results were found to be satisfactory.

Chapter 8

Discussion and conclusion

8.1 Summary

Microgrids represent a promising solution to integrate RESs efficiently into the modern power grid. In this thesis, the concept of a microgrid has been introduced in Chapter 3. Then some of the important challenges in controlling a microgrid have been recalled in Chapter 3. In this work, some significant control problems in an inverter-based islanded microgrid have been addressed, namely: (1) accurate network frequency restoration, (2) active power sharing, (3) load/PCC voltage regulation, (4) reactive power sharing and (5) voltage stability. Clock drift is a non-negligible parameter uncertainty observed in microgrids, which has an adverse effect on the steady-state performance of primary and secondary frequency control. Thus, the first two objectives mentioned above were investigated in the presence of clock drifts. These results have been summarized in Chapter 5. The last three control problems mentioned above were studied in the case of a microgrid with parallel-connected inverters, i.e., a parallel microgrid, which is a commonly encountered microgrid application. The observations and results regarding voltage control have been presented in Chapter 6.

In Chapter 4, it has been shown that the steady-state active power sharing provided by the standard frequency droop control is disturbed in the presence of clock drifts. Similarly, it has been observed that the secondary frequency control is also negatively affected by the presence of clock drifts. Inspired by this issue, in Chapter 5, the steady-state performance of various distributed secondary frequency controllers has been compared based on whether they achieve accurate network frequency restoration and active power sharing in the presence of clock drifts. These secondary controllers assume that the standard frequency droop control is active at the primary control layer.

For the comparative study, a *general distributed secondary control representation* has been proposed. This representation can be cast into some of the typically used distributed secondary frequency controllers like the DAI control [32, 51], the pinning control [40], and many more. Based on the proposed general control representation, necessary and sufficient conditions for accurate frequency restoration and active power sharing have been derived with explicit consideration of clock drifts. The DAI controller was found to be not satisfying any of the derived conditions. However, the pinning controller seems to achieve accurate frequency restoration, but not active power sharing. As a consequence of the observations thus far, a novel secondary frequency control, termed as the *generalized distributed averaging integral (GDAI)* control, has been proposed. The GDAI control achieves the aforementioned control objectives in the presence of clock drifts. The second part of Chapter 5 was focused on how to choose the parameters of the GDAI control such that the closed-loop system trajectories converge asymptotically to a desired synchronized motion. In this regard, a tuning criterion, in the form of a set of LMIs, has been derived, which renders robust stability in the presence of unknown-bounded clock drift values.

In Chapter 6, the problem of voltage control in parallel microgrids has been investigated. More precisely, two practically important control objectives of accurate reactive power sharing and voltage restoration at a joint load (at the PCC) in case of a lossless inverter-based parallel microgrid has been investigated in detail. At first, the existence and uniqueness properties of a positive voltage solution satisfying the non-linear algebraic equations corresponding to the above-mentioned objectives have been established. Later, a distributed voltage controller, which at steady-state yields this unique voltage solution, has been proposed. In the second part of Chapter 6, a stability criterion that guarantees asymptotic convergence of solutions of the proposed distributed controller to the desired unique voltage solution has been derived. As it was found that the stability criterion depends on the voltage equilibrium, a numerically verifiable condition to choose the parameters of the proposed controller has also been derived.

To validate the results and to check whether the presented control approaches work well in the presence of typical modeling uncertainties and disturbances, results from Chapter 5 and Chapter 6 have been extensively tested via simulation in Chapter 7. The tuning criteria derived in Chapter 5 and Chapter 6 were found to be feasible. Furthermore, the GDAI control proposed in Chapter 5 and the distributed voltage control presented in Chapter 6 were found to be working satisfactorily in the presence of (small) line resistances and load variations.

8.2 Discussion

Generally, distributed secondary frequency controllers achieve network frequency restoration in a fair manner [26]. Steady-state active power sharing is a nice property of such controllers [51, 110]. However, in the presence of clock drifts, the commonly employed distributed frequency controllers fail to achieve accurate network frequency restoration and active power sharing. Thus, a novel control approach termed as the generalized distributed averaging integral (GDAI) control has been proposed to address these issues in the presence of clock drifts. The GDAI control is similar to the pinning control [13, Equation 47] (see also (5.3.10)) and the DAI control [32, Equation 6] (see also (5.3.9)) with the difference that together with the mandatory secondary control input, internal frequency of an inverter should also be communicated with its neighbors, see (5.6.2). In practice, communicating such an extra signal is not an issue, since the topology used in the GDAI control to communicate internal frequencies is the same as that used for communicating secondary control inputs. More precisely, the two Laplacian matrices used in (5.6.2) are the same. Furthermore, the GDAI control only requires that a few grid-forming inverters (at least one) need an accurate clock, see (5.6.2). This avoids the requirement of a central unit communicating the global/accurate time signal to all the grid-forming inverters connected in the network.

The distributed voltage control presented in Chapter 6 also requires a–sparsely–connected communication network for its operation. Furthermore, in a parallel microgrid setting, it is often the case that grid-forming inverters require PCC voltage information for regulating the PCC voltage amplitude to the nominal value. In this regard, the proposed distributed voltage control (6.5.1) does not require that the PCC voltage be communicated to all the grid-forming inverters connected in the parallel microgrid, hence avoiding an undesired one-to-all communication setup. This is a direct implication of the assumption that the controller parameter E used in (6.5.1) is a sparse diagonal positive semi-definite matrix.

In summary, various frequency and voltage control objectives in islanded microgrids have been investigated in this thesis. The proposed frequency control solution accomplishes two important control objectives in an inverter-based microgrid in the presence of clock drifts. The voltage control solution presented in this thesis addresses three crucial control challenges in a microgrid with parallel-connected inverters.

8.3 Future research directions

In this section, some possible extensions to this work are outlined.

Similar to any distributed control approach, the GDAI control proposed in Chapter 5 also requires a–sparse–communication network for its operation. As a consequence, it is also prone to issues like communication delay and denial of service (DoS). Robustness of the DAI controller towards the above issues has been recently investigated in [36, 65, 67]. Thus, inspired by [36, 65, 67], a possible extension would be to explore the same with GDAI control. Another exciting extension to the results presented in Chapter 5 is to quantify the robustness of GDAI control towards exogenous disturbances, e.g., by calculating the L_2 gain [50]. This problem has been explored in the case of the DAI control in [65]. In practice, such undesired external disturbances are widespread, and hence, the aforementioned study is very relevant. Furthermore, extending the stability analysis presented in Chapter 5 to variable voltage amplitudes [30] is interesting. Another intriguing idea is to design the GDAI control for microgrids with constant power loads, yielding a differential algebraic system. See, e.g. [25, 110], where the case of the DAI control with constant power loads has been explored.

Regarding Chapter 6, an immediate extension would be investigate existence and uniqueness properties of voltage solution satisfying reactive power sharing and PCC voltage regulation with respect to a constant power load, or even a ZIP[1] load model. The next interesting step would be to design a distributed voltage controller which drives the system equations to the unique solution asymptotically.

Another idea would be to consider more than one parallel microgrid. Such a setting is especially relevant when it comes to a big battery power plant, where many inverter-interfaced batteries are present. More precisely, let there be $m > 1$ parallel microgrids and each parallel microgrid has $n > 1$ inverters connected in parallel to a load bus. The load bus of a parallel microgrid is connected to the load bus of another parallel microgrid through a power line. In such a setting, designing voltage controllers such that voltage amplitudes at m number of load buses are regulated, and at the same time, the reactive power demand of the system loads is shared fairly between $n \times m$ number of inverters is a vital control objective.

In a similar spirit to that of a bunch of parallel microgrids, consider an inverter-based microgrid with arbitrary topology. In such a meshed microgrid, often the

[1] ZIP stands for constant impedance/current/power, see [5, Chapter 3], [100, Chapter 3].

load buses and the inverter buses are different, see for example the benchmark grid presented in [128]. Furthermore, apart from normal loads, it is often the case that there are critical (high-priority) loads also connected in a microgrid. Recall that grid-forming inverters are responsible for controlling such a network to maintain a stable voltage equilibrium, achieve reactive power sharing, and restore voltage amplitudes at the critical loads to the desired nominal value. The latter objective is fundamental because the loads are designed to work near their nominal voltage value, and it is mostly the case that the loads are not controllable, e.g. ZIP loads. Therefore, designing a distributed voltage controller at each grid-forming inverter such that reactive power sharing, critical load voltage regulation, and voltage stability are ensured is interesting–albeit challenging–problem.

It is worthwhile to note that the system equations coupling reactive power and voltage amplitudes in the case of a lossless meshed AC microgrid[2] (see e.g., [24]) is exactly the same as that of a meshed DC microgrid (see e.g., [121]) by replacing *reactive power* with *active power* (or simply *power*) and *line susceptances* with *line conductances*. Hence, the idea mentioned above for AC microgrids can be extended to DC microgrids as well. Another interesting, but challenging, extension would be to combine the results in Chapter 5 and Chapter 6, i.e., a coupled distributed frequency and voltage control. Finally, exploring the results in Chapter 5 and Chapter 6 with consideration of power lines with mixed R/X (resistance/inductive reactance) ratio is also interesting.

In conclusion, there are many intriguing and challenging open problems regarding the control of an islanded microgrid. The author hopes that the work presented in this thesis helps to address at least some of these problems.

[2] Under the decoupling assumption, see Assumption 6.2.1.

Bibliography

[1] P. Kundur, *Power system stability and control*. McGraw-Hill, 1994.

[2] D. A. Jones, "Electrical engineering: the backbone of society," in *IEE Proceedings A, Science, Measurement and Technology*, vol. 138, no. 1. IET, 1991, pp. 1–10.

[3] P. Anderson and A. Fouad, *Power System Control and Stability*. J.Wiley & Sons, 2002.

[4] J. J. Grainger and W. D. Stevenson, *Power system analysis*. McGraw-Hill New York, 1994, vol. 621.

[5] J. Machowski, J. Bialek, and J. Bumby, *Power system dynamics: stability and control*. J.Wiley & Sons, 2008.

[6] P. P. Varaiya, F. F. Wu, and J. W. Bialek, "Smart operation of smart grid: Risk-limiting dispatch," *Proceedings of the IEEE*, vol. 99, no. 1, pp. 40–57, 2011.

[7] K. Alanne and A. Saari, "Distributed energy generation and sustainable development," *Renewable and Sustainable Energy Reviews*, vol. 10, no. 6, pp. 539–558, Dec. 2006.

[8] H. Farhangi, "The path of the smart grid," *IEEE Power and Energy Magazine*, vol. 8, no. 1, pp. 18 –28, Jan./Feb. 2010.

[9] X. Fang, S. Misra, G. Xue, and D. Yang, "Smart grid - the new and improved power grid: a survey," *Communications Surveys & Tutorials, IEEE*, vol. 14, no. 4, pp. 944–980, 2012.

[10] R. Lasseter, "Microgrids," in *IEEE Power Engineering Society Winter Meeting, 2002*, vol. 1, 2002, pp. 305 – 308 vol.1.

[11] T. Ackermann, G. Andersson, and L. Söder, "Distributed generation: a definition," *Electric power systems research*, vol. 57, no. 3, pp. 195–204, 2001.

[12] W. D. Stevenson, *Elements of power system analysis*. McGraw Hill Kogakusha Limited, 1975.

[13] A. Bidram, F. Lewis, and A. Davoudi, "Distributed control systems for small-scale power networks: Using multiagent cooperative control theory," *IEEE Control Systems*, vol. 34, no. 6, pp. 56–77, 2014.

[14] J. Rocabert, A. Luna, F. Blaabjerg, and P. Rodriguez, "Control of power converters in AC microgrids," *IEEE Transactions on Power Electronics*, vol. 27, no. 11, pp. 4734–4749, Nov. 2012.

[15] J. Lopes, C. Moreira, and A. Madureira, "Defining control strategies for microgrids islanded operation," *IEEE Transactions on Power Systems*, vol. 21, no. 2, pp. 916 – 924, May 2006.

[16] J. Schiffer, D. Zonetti, R. Ortega, A. Stanković, J. Raisch, and T. Sezi, "Modeling of microgrids - from fundamental physics to phasors and voltage sources," *Automatica*, vol. 74, no. 12, pp. 135–150, 2016.

[17] T. Green and M. Prodanovic, "Control of inverter-based micro-grids," *Electric Power Systems Research*, vol. Vol. 77, no. 9, pp. 1204–1213, July 2007.

[18] N. Hatziargyriou, H. Asano, R. Iravani, and C. Marnay, "Microgrids," *IEEE Power and Energy Magazine*, vol. 5, no. 4, pp. 78–94, 2007.

[19] F. Katiraei, R. Iravani, N. Hatziargyriou, and A. Dimeas, "Microgrids management," *IEEE Power and Energy Magazine*, vol. 6, no. 3, pp. 54–65, 2008.

[20] R. Lasseter and P. Paigi, "Microgrid: a conceptual solution," in *Power Electronics Specialists Conference, 2004. PESC 04. 2004 IEEE 35th Annual*, vol. 6, June 2004, pp. 4285 – 4290 Vol.6.

[21] C. A. Hans, P. Braun, J. Raisch, L. Grüne, and C. Reincke-Collon, "Hierarchical distributed model predictive control of interconnected microgrids," *IEEE Transactions on Sustainable Energy*, vol. 10, no. 1, pp. 407–416, Jan 2019.

[22] J. Schiffer, R. Ortega, A. Astolfi, J. Raisch, and T. Sezi, "Conditions for stability of droop-controlled inverter-based microgrids," *Automatica*, vol. 50, no. 10, pp. 2457–2469, 2014.

[23] J. Schiffer, "Stability and power sharing in microgrids," Ph.D. dissertation, Technische Universität Berlin, 2015.

[24] J. W. Simpson-Porco, F. Dörfler, and F. Bullo, "Voltage stabilization in microgrids via quadratic droop control," *IEEE Transactions on Automatic Control*, vol. 62, no. 3, pp. 1239 – 1253, March 2017.

[25] C. D. Persis, N. Monshizadeh, J. Schiffer, and F. Dörfler, "A Lyapunov approach to control of microgrids with a network-preserved differential-algebraic model," in *IEEE 55th Conference on Decision and Control (CDC)*, 2016, pp. 2595 – 2600.

[26] F. Dörfler, J. W. Simpson-Porco, and F. Bullo, "Breaking the hierarchy: Distributed control & economic optimality in microgrids," *IEEE Transactions on Control of Network Systems*, vol. 3, no. 3, pp. 241–253, Sept. 2016.

[27] J. Schiffer, T. Seel, J. Raisch, and T. Sezi, "Voltage stability and reactive power sharing in inverter-based microgrids with consensus-based distributed voltage control," *IEEE Transactions on Control Systems Technology*, vol. 24, no. 1, pp. 96–109, 2016.

[28] N. Bretas and L. F. C. Alberto, "Lyapunov function for power systems with transfer conductances: extension of the invariance principle," *IEEE Transactions on Power Systems*, vol. 18, no. 2, pp. 769–777, 2003.

[29] R. Ortega, M. Galaz, A. Astolfi, Y. Sun, and T. Shen, "Transient stabilization of multimachine power systems with nontrivial transfer conductances," *IEEE Transactions on Automatic Control*, vol. 50, no. 1, pp. 60 – 75, jan. 2005.

[30] C. D. Persis and N. Monshizadeh, "Bregman storage functions for microgrid control," *IEEE Transactions on Automatic Control*, vol. 63, no. 1, pp. 53–68, Jan. 2017.

[31] F. Dörfler and F. Bullo, "Synchronization and transient stability in power networks and non-uniform Kuramoto oscillators," *SIAM Journal on Control and Optimization*, vol. 50, no. 3, pp. 1616–1642, 2012.

[32] J. W. Simpson-Porco, Q. Shafiee, F. Dörfler, J. C. Vasquez, J. M. Guerrero, and F. Bullo, "Secondary frequency and voltage control of islanded microgrids via distributed averaging," *IEEE Transactions on Industrial Electronics*, vol. 62, pp. 7025–7038, 2015.

[33] J. W. Simpson-Porco, F. Dörfler, and F. Bullo, "Voltage collapse in complex power grids," *Nature Communications*, vol. 7, no. 10790, Feb. 2016.

[34] Q.-C. Zhong, "Robust droop controller for accurate proportional load sharing among inverters operated in parallel," *IEEE Transactions on Industrial Electronics*, vol. 60, no. 4, pp. 1281–1290, 2013.

[35] C. K. Sao and P. W. Lehn, "Autonomous load sharing of voltage source converters," *IEEE Transactions on Power Delivery*, vol. 20, no. 2, pp. 1009–1016, 2005.

[36] J. Schiffer, F. Dörfler, and E. Fridman, "Robustness of distributed averaging control in power systems: Time delays & dynamic communication topology," *Automatica*, vol. 80, pp. 261–271, 2017.

[37] F. Guo, C. Wen, J. Mao, and Y. D. Song, "Distributed secondary voltage and frequency restoration control of droop-controlled inverter-based microgrids," vol. 62, pp. 4355–4368, 2015.

[38] M. Chandorkar, D. Divan, and R. Adapa, "Control of parallel connected inverters in standalone AC supply systems," *IEEE Transactions on Industry Applications*, vol. 29, no. 1, pp. 136 –143, Jan./Feb. 1993.

[39] J. Guerrero, J. Vasquez, J. Matas, L. de Vicuna, and M. Castilla, "Hierarchical control of droop-controlled AC and DC microgrids: A general approach toward standardization," *IEEE Transactions on Industrial Electronics*, vol. 58, no. 1, pp. 158 –172, jan. 2011.

[40] A. Bidram and A. Davoudi, "Hierarchical structure of microgrids control system," *IEEE Transactions on Smart Grid*, vol. 3, no. 4, pp. 1963–1976, 2012.

[41] H. Kopetz, *Real-time systems: design principles for distributed embedded applications*. Springer, 2011.

[42] Anritsu, "Understanding frequency accuracy in crystal controlled instruments - application note," Anritsu EMEA Ltd., Tech. Rep., 2001.

[43] J. Schiffer, C. A. Hans, T. Kral, R. Ortega, and J. Raisch, "Modeling, analysis, and experimental validation of clock drift effects in low-inertia power systems," *IEEE Transactions on Industrial Electronics*, vol. 64, pp. 5942 – 5951, 2017.

[44] M. Castilla, A. Camacho, P. Martí, M. Velasco, and M. M. Ghahderijani, "Impact of clock drifts on communication-free secondary control schemes for inverter-based islanded microgrids," *IEEE Transactions on Industrial Electronics*, vol. 65, no. 6, pp. 4739 – 4749, June 2017.

[45] M. Castilla, A. Camacho, J. Miret, M. Velasco, and P. Marti, "Local secondary control for inverter-based islanded microgrids with accurate active-power sharing under high load conditions," *IEEE Transactions on Industrial Electronics*, vol. 66, no. 4, pp. 2529 – 2539, June 2018.

[46] J. T. Martínez, M. Castilla, J. Miret, M. M. Ghahderijani, and J. M. Rey, "Experimental study of clock drift impact over droop-free distributed control for industrial microgrids," in *43rd Annual Conference of the IEEE Industrial Electronics Society , IECON*, 2017, pp. 2479 – 2484.

[47] C. X. Rosero, P. Martí, M. Velasco, M. Castilla, J. Miret, and A. Camacho, "Consensus for active power sharing and frequency restoration in islanded microgrids subject to drifting clocks," in *IEEE 26th International Symposium on Industrial Electronics (ISIE)*, 2017, pp. 70 – 75.

[48] P. Marti, J. Torres-Martinez, C. X. Rosero, M. Velasco, J. Miret, and M. Castilla, "Analysis of the effect of clock drifts on frequency regulation and power sharing in inverter-based islanded microgrids," *IEEE Transactions on Power Electronics*, vol. 33, no. 12, pp. 10 363 – 10 379, Dec. 2018.

[49] H. K. Khalil, *Nonlinear systems*. Prentice Hall, 2002, vol. 3.

[50] A. van der Schaft, *L2-Gain and Passivity Techniques in Nonlinear Control*. Springer, 2000.

[51] C. Zhao, E. Mallada, and F. Dörfler, "Distributed frequency control for stability and economic dispatch in power networks," in *American Control Conference (ACC)*, July 2015, pp. 2359 – 2364.

[52] M. Andreasson, H. Sandberg, D. V. Dimarogonas, and K. H. Johansson, "Distributed integral action: Stability analysis and frequency control of power systems," in *51st Conference on Decision and Control*, Maui, HI, USA, 2012.

[53] C. Godsil and G. Royle, *Algebraic Graph Theory*. Springer, 2001.

[54] M. Mesbahi and M. Egerstedt, *Graph theoretic methods in multiagent networks*. Princeton University Press, 2010.

[55] R. Diestel, *Graph Theory*, 4th ed. Springer, 2010.

[56] R. Olfati-Saber, J. A. Fax, and R. M. Murray, "Consensus and cooperation in networked multi-agent systems," *Proceedings of the IEEE*, vol. 95, no. 1, pp. 215–233, 2007.

[57] E. Weitenberg, Y. Jiang, C. Zhao, E. Mallada, C. D. Persis, and F. Dörfler, "Robust decentralized secondary frequency control in power systems: Merits and trade-offs," *IEEE Transactions on Automatic Control (Early Access)*, Dec. 2017.

[58] J. Schiffer, R. Ortega, C. Hans, and J. Raisch, "Droop-controlled inverter-based microgrids are robust to clock drifts," *American Control Conference*, pp. 2341 – 2346, 2015.

[59] M. A. Pai, *Energy function analysis for power system stability*. Kluwer academic publishers, 1989.

[60] E. Planas, A. Gil-de Muro, J. Andreu, I. Kortabarria, and I. Martínez de Alegría, "General aspects, hierarchical controls and droop methods in microgrids: A review," *Renewable and Sustainable Energy Reviews*, vol. 17, pp. 147–159, 2013.

[61] C. A. Hans, V. Nenchev, J. Raisch, and C. Reincke-Collon, "Minimax model predictive operation control of microgrids," 2014, 19th IFAC World Congress, Cape Town, South Africa.

[62] J. W. Simpson-Porco, F. Dörfler, and F. Bullo, "Synchronization and power sharing for droop-controlled inverters in islanded microgrids," *Automatica*, vol. 49, no. 9, pp. 2603 – 2611, 2013.

[63] J. Guerrero, P. Loh, M. Chandorkar, and T. Lee, "Advanced control architectures for intelligent microgrids – part I: Decentralized and hierarchical control," *IEEE Transactions on Industrial Electronics*, vol. 60, no. 4, pp. 1254–1262, 2013.

[64] X. Fu, F. Dörfler, and M. R. Jovanović, "Topology identification and design of distributed integral action in power networks," in *American Control Conference (ACC)*, 2016, pp. 5921 – 5926.

[65] S. Alghamdi, J. Schiffer, and E. Fridman, "Distributed secondary frequency control design for microgrids: Trading off l2-gain performance and communication efforts under time-varying delays," in *European Control Conference*, 2018.

[66] S. Alghamdi, J. Schiffer, and E. Fridman, "Synthesizing sparse and delay-robust distributed secondary frequency controllers for microgrids," *IEEE Transactions on Control Systems Technology*, 2019.

[67] E. Weitenberg, C. D. Persis, and N. Monshizadeh, "Exponential convergence under distributed averaging integral frequency control," *Automatica*, vol. 98, pp. 103–113, Dec. 2018.

[68] C. D. Persis and P. Tesi, "Input-to-state stabilizing control under denial-of-service," *IEEE Transactions on Automatic Control*, vol. 60, no. 11, Nov. 2015.

[69] F. Dörfler, M. R. Jovanović, M. Chertkov, and F. Bullo, "Sparsity-promoting optimal wide-area control of power networks," *IEEE Transactions on Power Systems*, vol. 29, no. 5, Sept. 2014.

[70] C. X. Rosero, H. Carrasco, M. Velasco, and P. Martí, "Impact of clock drifts on active power sharing and frequency regulation in distributed-averaging secondary control for islanded microgrids," in *International Autumn Meeting on Power, Electronics and Computing*, 2017, pp. 1 – 6.

[71] R. R. Kolluri, I. Mareels, T. Alpcan, M. Brazil, J. de Hoog, and D. A. Thomas, "Power sharing in angle droop controlled microgrids," *IEEE Transactions on Power Systems*, vol. 32, no. 6, pp. 4743 – 4751, Nov. 2017.

[72] R. Majumder, G. Ledwich, A. Ghosh, S. Chakrabarti, and F. Zare, "Droop control of converter-interfaced microsources in rural distributed generation," *IEEE Transactions on Power Delivery*, vol. 25, no. 4, pp. 2768–2778, Oct. 2010.

[73] R. R. Kolluri, I. Mareels, T. Alpcan, M. Brazil, J. de Hoog, and D. A. Thomas, "Stability and active power sharing in droop controlled inverter interfaced microgrids: Effect of clock mismatches," *Automatica*, vol. 93, pp. 469–475, 2018.

[74] R. Solis, V. S. Borkar, and P. R. Kumar, "A new distributed time synchronization protocol for multihop wireless networks," in *CDC*, 2006, pp. 2734 – 2739.

[75] L. Schenato and F. Fiorentin, "Average timesynch: A consensus-based protocol for clock synchronization in wireless sensor networks," *Automatica*, vol. 47, no. 9, pp. 1878–1886, 2011.

[76] J. Guerrero, L. Garcia de Vicuna, J. Matas, M. Castilla, and J. Miret, "Output impedance design of parallel-connected UPS inverters with wireless load-sharing control," *IEEE Transactions on Industrial Electronics*, vol. 52, no. 4, pp. 1126 – 1135, aug. 2005.

[77] J. M. Guerrero, J. C. Vasquez, J. Matas, M. Castilla, and L. G. de Vicuna, "Control strategy for flexible microgrid based on parallel line-interactive UPS systems," *IEEE Transactions on Industrial Electronics*, 2009.

[78] J. Guerrero, J. Matas, L. G. de Vicuna, M. Castilla, and J. Miret, "Decentralized control for parallel operation of distributed generation inverters using resistive output impedance," *IEEE Transactions on Industrial Electronics*, vol. 54, no. 2, pp. 994 –1004, April 2007.

[79] A. Tuladhar, H. Jin, T. Unger, and K. Mauch, "Control of parallel inverters in distributed AC power systems with consideration of line impedance effect," *IEEE Transactions on Industry Applications*, vol. 36, no. 1, pp. 131 –138, Jan./Feb. 2000.

[80] J. Guerrero, J. Matas, L. de Vicuna, M. Castilla, and J. Miret, "Wireless-control strategy for parallel operation of distributed-generation inverters," *IEEE Transactions on Industrial Electronics*, vol. 53, no. 5, pp. 1461 –1470, oct. 2006.

[81] M. Marwali, J.-W. Jung, and A. Keyhani, "Control of distributed generation systems - part ii: Load sharing control," *IEEE Transactions on Power Electronics*, vol. 19, no. 6, pp. 1551 – 1561, Nov. 2004.

[82] U. Borup, F. Blaabjerg, and P. Enjeti, "Sharing of nonlinear load in parallel-connected three-phase converters," *IEEE Transactions on Industry Applications*, vol. 37, no. 6, pp. 1817 – 1823, Nov/Dec 2001.

[83] E. Coelho, P. Cortizo, and P. Garcia, "Small-signal stability for parallel-connected inverters in standalone AC supply systems," *IEEE Transactions on Industry Applications*, vol. 38, no. 2, pp. 533 –542, Mar./Apr. 2002.

[84] R. A. Horn and C. R. Johnson, *Matrix analysis*. Cambridge university press, 2012.

[85] R. Olfati-Saber and R. M. Murray, "Consensus problems in networks of agents with switching topology and time-delays," *IEEE Transactions on Automatic Control*, vol. 49, no. 9, pp. 1520–1533, Sept. 2004.

[86] A. Jadbabaie, J. Lin, and A. S. Morse, "Coordination of groups of mobile autonomous agents using nearest neighbor rules," *IEEE Transactions on Automatic Control*, vol. 48, no. 6, pp. 988–1001, June 2003.

[87] W. Ren and R. W. Beard, "Consensus seeking in multi-agent systems under dynamically changing interaction topologies," *IEEE Transactions on Automatic Control*, vol. 50, no. 5, p. 655–661, May 2005.

[88] L. Moreau, "Stability of multi-agent systems with time-dependent communication links," *IEEE Transactions on Automatic Control*, vol. 50, no. 2, pp. 169–182, Feb. 2005.

[89] J. D. Glover, M. S. Sarma, and T. J. Overbye, *Power system analysis and design*. Cengage Learning, 2011.

[90] H. Akagi, E. H. Watanabe, and M. Aredes, *Instantaneous power theory and applications to power conditioning*. John Wiley & Sons, 2007.

[91] F. Dörfler and F. Bullo, "Kron reduction of graphs with applications to electrical networks," *IEEE Transactions on Circuits and Systems I: Regular Papers*, vol. 60, no. 1, pp. 150–163, Jan. 2013.

[92] N. Pogaku, M. Prodanovic, and T. Green, "Modeling, analysis and testing of autonomous operation of an inverter-based microgrid," *IEEE Transactions on Power Electronics*, vol. 22, no. 2, pp. 613 –625, March 2007.

[93] S. Chowdhury and P. Crossley, *Microgrids and active distribution networks*. The Institution of Engineering and Technology, 2009.

[94] IEEE PES Task Force on Microgrid Stability Analysis and Modeling, "Microgrid stability definitions, analysis, and modeling," IEEE Power and Energy Society, Tech. Rep., June 2018.

[95] N. Lidula and A. Rajapakse, "Microgrids research: A review of experimental microgrids and test systems," *Renewable and Sustainable Energy Reviews*, vol. 15, no. 1, pp. 186–202, 2011.

[96] O. Palizban, K. Kauhaniemi, and J. M. Guerrero, "Microgrids in active network management—Part I: hierarchical control, energy storage, virtual power plants, and market participation," *Renewable and Sustainable Energy Reviews*, 2014.

[97] B. K. Poolla, S. Bolognani, and F. Dörfler, "Optimal placement of virtual inertia in power grids," *Automatica*, vol. 62, no. 12, pp. 6209 – 6220, Dec. 2017.

[98] B. K. Poolla, D. Gross, T. Borsche, S. Bolognani, and F. Dörfler, *Virtual inertia placement in electric power grids*. Springer, 2018, vol. 162.

[99] P. Kundur, J. Paserba, V. Ajjarapu, G. Andersson, A. Bose, C. Canizares, N. Hatziargyriou, D. Hill, A. Stankovic, C. Taylor, T. Van Cutsem, and V. Vittal, "Definition and classification of power system stability IEEE/CIGRE joint task force on stability terms and definitions," *IEEE Transactions on Power Systems*, vol. 19, no. 3, pp. 1387–1401, Aug. 2004.

[100] T. Van Cutsem and C. Vournas, *Voltage stability of electric power systems*. Springer, 1998, vol. 441.

[101] C. A. Hans, P. Sopasakis, A. Bemporad, J. Raisch, and C. Reincke-Collon, "Scenario-based model predictive operation control of islanded microgrids," in *54th IEEE Conference on Decision and Control (CDC)*, 2015, pp. 3272 – 3277.

[102] N. Mohan and T. M. Undeland, *Power electronics: converters, applications, and design*. John Wiley & Sons, 2007.

[103] R. Teodorescu, M. Liserre, and P. Rodriguez, *Grid converters for photovoltaic and wind power systems*. John Wiley & Sons, 2011, vol. 29.

[104] Q.-C. Zhong and T. Hornik, *Control of power inverters in renewable energy and smart grid integration*. John Wiley & Sons, 2012.

[105] R. W. Erickson and D. Maksimovic, *Fundamentals of power electronics*. Springer, 2001.

[106] X. Wang, J. M. Guerrero, F. Blaabjerg, and Z. Chen, "A review of power electronics based microgrids," *Journal of Power Electronics*, vol. 12, no. 1, pp. 181–192, 2012.

[107] J. T. Bialasiewicz, "Renewable energy systems with photovoltaic power generators: Operation and modeling," *IEEE Transactions on Industrial Electronics*, vol. 55, no. 7, p. 2752–2758, Jul. 2008.

[108] A. Engler, "Applicability of droops in low voltage grids," *International Journal of Distributed Energy Resources*, vol. 1, no. 1, pp. 1–6, 2005.

[109] R. Ortega, A. van der Schaft, B. Maschke, and G. Escobar, "Interconnection and damping assignment passivity-based control of port-controlled Hamiltonian systems," *Automatica*, vol. 38, no. 4, pp. 585–596, April 2002.

[110] J. Schiffer and F. Dörfler, "On stability of a distributed averaging PI frequency and active power controlled differential-algebraic power system model," in *European Control Conference (ECC)*, 2016, pp. 1487 – 1492.

[111] J. Simpson-Porco, "A theory of solvability for lossless power flow equations – part I: Fixed-point power flow," *IEEE Transactions on Control of Network Systems*, vol. 5, no. 3, pp. 1361 – 1372, Sept. 2017.

[112] Y. W. Li and C.-N. Kao, "An accurate power control strategy for power-electronics-interfaced distributed generation units operating in a low-voltage multibus microgrid," *IEEE Transactions on Power Electronics*, vol. 24, no. 12, pp. 2977 –2988, Dec. 2009.

[113] L. Schenato and G. Gamba, "A distributed consensus protocol for clock synchronization in wireless sensor network," in *46th IEEE Conference on Decision and Control*. IEEE, 2007, pp. 2289–2294.

[114] Y. Kikuya, S. M. Dibaji, and H. Ishii, "Fault tolerant clock synchronization over unreliable channels in wireless sensor networks," *IEEE Transactions on Control of Network Systems*, vol. 5, no. 4, pp. 1551 – 1562, July 2017.

[115] Y. Kadowaki and H. Ishii, "Event-based distributed clock synchronization for wireless sensor networks," *IEEE Transactions on Automatic Control*, vol. 60, no. 8, pp. 2266 – 2271, August 2015.

[116] A. Krishna, C. A. Hans, J. Schiffer, J. Raisch, and T. Kral, "Steady state evaluation of distributed secondary frequency control strategies for microgrids in the presence of clock drifts," in *25th Mediterranean Conference on Control and Automation (MED)*, 2017, pp. 508 – 515.

[117] A. Krishna, J. Schiffer, and J. Raisch, "A consensus-based control law for accurate frequency restoration and power sharing in microgrids in the presence of clock drifts," in *European Control Conference (ECC)*, 2018, pp. 2575 – 2580.

[118] A. Krishna, J. Schiffer and J. Raisch, "Distributed secondary frequency control in microgrids: Robustness and steady-state performance in the presence of clock drifts," *European Journal of Control (In press)*, 2019.

[119] J. Schiffer, D. Goldin, J. Raisch, and T. Sezi, "Synchronization of droop-controlled microgrids with distributed rotational and electronic generation," in *52nd Conference on Decision and Control*, Florence, Italy, 2013, pp. 2334–2339.

[120] J. Löfberg, "YALMIP : A toolbox for modeling and optimization in MATLAB," in *IEEE International Symposium on Computer Aided Control Systems Design*, Sept. 2004, pp. 284 –289.

[121] C. D. Persis, E. R.A.Weitenberg, and F. Dörfler, "A power consensus algorithm for dc microgrids," *Automatica*, vol. 89, pp. 364–375, Mar. 2018.

[122] A. Krishna, J. Schiffer, N. Monshizadeh, and J. Raisch, "A consensus-based voltage control for reactive power sharing and pcc voltage regulation in microgrids with parallel-connected inverters," in *European Control Conference*, 2019.

[123] S. Bolognani, G. Cavraro, and S. Zampieri, "A distributed feedback control approach to the optimal reactive power flow problem," in *Control of Cyber-Physical Systems*. Springer, 2013, pp. 259–277.

[124] "DIN EN 50160:2010 - Merkmale der Spannung in öffentlichen Elektrizitätsversorgungsnetzen, (engl: "Voltage characteristics of electricity supplied by public distribution networks)," february 2011.

[125] Plexim GmbH, "Plecs software, www.plexim.com," 2013.

[126] S. Golestan, M. Monfared, and F. D. Freijedo, "Design-oriented study of advanced synchronous reference frame phase-locked loops," *IEEE Transactions on Power Electronics*, vol. 28, pp. 765–778, Feb. 2012.

[127] Mosek, "The mosek optimization toolbox, www.mosek.com."

[128] K. Rudion, A. Orths, Z. Styczynski, and K. Strunz, "Design of benchmark of medium voltage distribution network for investigation of DG integration," in *IEEE Power Engineering Society General Meeting*, 2006.